

**Sustainable Aromatics: Synthesis and Hydrogenolysis of
Lignin Monomer Compounds**

Yuhan Zhao

Submitted in accordance with the requirements for the degree of

Doctor of Philosophy

The University of Leeds

School of Chemistry

December 2014

The candidate confirms that the work submitted is his/her own and that appropriate credit has been given where reference has been made to the work of others.

This copy has been supplied on the understanding that it is copyright material and that no quotation from the thesis may be published without proper acknowledgement.

The right of Yuhan Zhao to be identified as Author of this work has been asserted by her in accordance with the Copyright, Designs and Patents Act 1988.

© 2014 The University of Leeds and Yuhan Zhao

Acknowledgement

I would like to express my deep appreciation and thanks to my supervisor Prof. John Blacker, who is encouraging my research and helping me build my chemistry knowledge. With his guidance and patience, I become more confident and grow as a research scientist. Thanks for John's support for offering me many opportunities to present my work at international conferences.

I would also like to thank my co-supervisor Prof. Steve Marsden, thanks for his suggestions and comments for this research. I appreciated Prof. Philip Kocienski's kindness and help. I am grateful to Dr Julie Fisher for her kindness and helpful advice for my PhD study in general.

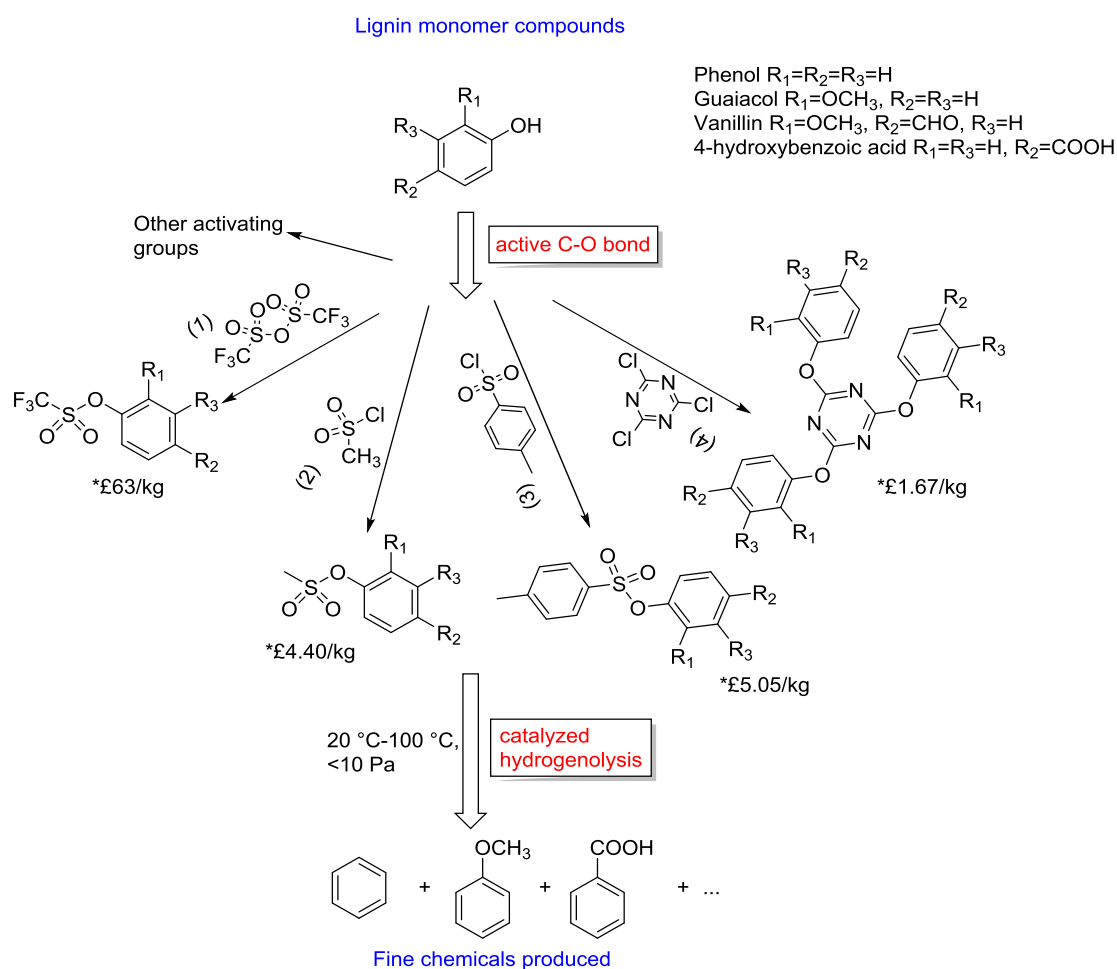
I would like to thank my family, without their support, my PhD would not be possible. I will forever be thankful my parents who have raised me with understanding, encouraging and supporting me. For my grandparents, they give me faith to overcome difficulties and stand on my behalf. I am grateful to my boyfriend Mark. He has been patient and faithful supporting me during my final stage of this PhD.

I have appreciated the iPRD group in the basement. Thanks to Dr Katie Jolly, Dr William Reynolds, Dr Jessica Breen and Dr John Cooksey for their support on my research. Thanks for them to read my reports and help me improve my language.

Lastly, I gratefully acknowledge my friends. I had enjoyable time in Leeds. The life being a PhD is not easy, however, you brought so much laughter into it. I want to thank my best friend Qi Meng, who I met on the first day of my PhD. We worked together in the late nights and most weekends, but we also travelled together in many places in Europe. When I lost my faith, you encouraged me not to give up.

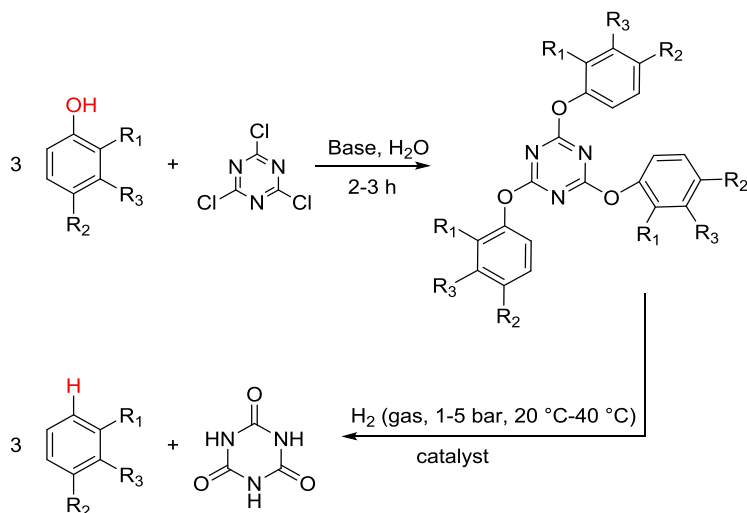
Abstract

Plant biomass is an ideal alternative source to address the increasing demand for oil-derived chemicals. Lignin constitutes *ca* 35% of dry woody biomass and is produced as a non-commercial waste by-product from the Kraft Pulping industry. The polyphenolic chemical structures of lignin are built largely from guaiacolpropane sub-units units linked through C-C and ether C-O bonds, which resist degradation of the woody biomass. Guaiacol represents around 40% of the phenolic monomers within digested lignin. We have investigated processes that might be commercially viable for the hydrodeoxygenation of poly-oxygenated aromatic compounds including guaiacol and vanillin, which could come from digested lignin. The use of mild, low energy conditions have been achieved efficiently using phenolic activation with cyanuric chloride; the subsequent hydrogenolysis reactions have been developed into a flow process that gives selective and high yielding formation of aromatic fine chemicals such as anisole, *meta*-methoxybenzyl alcohol and benzoic acid.

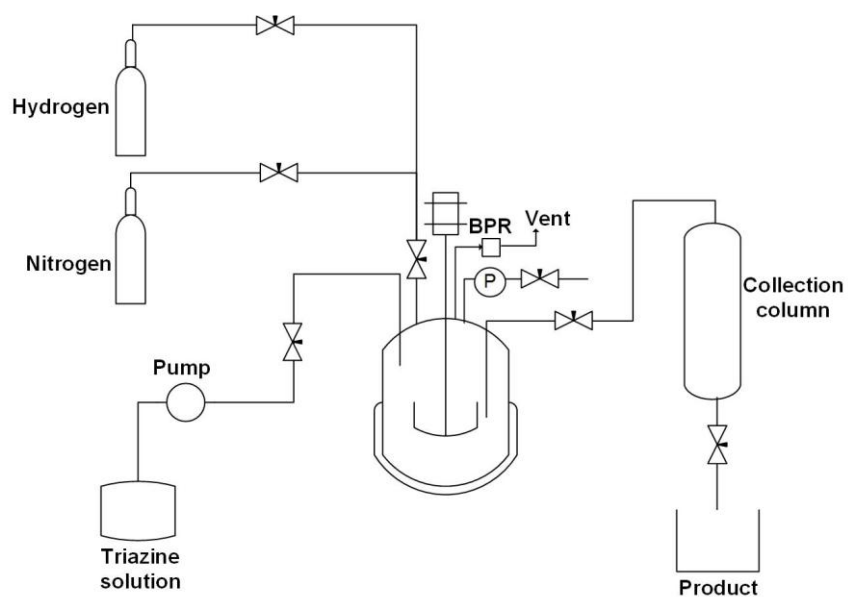


* The prices are estimated bulk raw material costs

Cyanuric chloride is a potentially cheaper and/or recyclable reagent for the activation/hydrogenolysis of lignin monomer compounds.



A viable flow hydrogenolysis process has been developed for tri-substituted triazine compounds using a cascade continuous stirred tank reactor.



Contents

Acknowledgement	ii
Abstract	iii
Contents	v
List of Figures	iii
List of Tables	vii
Abbreviations	ix
Chapter 1 Introduction to Lignin	1
1.1 Introduction	1
1.2 Basics of lignin and state of the art	8
1.2.1 Lignin in wood and its structure.....	8
1.2.2 Industry lignin production	12
1.3 Degradation of lignin	17
1.3.1 Biocatalytic degradation of Lignin.....	17
1.3.2 Chemical Degradation of Lignin.....	19
1.4 Applications of lignin	22
1.4.1 Energy supply.....	23
1.4.2 Macromolecules of lignin.....	23
1.4.3 Aromatic chemicals from depolymerised lignin	23
1.5 Objectives and outlines	25
1.6 References	29
Chapter 2 Introduction to upgrading pyrolysis bio-oil to produce lignin derived aromatics and cycloalkanes	32
2.1 Transition metal sulfide (TMS) catalysts	35
2.2 Noble metal catalysts	39
2.3 Non noble metal catalysts	42

2.4 Deactivation of catalysts	45
2.5 Activation of aryl C-O bonds	46
2.6 References	48
Chapter 3 Results and Discussion for Activation of C_{arom}-O bonds in Lignin Model Compounds.....	52
3.1 Metal guaiacolate	52
3.1.1 Calcium and iron guaiacolate	52
3.1.2 Sodium and potassium guaiacolate	55
3.2 Activation of phenols <i>via</i> sulfite and sulfate compounds.....	56
3.2.1 Synthesis of guaiacol sulfite and sulfate	56
3.2.2 Hydrodeoxygenation of guaiacol sulfite	58
3.3 Activation of phenols by sulfonate esters	59
3.3.1 Synthesis of triflates, tosylates, and mesylates.....	59
3.3.2 Hydrogenolysis of triflate, tosylate and mesylate	60
3.4 Conclusions	64
3.5 References	66
Chapter 4 Removing phenolic hydroxyl groups with strong electron-withdrawing groups	67
4.1 Synthesis and hydrogenolysis of tetrazoles	67
4.1.1 Synthesis of 5-(2-methoxy-phenoxy)-1-phenyl-1 <i>H</i> -tetrazole	68
4.1.2 Catalytic hydrogenolysis of 5-(2-methoxy-phenoxy)-1-phenyl-1 <i>H</i> -tetrazole	70
4.2 Synthesis of tri-substituted triazines from lignin monomer compounds	73
4.2.1 Synthesis of guaiacolate-cyanurate complex (1,3,5-triazines)	73
4.2.2 Synthesis of trisubstituted-1,3,5-triazines by lignin monomers	76
4.2.3 Reaction mechanism	77
4.3 Mixed phenol addition – “the lignin soup model”	79
4.4 Conclusions	80

4.5 References	81
Chapter 5 Hydrogenolysis of lignin monomer compounds	83
5.1 Hydrogenolysis of 2,4,6-tris(aryloxy)-1,3,5-triazine derivatives in batch	83
5.1.1 Transfer hydrogenolysis	83
5.1.2 Catalytic hydrogenation using hydrogen gas	85
5.1.3 Reaction kinetic study of hydrogenolysis of tetrazine compound in a batch reactor	91
5.2 Process development for the hydrogenolysis of trisubstituted triazines in a continuous stirred-tank reactor	93
5.2.1 Optimisation of flow hydrogenolysis with CSTR	93
5.2.2 Characterisation of Pd/C catalyst	98
5.3 Economic evaluation	100
5.3.1 Comparison of batch and CSTR productivity	100
5.3.2 Process cost estimation.....	101
5.4 Conclusions	103
5.5 References	104
Chapter 6 Conclusion and future work	105
Chapter 7 Experimental	108
7.1 General Procedures.....	108
7.2 Synthesis of metal guaiacولات	113
7.2.1 Synthesis of sodium guaiacolate	113
7.2.2 Synthesis of potassium guaiacolate	114
7.3 Synthesis of diguaiacol sulfite and sulfate	115
7.3.1 Synthesis of diguaiacol sulfite.....	115
7.3.2 Synthesis of diguaiacol sulfate	116
7.4 Synthesis of aryl sulfonates	118
7.4.1 General procedure for synthesis of aryl triflates	118
7.4.2 General procedure for synthesis of aryl tosylates	121

7.4.3 General procedure for synthesis of mesylate	124
7.5 Synthesis of tetrazoles	127
7. 6 Synthesis of 2,4,6-<i>tris</i>(aryloxy)-1,3,5-triazine derivatives.....	128
7.7 Hydrogenolysis of lignin monomer compounds	141
7.7.1 H ₂ gas hydrogenolysis in batch	141
7.7.2 Hydrogenolysis of 2, 4, 6- <i>tris</i> (aryloxy)-1, 3, 5-triazines.....	142
7.7.3 Hydrogenolysis using a hydrogen transfer reagent in batch	144
7.7.4 Hydrogenolysis using Continuous Stirred Tank Reactor (CSTR).....	145
7.6 Reference.....	146
Appendix.....	148

List of Figures

Figure 1.1 World energy consumption by different sources.....	1
Figure 1.2 Petroleum consumption by end-use sector in 2010.....	2
Figure 1.3 The fully integrated agro-biofuel-biomaterial-biopower cycle for sustainable technologies.....	4
Figure 1.4 Structure of woody biomass components.....	5
Figure 1.5 Lignin degradation pathways.....	6
Figure 1.6 Bioethanol production from biomass.....	7
Figure 1.7 Levulinic acid from hydrolysis of cellulose	8
Figure 1.8 Dominant substructure of lignin	9
Figure 1.9 Three basic phenylpropane structures of lignin.....	9
Figure 1.10 Kraft pulping process.....	13
Figure 1.11 α -aryl ether bonds cleavage in free phenolic unit.....	14
Figure 1.12 Sulfidolytic cleavage of β -aryl ether bonds in phenolic arylpropane units and conversion into enol-ether units	15
Figure 1.13 Alkaline cleavage of β -aryl ether bonds in nonphenolic arylpropane units	16
Figure 1.14 Biocatalytic degradation of lignin	18
Figure 1.15 Bubbling fluid bed reactor for pyrolysis.....	20
Figure 1.16 Phenolic monomers produced from pyrolysis of lignin	21
Figure 1.17 Hydrodeoxygenation of lignin model compound.....	22
Figure 1.18 Applications of lignin	22
Figure 1.19 Utilization of lignin.....	23
Figure 1.20 Chemicals derived from BTX	24

Figure 1.21 The catalyzed HDO of guaiacol	27
Figure 1.22 Activation routes for the hydroxyl groups in lignin monomer compounds	28
Figure 2.1 Reactions for upgrading lignin-derived compounds.....	32
Figure 2.2 Reaction pathway of guaiacol (Solid black arrows represent MT reaction, dash green, blue and black arrows represent HDO, DDO and HYD processes respectively). Drawing modified from reference 6.	34
Figure 2.3 Degradation pathways of phenol on TMS catalyts	35
Figure 2.4 (a) mechanism of HDO of 2-ethylphenol with a CoMoS/Al ₂ O ₃ catalyst (b) mechanism of DDO of 2-ethylphenol with a CoMoS/Al ₂ O ₃ catalyst	36
Figure 2.5 Yields of HDO of pyrolysis oil (250 °C, 100 bar, 4 h) by different noble metal catalyts. Data from ref. 13	40
Figure 2.6 The main products of guaiacol HDO over nickel catalyts at 320 °C and 170 bar H ₂ for 1 hour.....	44
Figure 2.7 Mechanism of Fe/SiO ₂ catalysed HDO of guaiacol.....	44
Figure 2.8 Pyrolysis of softwood kraft lignin over zeolite	45
Figure 2.9 Pathway for degradation of aryl toluenesulfonate	48
Figure 3.1 IR of calcium guaiacol half salt	54
Figure 3.2 Leaving groups for the activation of phenolic hydroxyl group	57
Figure 3.3 Product selectivity of vanillin triflate hydrogenolysis.....	62
Figure 3.4 Hydrogenolysis of benzaldehyde.....	63
Figure 4.1 Molecular modelling of guaiacol and 5-(2-methoxy-phenoxy)-1-phenyl-1H-tetrazole	69
Figure 4.2 X-ray structure of 5-(2-methoxy-phenoxy)-1-phenyl-1H-tetrazole	70
Figure 4.3 Molecular modeling of 2,4,6- <i>tris</i> (2-methoxyphenoxy)-1,3,5-triazine	75
Figure 4.4 X-ray structure of 2,4,6- <i>tris</i> (2-methoxyphenoxy)-1,3,5-triazine.....	75

Figure 5.1 Hydrogen donors for the transfer hydrogenolysis of 2,4,6- <i>tris</i> (2-methoxyphenoxy)-1,3,5-triazine	84
Figure 5.2 Possible mechanism of hydrazine reaction with TMPT to produce guaiacol	85
Figure 5.3 Hydrogenolysis of 2,4,6- <i>tris</i> (2-methoxyphenoxy)-1,3,5-triazine over 10 wt% Pt/C and 10 wt% Ru/C.....	87
Figure 5.4 IR of (a) recovered CYA after hydrogenolysis; (b) commercial CYA 98%, Aldrich.....	90
Figure 5.5 Decomposition of cyanuric acid	90
Figure 5.6 Hydrogenolysis of 5.1.1 at different concentrations in EtOAc	91
Figure 5.7 Temperature effect of the hydrogenolysis reaction	92
Figure 5.8 Line diagram of the CSTR set-up used in the catalytic hydrogenolysis.....	93
Figure 5.9 Yield of anisole produced by catalytic hydrogenolysis in a continuous flow CSTR (method A) at different flow rates.....	94
Figure 5.10 CSTR hydrogenolysis with flow rate 4 mL/min over 10 bar H ₂ at 50 °C with 30 mL reactor volume	95
Figure 5.11 Hydrogen pressure effect on the catalytic hydrogenolysis of 5.1.1 in the CSTR.....	96
Figure 5.12 Reported reduction of anisole to give a mixture of aromatic products	96
Figure 5.13 Selectivity of hydrogenolysis products produced in CSTR (a) 4mL/min, 10 bar; (b) 4 mL/min, 5 bar	97
Figure 5.14 Conversion of CSTR hydrogenolysis with 4mL/min and 8 mL/min flow rate.....	98
Figure 5.15 Hydrogenolysis over Pd/C and recycled Pd/C.....	98
Figure 5.16 (a) 5% Pd/C (Johnson Matthey 87L); (b) Pd/C collected from a CSTR hydrogenolysis over 10 bar H ₂ and flow rate 4 mL/min for 1 hour; (c) Pd/C collected from a CSTR hydrogenolysis with Et ₃ N over 10 bar H ₂ and flow rate 4 mL/min for 1	

hour; (d) One-time recycled Pd/C collected from a CSTR hydrogenolysis over 10 bar H ₂ and flow rate 4 mL/min for 1 hour.	99
Figure 5.17 Particle size distribution of Pd/C catalysts	99
Figure 5.18 Anisole productivity of (a) batch reactor, 1 bar and (b) CSTR system, 5 bar, 4 mL/min.....	101
Figure 7.1 Two-stage cascade pressure CSTR, automated Parr reactors.....	111

List of Tables

Table 1.1 Compounds derived from crude oil	3
Table 1.2 Major components of wood cell walls	5
Table 1.3 Major functional groups in lignin per 100 phenyl propane unites	10
Table 1.4 Different linkages between lignin units	11
Table 1.5 Some aromatic productions from lignin, market size/value and applications ⁴⁸	25
Table 2.1 Bond dissociation energies (BDE).....	33
Table 2.2 Components of pyrolysis oil and its HDO products	33
Table 2.3 Selective conversion (%) of lignin model compounds on sulfated CoMo/Al ₂ O ₃ catalyst at 50 bar of H ₂ and 300 °C for 4 h.....	38
Table 2.4 Recent research into reduction of bio-oil model compounds with noble metal catalysts	41
Table 3.1 Synthesis of aryl sulfonates from lignin monomers.....	60
Table 3.2 Pd/C catalysed hydrogenolysis of aryl sulfonates	61
Table 3.3 Estimated material cost for the hydrogenolysis of guaiacol triflate.....	65
Table 4.1 Bond lengths and bond angles of some 5-aryloxy-1-phenyltetrazole ethers	68
Table 4.2 Reaction conditions for synthesis of tetrazole compound	69
Table 4.3 Solvent effects on the production.....	71
Table 4.4 Transfer hydrogenation of tetrazole with different hydrogen donor and catalysts	72
Table 4.5 pH and temperature influence on the effectiveness of cyanuric chloride reaction.....	74
Table 4.6 Synthesis of trisubstituted-1,3,5-triazines by lignin monomers.....	77

Table 5.1 Catalysts used hydrogenolysis reactions of 2,4,6- <i>tris</i> (2-methoxyphenoxy)-1,3,5-triazine	86
Table 5.2 Hydrogenolysis of 2,4,6- <i>tris</i> (aryloxy)-1,3,5-triazines	88
Table 5.3 TOF of hydrogenolysis of compound 5.1.1	92
Table 5.4 Wt% and Wt ratio of carbon and palladium from catalysts: a. fresh b. after 1 use c. with triethylamine d. second use.....	100
Table 5.5 Raw material cost estimation of anisole production	102
Table 7.1 The GC retention time of commercial standards or pure products	111
Table 7.2 Transfer hydrogenation for the hydrogenolysis of triazine compound.....	144
Table 7.3 Experimental conditions for CSTR hydrogenolysis	145

Abbreviations

°C	Degree Celsius
Å	Angstrom, 0.1 nm
Arom/Ar	Aromatic ring
BCD	Based-catalyzed depolymerisation
BDE	Bond dissociation energy
BTX	Benzene, Toluene, Xylene
CNT	Carbon nanotube
COD	1,5-Cyclooctadiene
CSTR	Continuous stirred-tank reactor
DAO	Dealkoxylation
DDO	Deoxygenation
DIPEA	<i>N,N</i> -diisopropylethylamine
DME	Demethylation
DMO	Demethoxylation
DMSO	Dimethyl sulfoxide
EDS	Energy-dispersive X-ray spectroscopy
Equiv.	Equivalent
EtOAc	Ethyl acetate
GC	Gas chromatography
GC-MS	Gas chromatography–mass spectrometry
h	Hour
H	Hydrogen

HDO	Hydrodeoxygenation
HRMS	High-resolution mass spectrometry
HYD	Hydrogenation
HZSM	Zeolite socony mobil
IR	Infrared
IS	Internal standard
<i>m</i>	Meta
MT	Methyl transfer
MTHF	Methyltetrahydrofuran
MZ	Mesoporous zeolite
NMR	Nuclear magnetic resonance
<i>o</i>	Ortho
OTf	Ethyl trifluoromethanesulfonate
OTs	Ethyl p-toluenesulfonate
<i>p</i>	Para
PET	Polyethylene terephthalate
PF	Phenol formaldehyde
Pr	Propyl
SC	Standard specific compound of interest
SEM	Scanning electron microscopy
^t Bu	Tert-butyl
THF	Tetrahydrofuran
TLC	Thin layer chromatography

TMPT	2,4,6- <i>tris</i> (2-methoxyphenoxy)-1,3,5-triazine
TMS	Transition metal sulphite catalyst
Wt %	Weight percentage

Chapter 1 Introduction to Lignin

1.1 Introduction

World energy sources include fossil fuels, nuclear power and renewable energy. Fossil fuels contribute the majority of energy production to the world energy market. According to BP Energy Outlook 2035, the growth of oil supply will be slower than other fuels; nevertheless, the demand for oil will rise dramatically by over 20% from 90 million barrels per day to 109 million barrels per day by 2035.¹ The price of crude oil is predicted to rise steadily, reaching \$106 per barrel in 2020 and \$163 per barrel in 2040.²

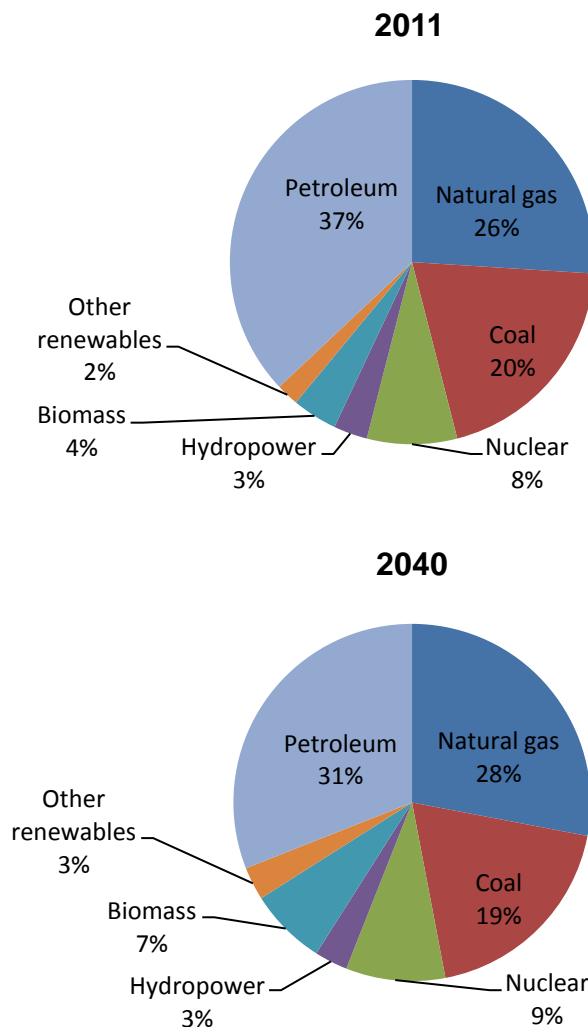


Figure 1.1 World energy consumption by different sources¹

Over fifty percent of the petroleum in the world is used by the transportation sector, whilst the use of petroleum to generate electric power has declined. However, the chemicals industry continues to consume large amounts of petroleum.

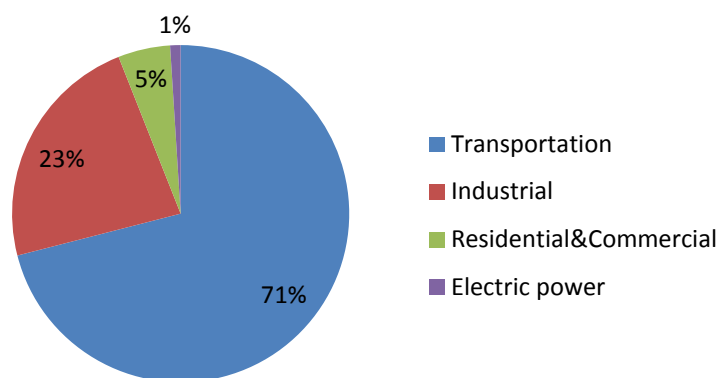


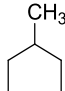
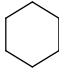
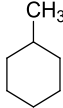
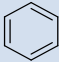
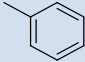
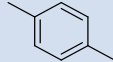
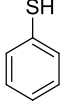
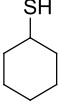
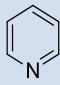
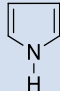
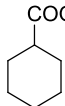
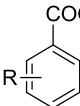
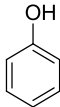
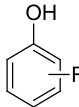
Figure 1.2 Petroleum consumption by end-use sector in 2010

Fossil fuels display a double impact in the chemical industry, as it is a large consumer of energy and non-recoverable fossil products serve as raw materials to be converted into synthetic substances used in our daily life. The manufacture of primary petrochemicals is based on natural gas and crude oils. Furthermore, the expanding production of secondary raw materials is obtained by using different processes to extract them from natural gas and crude oil.

In crude oils there are hydrocarbons mixed with sulfur, nitrogen and oxygen components. However, crude oils are not directly used for chemical production because they are complex mixtures with corrosive impurities. Therefore, crude oils are refined into more useful feedstocks such as liquid gas, petroleum naphtha, jet fuel, gasoline, diesel oil, heavy fuel oil and oil coke. Most paraffins, naphthenes and aromatics are derived from crude oils (Table 1.1).

With continued reliance on fossil fuels, the prices of petrochemicals will keep rising. In addition there are numerous concerns and issues surrounding the use of fossil fuels including: the depletion of fossil fuels, energy security, and the impact of CO₂ emissions on the environment and the increasing price of petroleum. To combat these problems, it is important to develop alternative fuels derived from renewable sources, such as biomass, hydropower, wind and solar energy.

Table 1.1 Compounds derived from crude oil

Crude oil composition	Example compounds		
Alkanes	Methane, Ethane, Propane, Butanes		
Naphthenes	 CH ₃ Methylcyclopentane	 Cyclohexane	 CH ₃ Methylcyclohexane
Aromatics	 Benzene	 Toluene	 p-Xylene
Sulfur compounds	CH ₃ SH Methyl mercaptan	 SH Thiophenol	 SH Cyclohexylthiol
Nitrogen compounds	 Pyridine	 Pyrrole	
Oxygen compounds	CH ₃ (CH ₂) _n COOH Carboxylic acid	 COOH Cyclohexane carboxylic acid	 COOH R Aromatic acids
	 OH Phenol	 OH R Cresylic acid	

Produced by all naturally-occurring energy sources, biomass is a major non-fossil organic source which provides an abundant carbon resource to reduce the dependence on petrochemicals.

Biomass is produced with sunlight and nutrients via photosynthesis and consumes atmospheric carbon dioxide whilst it grows (Figure 1.3). Biomass is an important renewable feedstock to provide fuels, chemicals or heat energy.

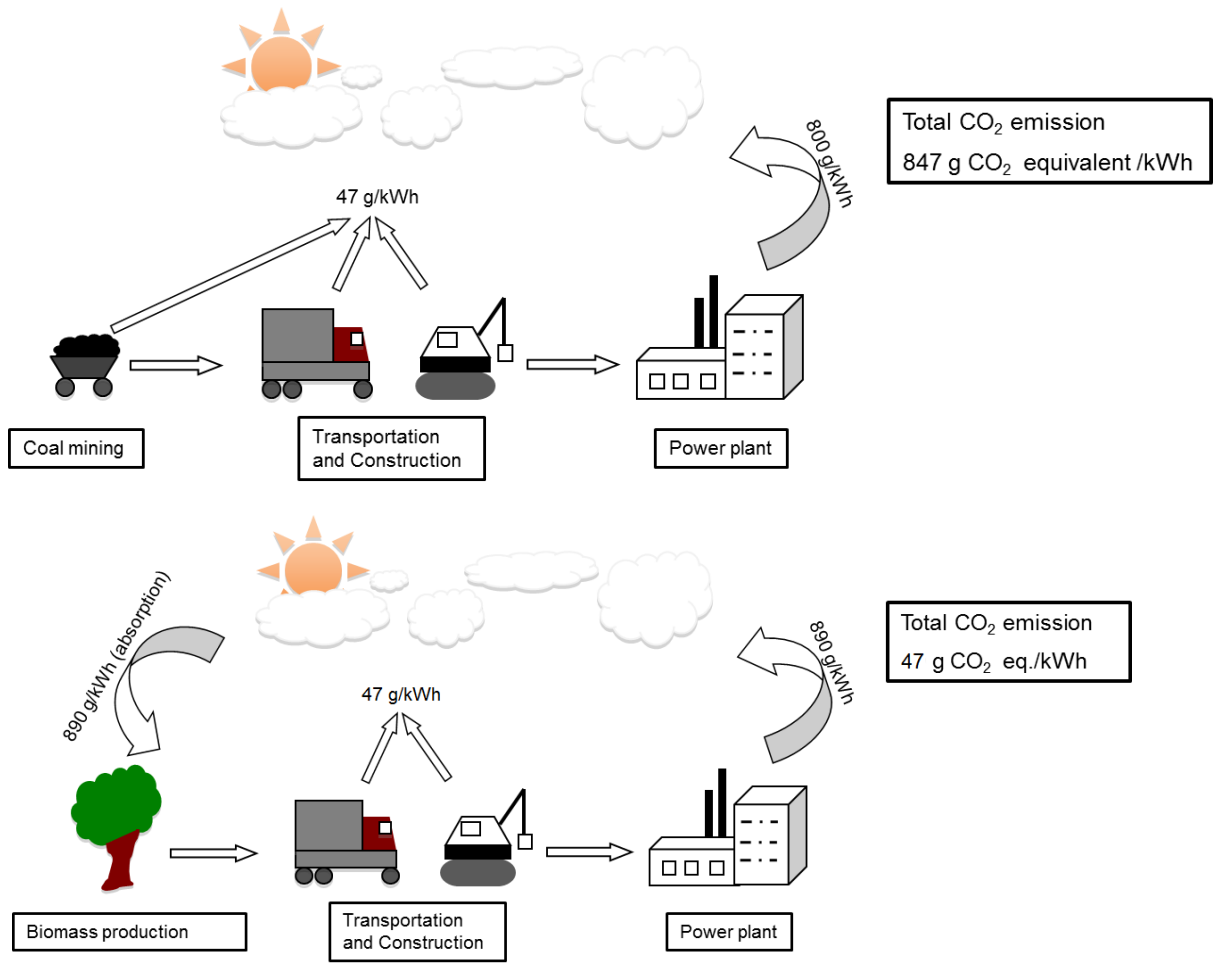


Figure 1.3 The fully integrated agro-biofuel-biomaterial-biopower cycle for sustainable technologies³

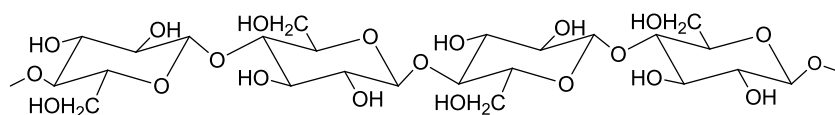
For the biorefinery process, diverse raw materials are supplied. These range from corn, sugar cane or wood to other agriculture materials. The production of the first generation of biofuels are taken directly from food sources, these include vegetable oils, crops and trees. First generation biofuels encourage improving fuel security and support for agricultural industries.

Technology for first generation biofuels is commercially developed, which produces large quantities of biodiesel, ethanol and biogas. However, there are some significant drawbacks to the first generation biofuels. The use of food sources contributes to higher food prices. Additionally, the usage of the land can accelerate deforestation and thus adversely affect biodiversity. To avoid competing with food production, second generation biofuels were developed as more sustainable alternatives. These biomass fuels use the waste of biomass from food crops and from physical (sawdust), chemical (black liquor from pulping process) and biological (manure from animals) processes.

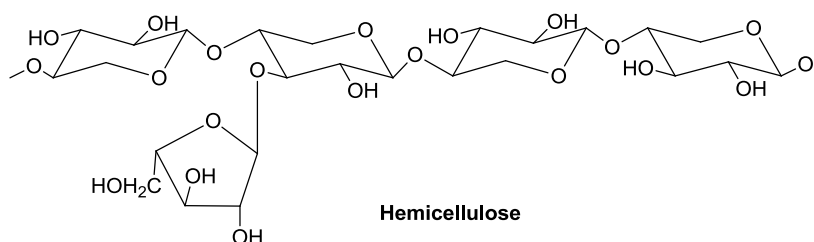
High molecular weight woody biomass is composed of three components: cellulose, containing hexoses; hemicelluloses, containing a mixture of hexoses and pentoses; lignin, composed of aromatic rings with carbon-carbon bonds and carbon-oxygen-carbon bonds (Figure 1.4).⁴

Table 1.2 Major components of wood cell walls

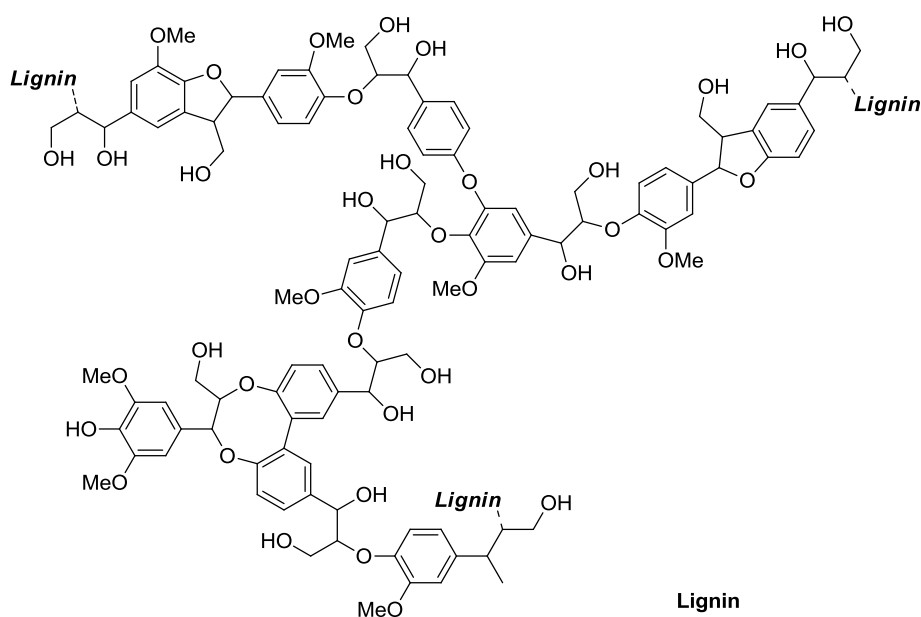
Components	Softwood %	Hardwood %
Cellulose	42–44	43–47
Hemicellulose	25–30	20–43
Lignin	25–30	17–26



Cellulose
1.1.1



Hemicellulose
1.1.2



Lignin
1.1.3

Figure 1.4 Structure of woody biomass components

Separating the raw materials provides three building blocks: carbohydrates, aromatics and hydrocarbons. These are in the form of cellulose and hemicelluloses, lignin and triglycerides respectively.⁵ To date, many pathways can convert lignin-cellulosic biomass into industry value added chemicals, e.g. alcohol and acid products derived from the fermentation of cellulose and hemicelluloses; carbohydrates derived from hydrolysis, using a hydrogenation or oxidation process; breaking down biomass into fragment chemicals via pyrolysis; or into a synthesis gas by means of gasification (Figure 1.5).^{6,7}

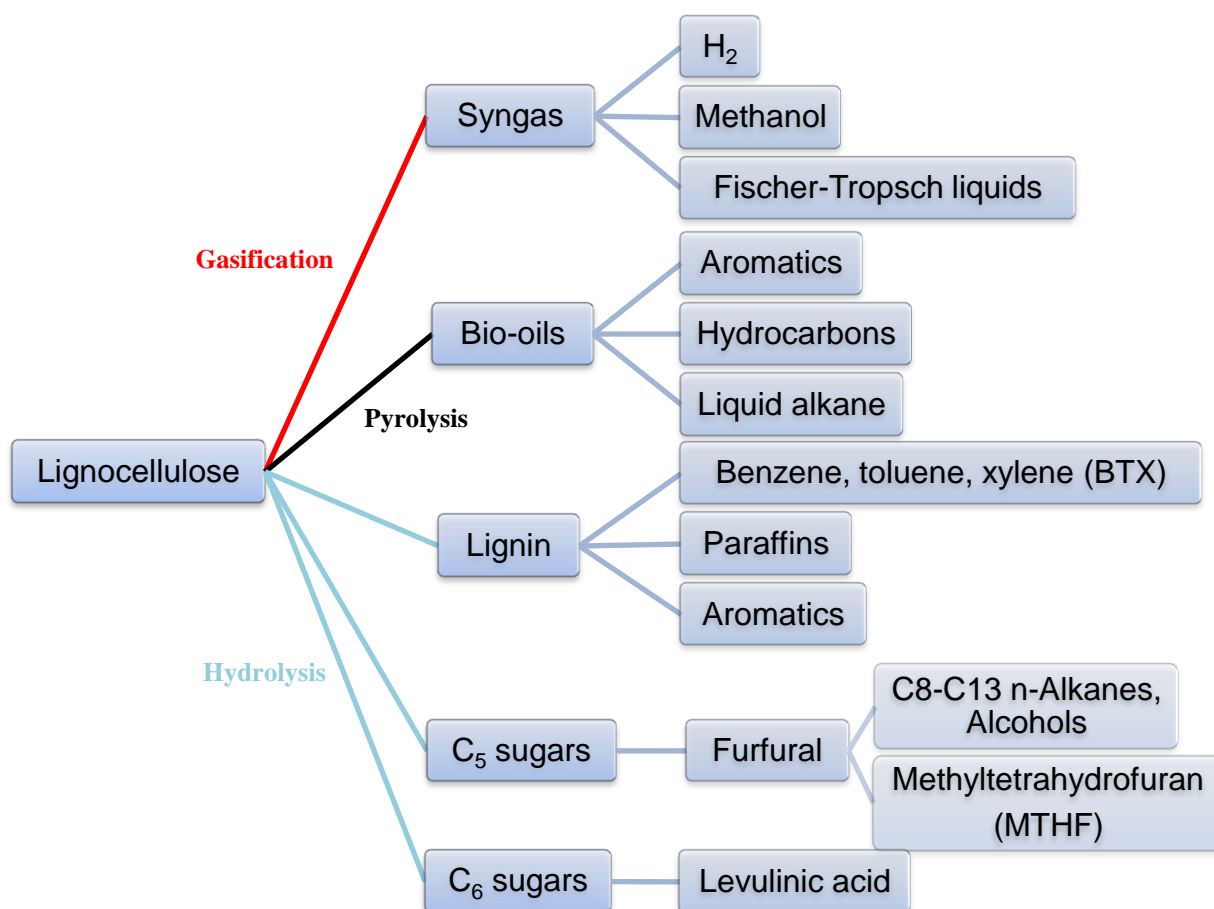


Figure 1.5 Lignin degradation pathways^{6,7}

Bioethanol

Bioethanol is a renewable biofuel whose production has increased dramatically from 6.2 billion litres to 50 billion litres in a decade (2000–2010) in the United States.⁸ The production of ethanol at low cost is the key to making it into a competitive additive for gasoline. Most bioethanol is manufactured using first generation biofuel production techniques, generated from fermentation of sugars in corn. However, the cost of the corn feedstock limits the price and supply of ethanol. Replacing corn starch with cellulose from other renewable sources will greatly reduce the cost of ethanol

production due to plentiful raw materials, such as wood, straw, agriculture waste or industry waste. Ethanol is produced by converting cellulose into sugar via enzyme hydrolysis, followed by fermentation (Figure 1.6). Currently, the lack of commercial use of cellulosic ethanol is due to the cost of cellulose enzymes. However, with more research into cellulosic ethanol, the price of these enzymes could be reduced to a level that would make it commercially viable.

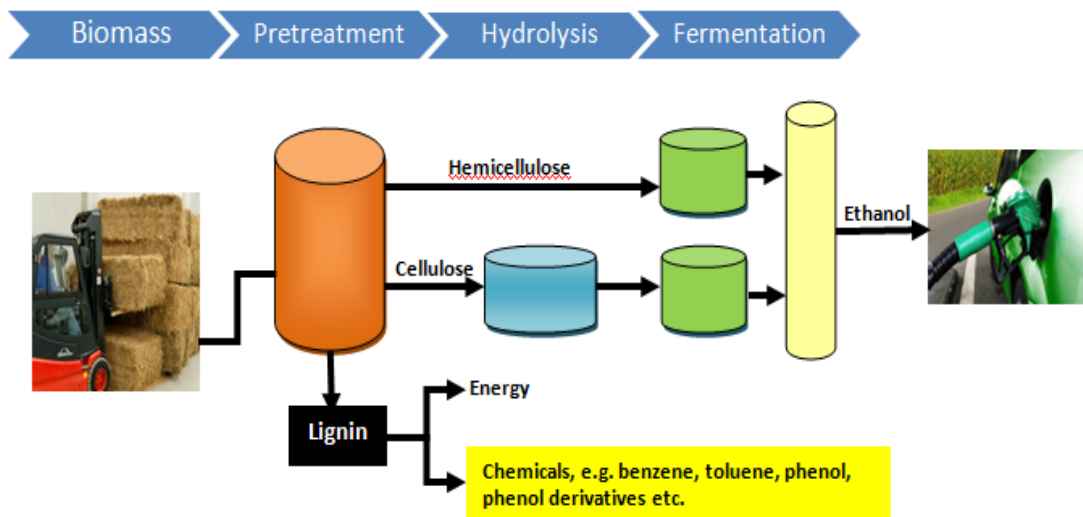


Figure 1.6 Bioethanol production from biomass

Levulinic acid

Levulinic acid is the acid-catalyzed hydrolysis product from cellulose or six carbon sugars (Figure 1.7).⁹

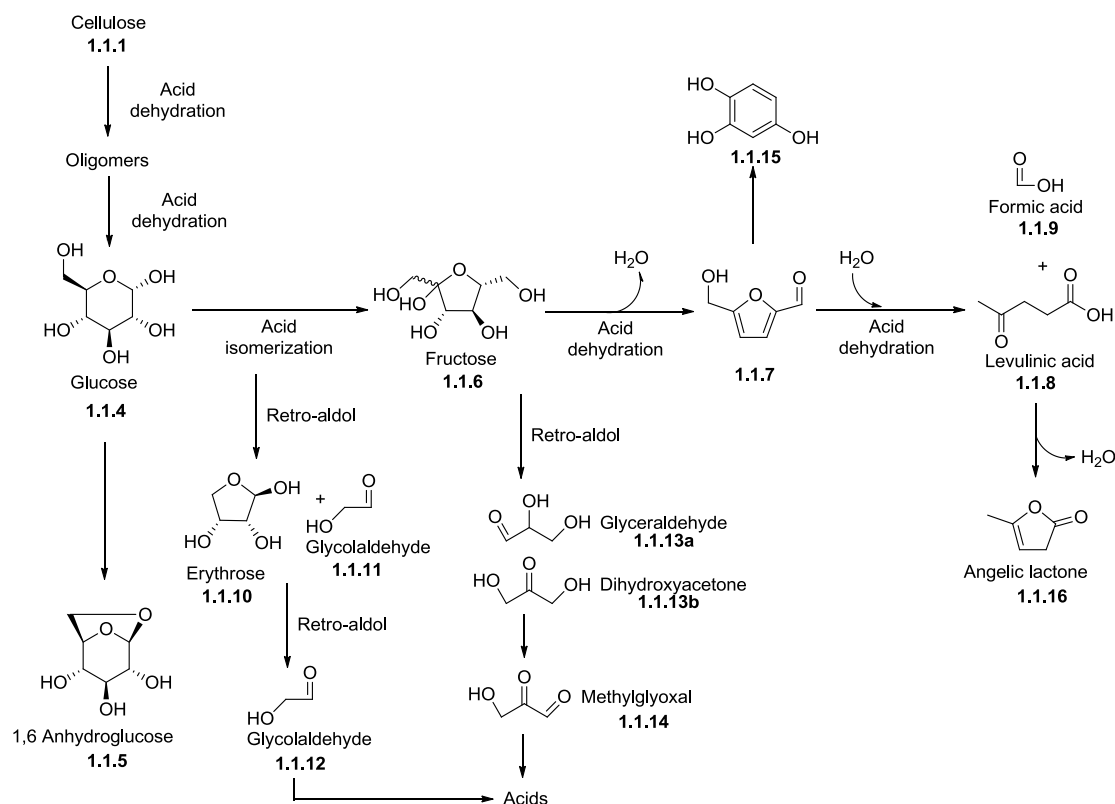


Figure 1.7 Levulinic acid from hydrolysis of cellulose⁹

It is a valuable building block that is used as a starting material for many compounds.^{7a} Levulinic esters and methyltetrahydrofuran are biodiesel and gasoline additives respectively.

1.2 Basics of lignin and state of the art

1.2.1 Lignin in wood and its structure

Lignin is derived from a *Latin* word, lignum, meaning wood. Lignin is one of the major components of plant cell walls and it plays an important role for plant survival. As a building material in woody tissues, lignin compresses wood fibres together by its mechanical resistance. On the other hand, lignin also prevents biological degradation by stopping microbial penetration. In softwoods and hardwoods, lignin content ranges between 24–33% and 19–35% respectively.¹⁰ It is also found in smaller amounts in non-wood crops (<3%) and grasses (from 15–25%).¹¹

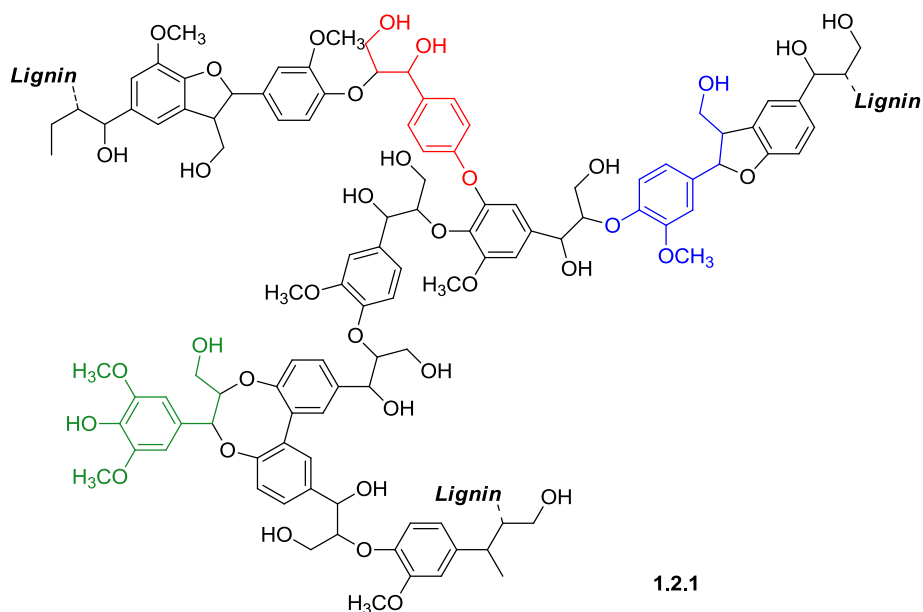


Figure 1.8 Dominant substructure of lignin. The structure of red is hydroxyphenyl/coumaryl unit, the structure of blue is guaiacyl/coniferyl unit and the structure of green is syringyl unit

The polyphenolic chemical structures of lignin are built from three dimensional guaiacolpropane linking with C-C bonds and ether C-O bonds¹², which resist the degradation of woody biomass. The extraction of lignin fragments showed that demethylation or demethoxylation of the structure helps repair the cell wall itself. So the exact lignin structure is not well defined, but the dominant substructure of lignin is presented (Figure 1.8).

Lignin can be regarded as arising from coupling of three basic phenylpropane units, syringyl-(S), guaiacyl/coniferyl-(G) and *p*-hydroxyphenyl/coumaryl-(H). The variety of lignin structure observed is due to the different monomer species and their composition. For example, in softwood, lignin is composed mainly of coniferyl monolignol (95%), whilst coumaryl alcohol is the typical unit found in grasses.

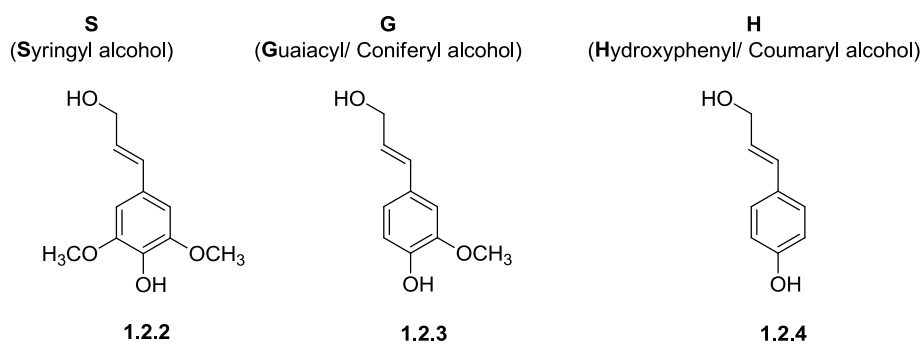


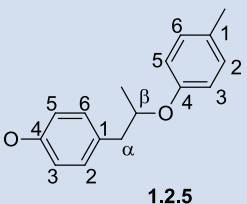
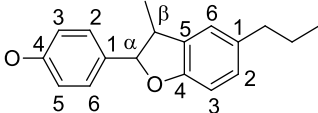
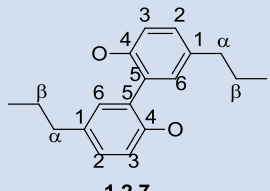
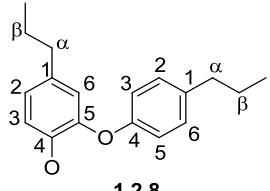
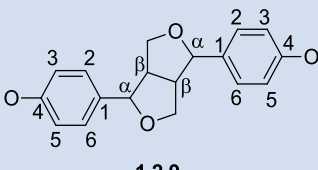
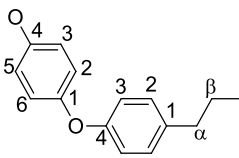
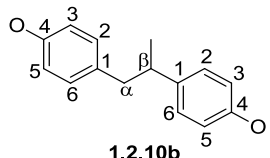
Figure 1.9 Three basic phenylpropane structures of lignin.

The natural degradation of lignin is caused by a variety of enzymes and sunlight, but this is a slow process because of its complex and resilient structure.¹³ The majority of the functional groups in lignin are aromatic, aliphatic hydroxyl groups and carboxyl groups (Table 1.3). The β -O-4 linkages are dominant to the C-O-C ether bonds between its units (Table 1.4).

Table 1.3 Major functional groups in lignin per 100 phenyl propane unites¹³

Functional group	Abundance per 100 C9 units
Benzyl alcohol	15-20
Phenolic hydroxyl (free)	15-30
Methoxyl	92-96
Carbonyl	10-15

Table 1.4 Different linkages between lignin units^{3a}

Type	Structure	Softwood %	Hardwood %
β -O-4	 <p>1.2.5</p>	40-50	50-60
β -5	 <p>1.2.6</p>	10-12	3
5-5	 <p>1.2.7</p>	13	3
4-O-5	 <p>1.2.8</p>	3	3
β - β	 <p>1.2.9</p>	3	3
Bonds to 1-position	 <p>1.2.10a</p>	1-3	3
	 <p>1.2.10b</p>		

1.2.2 Industry lignin production

1.2.2.1 Industrial lignins

A large amount of technical lignins from lignosulfonates and Kraft lignin are considered as potential raw materials, while soda lignin, organosolve lignin, ionic liquid lignin and hydrolysis lignin are only produced small amounts in industry and there is not much conventional industrial availability.

Lignosulfonates are water-soluble anionic polyelectrolytes generated from sulfite pulping process. The cleavage of α -carbon ether bonds occurs followed by sulfonation on the side chain. Important utilizations of lignosulfonates are stabilizing concrete, applying on the road surface to control dust and dispersing insoluble materials into water.¹⁴

1.2.2.2 Kraft pulping processes

The chemical pulping process contributed 80 percent of world pulp production in 2013.¹⁵ It is a process separating cellulose by breaking down lignin (delignification) and hemicellulose into small water-soluble molecules or fragments.

The Kraft (or sulfate) pulping process is the most common chemical pulping process due to its shorter processing time and stronger pulps compared to other processes. This is because in the other pulping processes, either lignin is left with fibres or cellulose is degraded.¹⁶ Kraft pulping removes most of the lignin in the wood. This results in a reduction of the hydrophobic effect caused by hydrogen bonding between lignin and cellulose or hemicelluloses in the fibres (Figure 1.9). During Kraft pulping, delignification takes place by two different cleavages of the lignin polymer that increase its solubility in water. One pathway involves the breakdown of interunit linkages of lignin into smaller molecules. The other increases the hydrophilicity of lignin fragments by the cleavage of phenylpropane units forming phenolic hydroxyl groups.

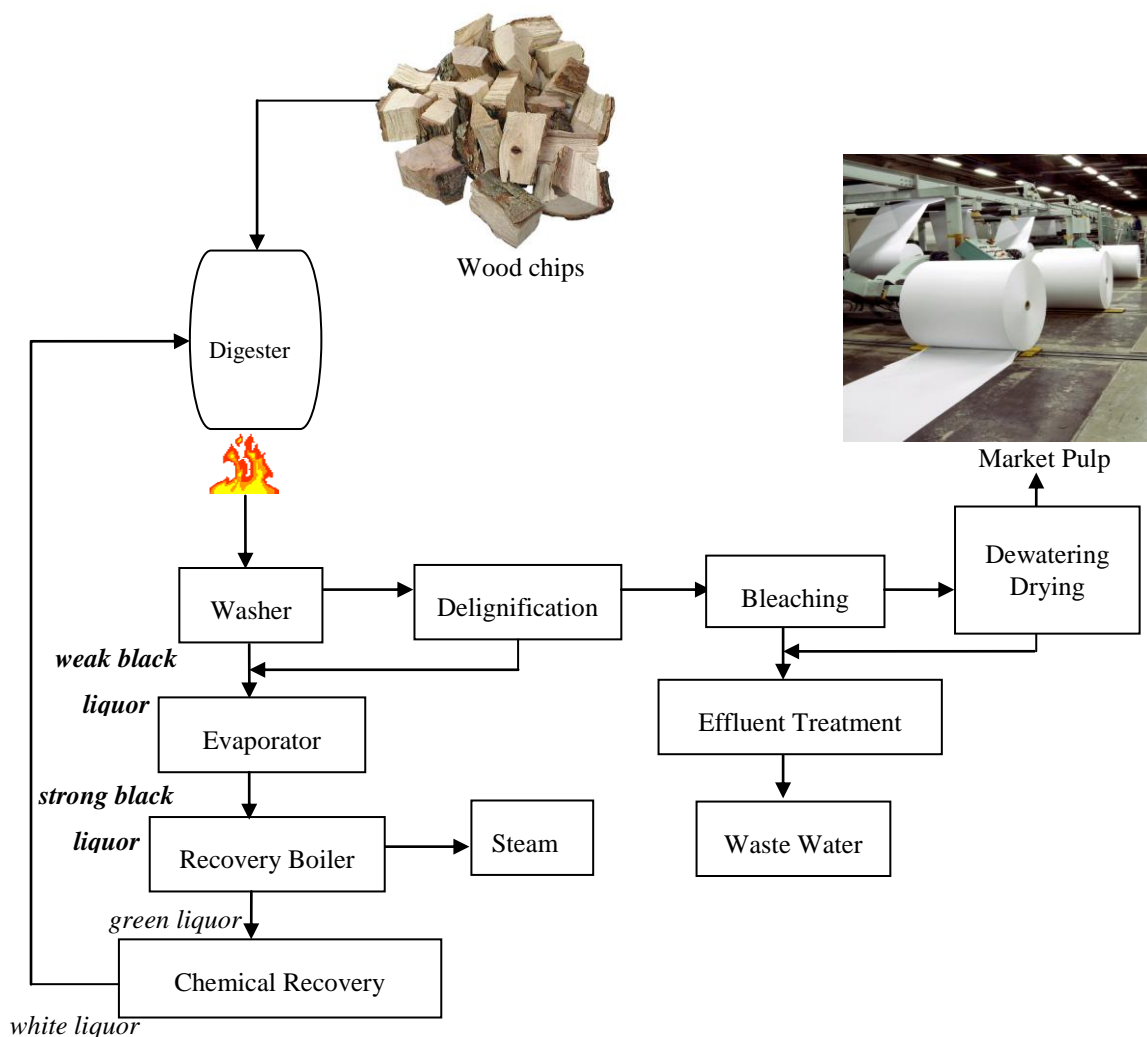


Figure 1.10 Kraft pulping process¹⁷

In a digester, lignin from wood chips is dissolved in a sodium hydroxide or sodium sulfide solution (known as white liquor) and selectively cleaved at high temperature (about 170°C) resulting in black liquor. Delignification occurs during this treatment, caused by lignin reacting with hydroxyl and hydrosulfide ions to generate smaller water soluble fragments. At the end, the pulp is separated from the wood waste by washing and then bleached to whiten fibres to form into paper (Figure 1.10).¹⁷

In Kraft pulping chemistry, the basic reactions of lignin can be divided into two categories: degradation and condensation. The degradation reaction is favoured because lignin fragments are formed, whilst in the condensation reactions, the lignin molecular size is increased by forming alkali-labile linkages. In the degradation stage, various fragments are obtained by cleavage of the α -aryl ether bonds present in the lignin polymer using a solution of sodium hydroxide and sodium sulfide. When these bonds are broken, free phenolic groups are generated which increases the hydrophilicity of lignin and its fragments in the aqueous solution. In the residual lignin

from Kraft pulping, there are 27 phenolic hydroxyl groups/100 C-9 units which affect the activity of Kraft lignin because they activate the *ortho*-position of the aromatic ring and form quinone methide intermediates.¹⁸

In the α -aryl ether linkage **1.2.11**, the phenolate unit is converted to quinone methide **1.2.12** by elimination of an α -aryloxy group **1.2.13** (Figure 1.11).¹⁸

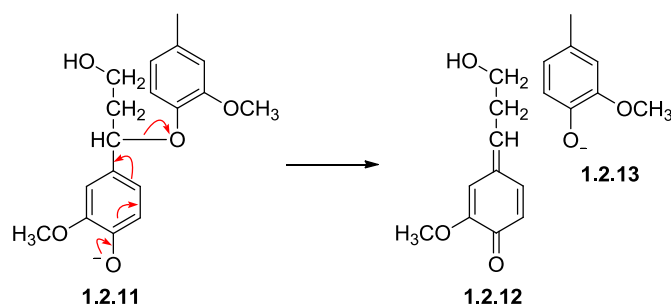


Figure 1.11 α -aryl ether bonds cleavage in free phenolic unit

β -Aryl ether bonds are the main type of linkage in lignin and their cleavage in Kraft pulping is important for lignin depolymerisation and fragmentation. In the β -aryl ether linkage **1.2.14**, the quinone methides **1.2.15** are formed when a good leaving group is present at the α -position. In Kraft pulping, nucleophilic addition of the hydrosulfide ion to compound **1.2.15** re-establishes the aromatic ring and gives a benzyl mercaptide intermediate **1.2.17**. The resulting mercaptide anion undergoes a nucleophilic substitution reaction at the β -carbon in **1.2.17** to give compound **1.2.18** and the β -aryloxy group **1.2.19**. The intermediate structure will lose sulfur to form a coniferyl alcohol (Figure 1.12).¹⁸ The cleavages of α -aryl ether linkage and β -aryl ether linkage occur in the initial degradation of lignin, and the phenolic groups will be broken down until there are no α -aryl or β -aryl ether bonds.

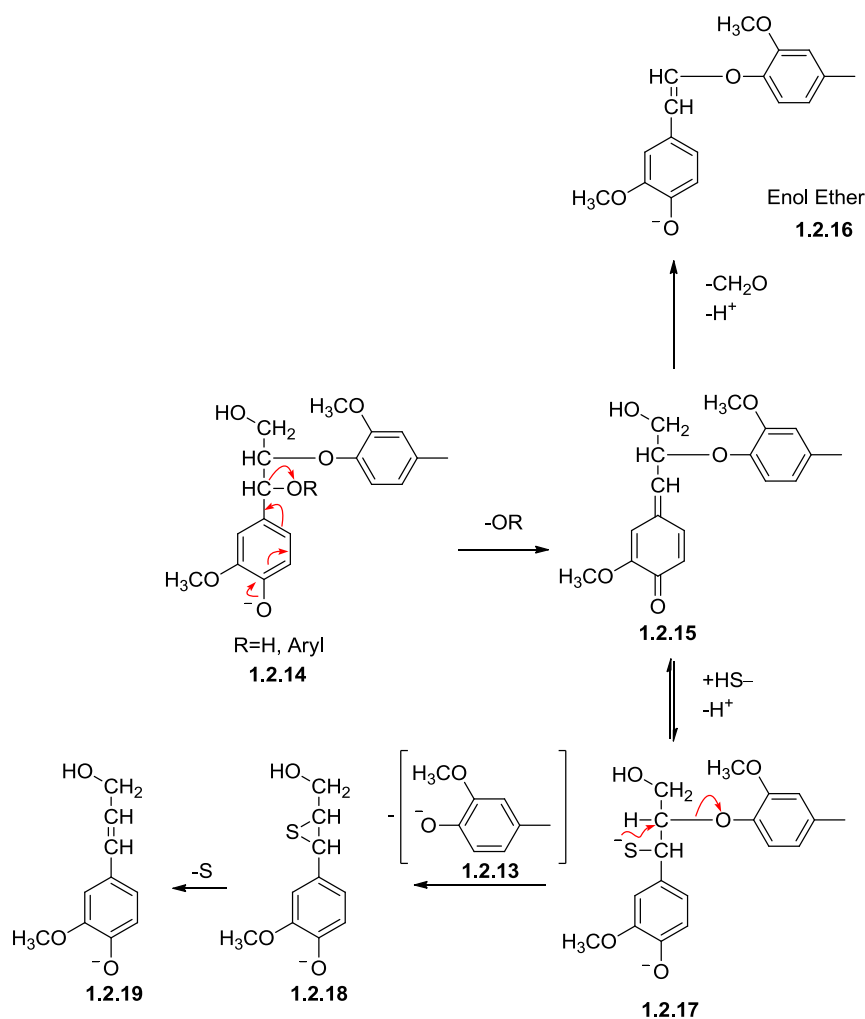


Figure 1.12 Sulfidolytic cleavage of β -aryl ether bonds in phenolic arylpropane units and conversion into enol-ether units

Meanwhile, the enol ether **1.2.16** can be formed by eliminating the hydroxymethyl group from the quinone methide intermediate **1.2.15**. Similarly, in the case of non-phenolic subunits present in lignin **1.2.20**, the deprotonated α -hydroxyl group can undergo a nucleophilic substitution reaction at the β -carbon to generate an intermediate epoxide **1.2.21**, resulting in elimination of a β -aryloxy substituent. Hydroxide or hydrosulfide anions in the white liquor act as nucleophiles, breaking the epoxide ring to produce diols **1.2.22** or thioglycols (Figure 1.13).¹⁸

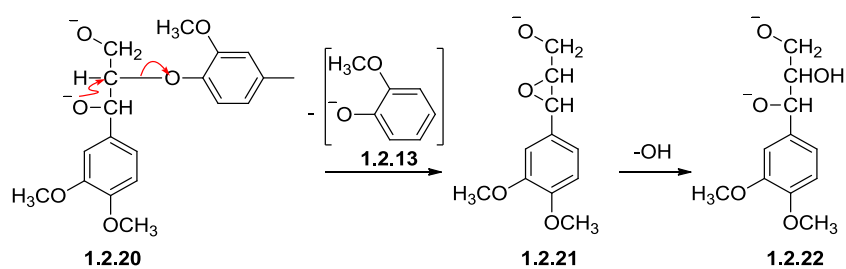


Figure 1.13 Alkaline cleavage of β -aryl ether bonds in nonphenolic arylpropane units

1.2.2.3 The challenge of lignin utilisation

Several properties of technical lignins restrict their applications in high added value chemicals. Impurities such as sulfur, ash or carbohydrates are extracted from the delignification process, so it is necessary to purify technical lignins before using them in either chemical or biochemical processes. Although there are many methods that have been used for purification of technical lignins, most of them are not economical processes and impurities that are chemically bonded with lignin cannot be removed completely. The other limitation is the complex reactivity of technical lignins due to various structures of different sizes, linkage type, functional groups and polymer and monomer composition. One way to reduce this restriction is to depolymerize lignin into oligomers or monomers.¹⁹

The Kraft pulping process is a low yield process; only 45% of wood can be used to produce pulp and major amounts of black liquor (Kraft lignin solution) are combusted.²⁰ In addition, with the increasing demand of the pulping industry, expanding the capacity of recovery boilers is a bottleneck in production, because the calorific load limits them and redesigning recovery boilers is very expensive. An estimated amount of lignin produced by the pulping and papermaking industries is about 70 million tons annually; in spite of this, only 1–2 per cent of lignin is extracted from pulp mills and used for further products or applications.^{21 22} Therefore separating the Kraft lignin by acidifying the black liquor to precipitate lignin sodium salt becomes an economic and convenient way to satisfy the high calorific load of the recovery boilers. Currently, only a few companies have developed Kraft lignin from black liquor and applied it towards the manufacture of commercial products, e.g. MeadWestvaco in the US is the only supplier worldwide for Kraft lignin and its derivatives.

1.3 Degradation of lignin

1.3.1 Biocatalytic degradation of lignin

The different cleavage pathways in lignin result from the different stabilities of the linkage bonds. The ester and ether bonds are the most easily broken bonds in lignin. Lignin can be metabolised by a microbial pathway.²³ Under aerobic conditions, the degradation of lignin was found to be associated with a variety of bacteria and fungi, especially white-rot fungi.²⁴ Lignin peroxidases (e.g. *P. putida mt-2* and *R. jostii RHA1*) and manganese peroxidases (e.g. *Dichomitus squalens*),²⁵ have high activities on depolymerisation of lignin and metabolise low molecular weight aromatic chemicals.²⁶ As shown in Figure 1.14, laccases or peroxidases act as an oxidizer for polymeric lignin. The produced lignin fragments are involved in different reactions, including hydrolysis of C₄-ether bonds, demethoxylation, aromatic ring opening and C_α-C_β break down. The aromatic aldehydes are generated and reduced to alcohols and quinines, followed by a redox cycle reaction via aryl alcohol oxidase and laccase respectively.²⁷ Hydrogen peroxide (H₂O₂) is created by the regeneration of aldehydes via arylalcohol dehydrogenases, and followed by Fenton's reaction ($\text{Fe}^{2+} + \text{H}_2\text{O}_2 \rightarrow \text{Fe}^{3+} + \text{OH}^\cdot + \text{OH}^-$) producing a hydroxyl radical (OH[·]), which is a strong oxidizer and attacks lignin at the initial wood degradation stage when the small pores prevent ligninolytic enzymes penetrating plant cell walls.²⁸

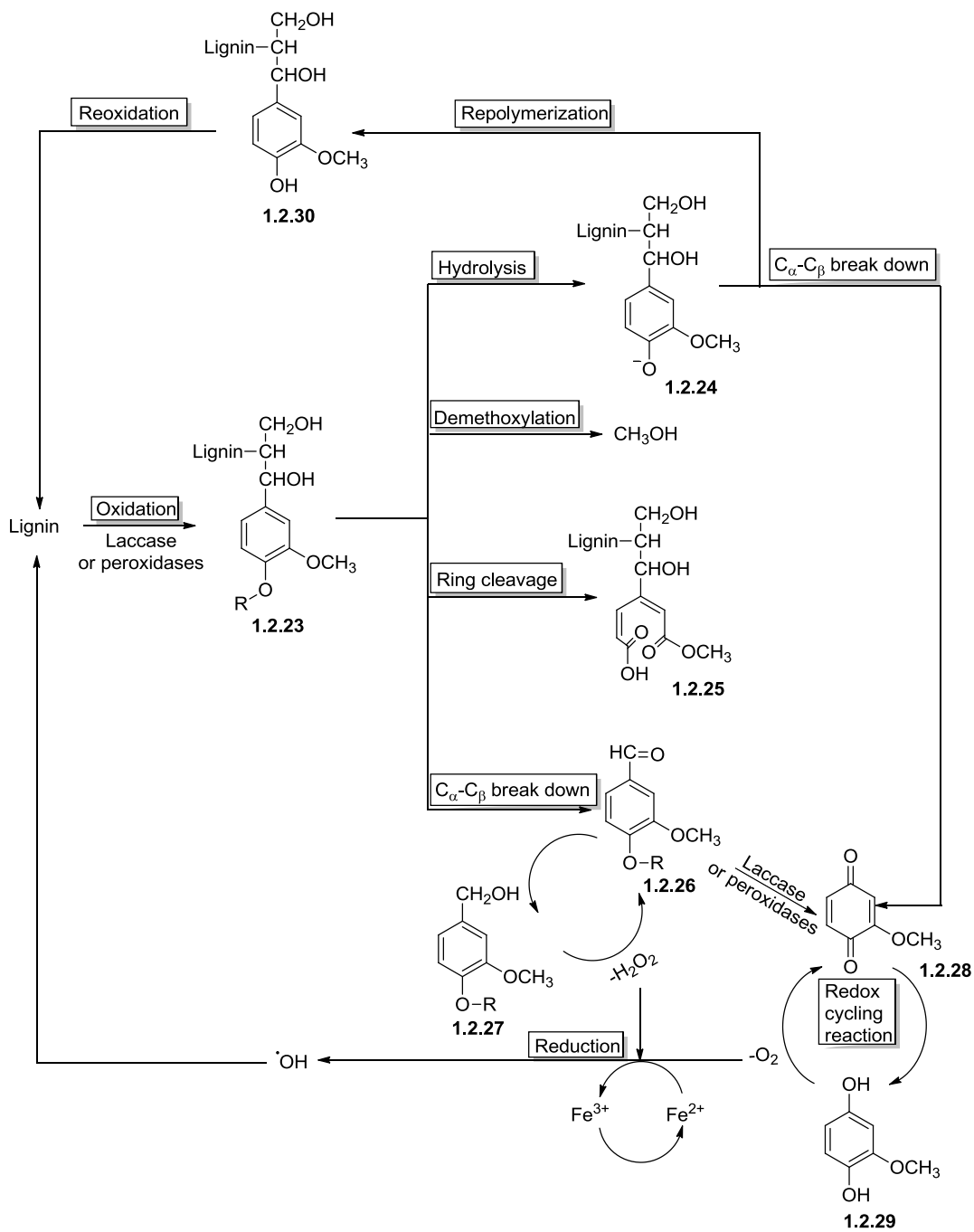


Figure 1.14 Biocatalytic degradation of lignin²⁷

1.3.2 Chemical Degradation of Lignin

A significant obstacle to the biocatalytic degradation of lignin is the inhibition of the bacterial growth by the degradation of products.²⁹ Therefore, chemical degradation of lignin is an attractive alternative.

1.3.2.1 Base-catalyzed depolymerisation (BCD)

Lignin can be depolymerised under alkaline conditions as we have already discussed in section 1.2.2.2 (Figure 1.10). Methoxy groups are removed by BCD to breakdown lignin. The hydrolysis rate is greatly influenced by the substituents on the aryloxy rings. One problem is that repolymerisation products may be formed through condensation reactions and the fragments of lignin connected with new bonds, e.g. methine, methylene, methyl and carboxyl linkages.³⁰ There were 26 compounds obtained from the depolymerisation of softwood lignin with 5 wt% NaOH at 300 °C. The main products were guaiacol (*ca.* 28%), catechol (*ca.* 7.5%) and vanillin (*ca.* 4.5%).³¹ At 315 °C in a continuous flow reactor with NaOH, Kraft lignin was converted into 19.1 wt% monomer fractions including phenol, guaiacol, vanillin and catechols.³² The BCD process is dependent on reaction temperature rather than time, rapid bond cleavage usually occurs at temperatures above 200 °C.^{19, 33} Another limitation of BCD is an economic problem; large amounts of strong base like NaOH are consumed in the process.

1.3.2.2 Thermal depolymerisation

Pyrolysis

The pyrolysis of lignin was studied by thermal analysis and reveals that the degradation is slow and occurs over a broad temperature range (300–1000 °C).³⁴ The selective cleavage of the different bonds results from the bonds having different bond energies. Phenolic compounds with low molecular weight will be produced at high temperatures, whilst at lower temperatures, the breakage of the β - β and C-C bonds will form reactive free radicals and the product stability is enhanced by the condensation reaction. The slow pyrolysis of lignin is not an attractive commercial approach to degrade lignin because of its low yield and poor selectivity for high-value products. Around 30–35 wt% of char is formed and further treatments are required to obtain pure monomers (Figure 1.15).³⁵ In contrast, fast pyrolysis generates a dark brown liquid, which is known as ‘bio oil’, by rapidly heating the finely ground dry biomass feed to 500 °C and then rapidly cooling the vapours to yield 80% pyrolysis oil by dry feed. The by-products char and gas are used in the process.³⁶

In the pyrolysis liquid products, monomeric phenols are the dominant components (*ca.* 69%).³⁷ These monomeric phenols can be categorized into three different types. Guaiacol and its derivatives are guaiacyl (G)-type monomers, which contribute to 83.4% in the total phenols. The other types of monomers are composed of syringol and its derivatives, which are known as syringyl (S)-type monomers accounting for 7.8% of the total liquid product. A small amount of polyphenols are distributed in the final phenols (5.2%), including phenol, catechol and 3-cresol (Figure 1.16).

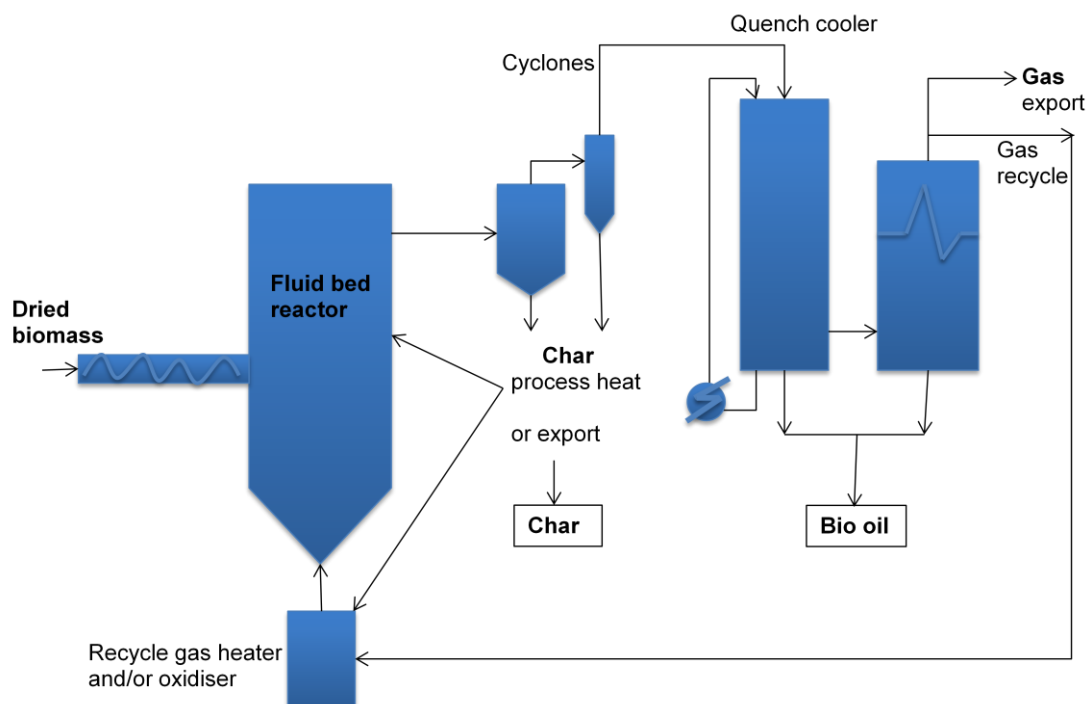


Figure 1.15 Bubbling fluid bed reactor for pyrolysis

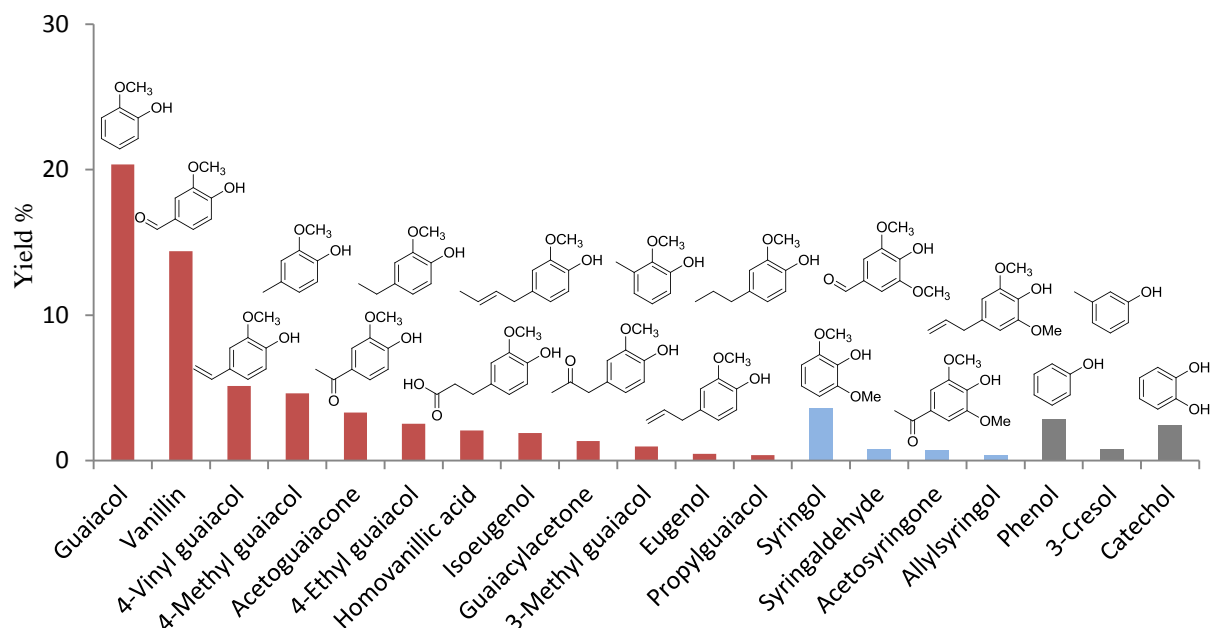


Figure 1.16 Phenolic monomers produced from pyrolysis of lignin^{34, 37-38}

Hydrodeoxygenation (HDO)

High yield monophenols, like cresol, anisole, phenol, benzene and cyclohexane, are produced at 250–350 °C by using HDO.³⁹

The key step of hydrodeoxygenation is the carbon-oxygen bond breaking via reduction and the formation of water. An example of a polyphenolic that can be derived as a significant fraction of lignin digestion is guaiacol. This molecule contains both hydroxy and methoxy substituents and for this reason is not in itself a particularly useful starting material. If selective removal of either or both these functional groups is possible the products phenol, anisole, or benzene would enable more useful chemicals (The worldwide market size and value of these components will be discussed on Table 1.6, page 26). Similarly, if the methyl-oxygen bond were reduced with high selectivity the product catechol would also be again be a useful fine chemical. Selective cleavage can be envisaged through the different bond energies of each of the oxygen-bearing bonds, and indeed previous studies indicate partial selectivity is already achievable under a variety of conditions and catalysts. For example catalytic hydrogenation at high temperature and pressure gives mixtures of *n*-hexane, *n*-heptane, methanol, 1-heptanol, heptanal, as products (Figure 1.17).^{40,41}

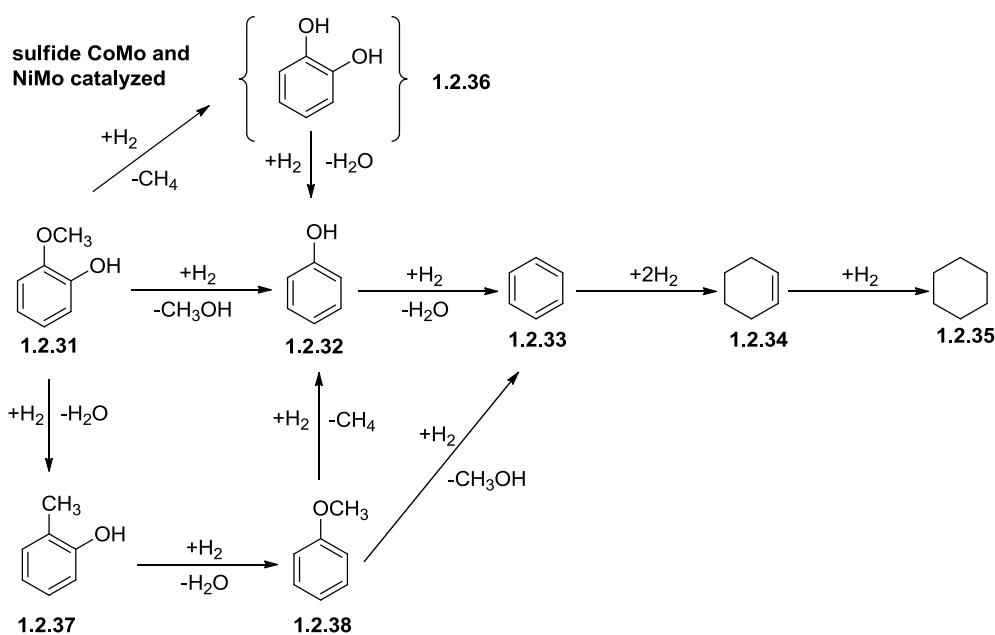


Figure 1.17 Hydrodeoxygenation of lignin model compound³⁹

1.4 Applications of lignin

For a long time, lignin was labelled as a ‘waste material’. Traditionally, lignin is used in low-value energy production. Development of lignin’s potential use in value-added chemicals has benefits for the environment. The application of lignin can be classified into three categories: a) Energy and syngas; b) macromolecules; c) aromatics and monomeric molecules (Figure 1.18).⁴²

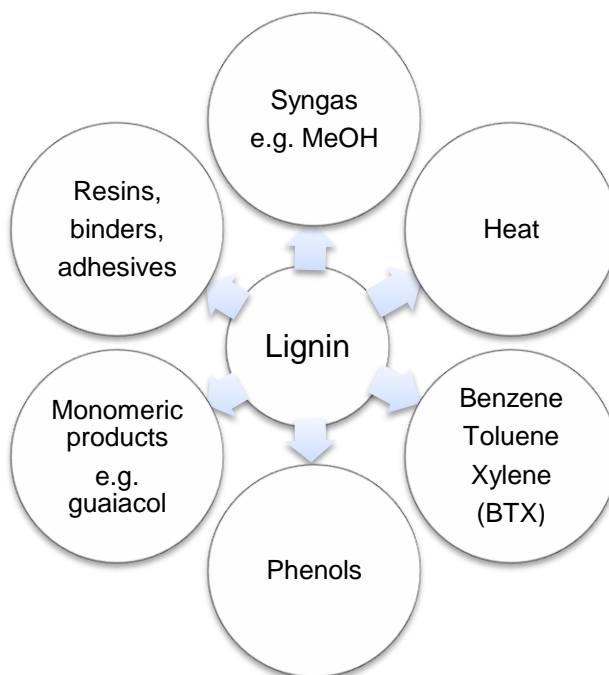


Figure 1.18 Applications of lignin

1.4.1 Energy supply

There are a few technologies that have been used for lignin that provide heat, power and fuels. In paper mills, combustion of lignin could supply the heat and power for the process. Syngas such as hydrogen and methanol is generated by gasification of lignin. Pyrolysis of lignin can produce bio-oil and syngas which integrate with petroleum chemical platforms. Hence, improvements in large scale purification and catalyst design are valuable goals for exploiting lignin as a feedstock.

1.4.2 Macromolecules of lignin

In wood, one important role of lignin is to act as a glue binding wood cell walls together. The application of lignin in phenolic and epoxy resins has been investigated because of its similar structure to phenol. Hence lignin is used as a replacement of phenol in the synthesis of phenol-formaldehyde (PF) resins.⁴³ Methylated lignin enhances the reactivity of lignin towards formaldehyde, used as a polywood adhesive, and provides good resin properties.⁴⁴ It is known that phenol is toxic even in small amounts and it is expensive, so the production of lignin-phenol-formaldehyde is valuable.

1.4.3 Aromatic chemicals from depolymerised lignin

Recently, there has been greater research interest in the recovery of lignin and its biotransformation to value-added products (Figure 1.19).

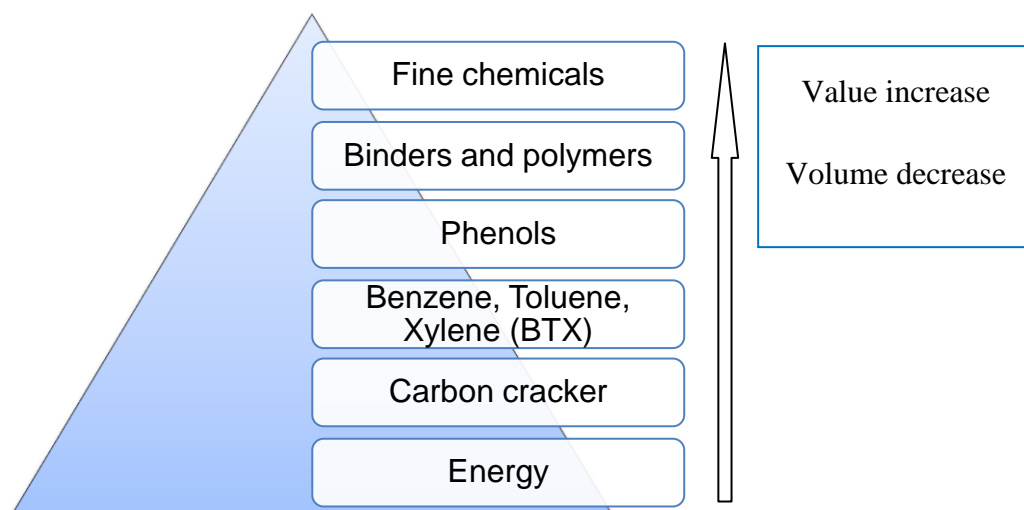


Figure 1.19 Utilization of lignin

Due to diminishing petroleum resources and limited feedstock, the use of lignin to produce aromatic fine chemicals is desirable. Non-selective depolymerisation of lignin

C-C and C-O bonds results in the generation of benzene, toluene, xylene (BTX) and phenols, and these products can be directly used as starting materials in the synthesis of most aromatics (Figure 1.20).⁴⁵ In 2010, the demand for benzene was 41 million tonnes, of which 21 million tonnes were used to produce styrene for subsequent applications, such as polystyrene, plastics or synthetic rubbers. A further 8 million tonnes of benzene was used in the production of cumene and phenol to make phenolic resins and construction products. Cyclohexane was derived from about 12 million tonnes of benzene and used for the manufacture of nylon, which is widely used in textiles.⁴⁶ Toluene is a general solvent and used as raw material to produce toluene diisocyanate for the manufacture of polyurethanes. The applications of toluene are comparatively smaller than benzene, so a large amount of toluene is hydrodealkylated to generate benzene.⁴⁵ There are relatively few applications of *meta*-xylene and *ortho*-xylene, but *para*-xylene represents a relatively large market as a source of polyethylene terephthalate (PET) in the production of fibres, resins and a diversity of applications.⁴⁷

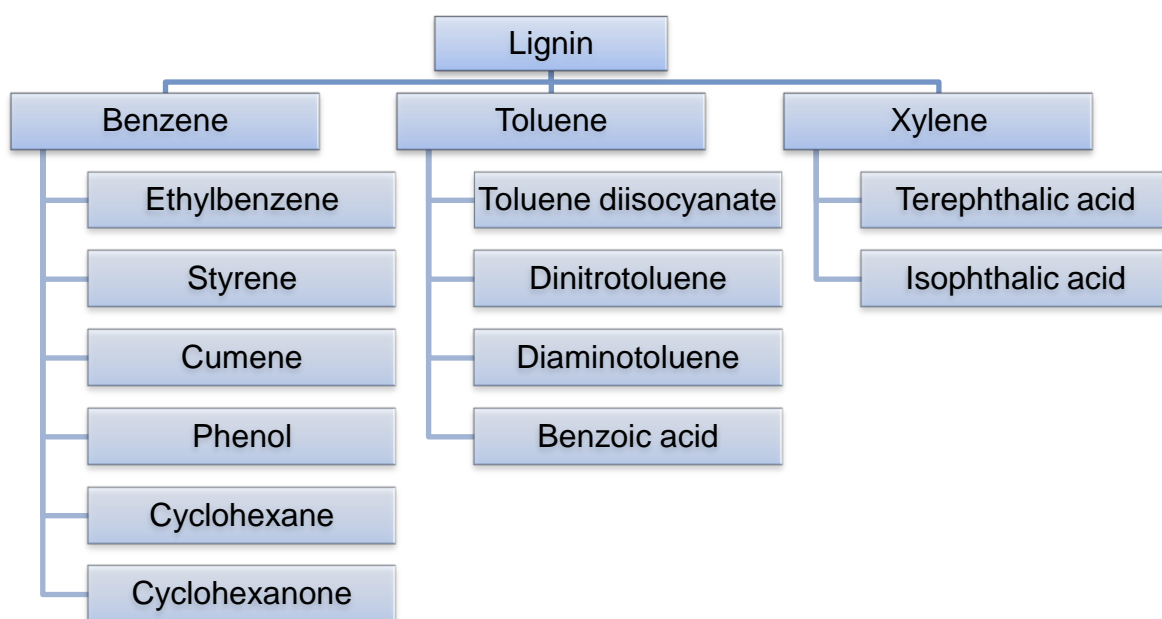


Figure 1.20 Chemicals derived from BTX⁴⁵

The prices of aromatic chemicals could be reduced as a result of the high value, low molecular weight chemicals extracted directly from lignin (Table 1.5).⁴⁸ On the other hand, the current manufacture of 11.9 million tonnes BTX produces 6.6 million tonnes of CO₂ equivalent (this equates to 0.55 tonnes CO₂ /tonne BTX), which is about 3.5 percent of the total CO₂ emissions of the chemical industry in Europe.⁴⁹ Lignin derived BTX could reduce the CO₂ emissions. However, the complex structure makes this a

challenge for the conversion of lignin. Oxygen containing groups in lignin, like hydroxyl, methoxyl, carboxyl and carbonyl groups, should be removed completely to form aromatic chemicals. The process of making BTX from fossil fuels has been optimised for a long time whereas the degradation of lignin is a more recent development.

Table 1.5 Some aromatic productions from lignin, market size/value and applications⁴⁸

Product	World production M ton / year	Market value \$/ ton	Applications
Benzene	30	1115	Production of ethylbenzene, styrene, cumene, cyclohexane.
Toluene	20	1075	Solvent, octane booster, fuels, coolant.
Xylenes	0.5	1280	Printing, rubber, ink, leather.
Phenol	6.5	1649	Phenolic resins, drugs, cosmetics, herbicides.
Cresol	0.18	1350-1850	Antioxidants, herbicides, cleaners, disinfectants.
Aniline	0.09	836	Preparing methylene diphenyl diisocyanate (MDI), pigments, rubber.

1.5 Objectives and outlines

Lignin is highly oxygenated and contains primarily phenols and alkanols as well as aryl and alkyl ether bonds. Therefore, in order to use lignin as a hydrocarbon feedstock a series of (reductive) deoxygenation reactions are required. However, a few challenges remain which limit the application of hydrodeoxygenation of lignin:

- (1) Lignin is a complex, highly cross-linked polymer in which access of the monomeric subunits to chemical reagents or catalysts is highly restricted.
- (2) Each monomeric subunit can be cross-linked by up to 3 bonds with neighbouring subunits; hence, at least 3 enthalpically difficult reactions are required before any entropic advantage is gained in the depolymerisation process.

- (3) Hydrogenation reactions on electron-rich phenols or phenol ethers are complicated by the powerful electron-donating nature of the oxygen atoms. Since hydrogenation (an electron donation process) on an electron-rich substrate is difficult, phenolic C–O bonds typically requires activation of the oxygen.
- (4) Some C–O bond cleavage reactions in lignins generate carbocation intermediates that can undergo intermolecular electrophilic substitution reactions in the polymer framework leading to inert products with strong C–C bonds.

The interest of studying lignin hydrodeoxygenation (HDO) has been raised recently. Hartwig⁵⁰ has demonstrated that dimeric lignin model compounds can be reduced by a homogeneous nickel catalyst combined with acid under mild conditions (1 bar H₂ and 80–120 °C). However, high catalyst loading (20 mol %) is needed in this process. A wide range of noble metal catalysts have been investigated as efficiently diminishing the energy intensity of HDO. For lignin monomeric model compounds, hydrodeoxygenation of guaiacol and cresol has been studied over Pt/Al₂O₃ and Pt/MZ-5 at 200 °C and 40 bar.⁵¹ Despite this, oxygen has been removed from the model compounds and converted into saturated hydrocarbons, such as cyclohexane, methylcyclohexane, methylhexane and methylhexanol.

On the other hand, historically the way in which organic chemists have carried out aromatic HDO is by activating the phenolic oxygen using a sulfonyl ester such as triflate, and using either stoichiometric hydride or catalytic (transfer)hydrogenation.⁵² The problem with this method for industrial use is the cost of the triflate and the waste it generates. For example, triflic anhydride costs around £40/kg in bulk, methanesulfonyl chloride around £4/kg, whereas the anisole product generated costs around £1/kg. Using either of these activating agents would generate 3–5kg of non-solvent waste / kg product. In this study alternative activating groups to enable selective HDO will be investigated which have the potential to be cheaper and/or be recyclable. In Chapter 2, a variety of catalysts systems and activating groups for C_{arom}–O bonds for the HDO of lignin model compounds will be reviewed.

The commercial application of lignin derived bio-oil realistically still has difficulties, such as low selectivity of the products, high process costs due to high pressure and high temperature are required for the process as well as the high loading amount of catalysts. Investigation of hydrodeoxygenation of lignin model compounds is at an

early stage; the catalysts need to be improved and economic processes have to be developed.

The aim of this project is to investigate commercially viable processes for the selective hydrodeoxygenation (HDO) of poly-oxygenated aromatic compounds formed from digested lignin.

Initially, the catalyzed HDO of guaiacol, a model for lignin derived aromatics will be studied using mild reaction conditions, to provide selective and high yielding formation of the chemicals benzene, anisole, phenol or catechol (Figure 1.21).

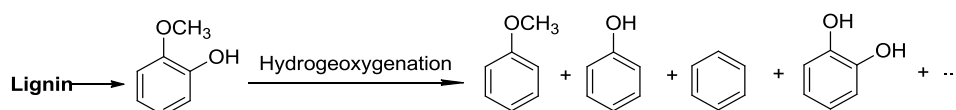


Figure 1.21 The catalyzed HDO of guaiacol

The low boiling point and high volatility of the mixture of products makes them separable by fractional distillation. Anisole is the preferred product to be obtained, due to its high value as one of the green solvents recommended by AstraZeneca and GSK.⁵³ The formation of phenol would avoid the current cumene-hydroperoxide process that generates equivalent volumes of co-product acetone. The commercial linkage of phenol and acetone has long been problematic in industry as the demands of each are different.

In Chapter 3, hydrodeoxygenation of guaiacol will be carried out using simple procedures that facilitate catalytic cleavage of the phenolic bond. This will be achieved by making metal-oxygen (M-O) complexes of guaiacol in which the M-O bonds are stronger than the C_{arom}-O bonds. Our investigation will also include hydroxyl-activated substrates with low cost carbon (carbonate, triarylcyanourate), silicon (silicate), sulfur (diarylsulfate, diarylsulfite, arylsulfate salts) and phosphorus (diarylphosphate, arylphosphate salt). These compounds will then be subjected to catalytic hydrogenation reactions and the yields, selectivities and rates compared.

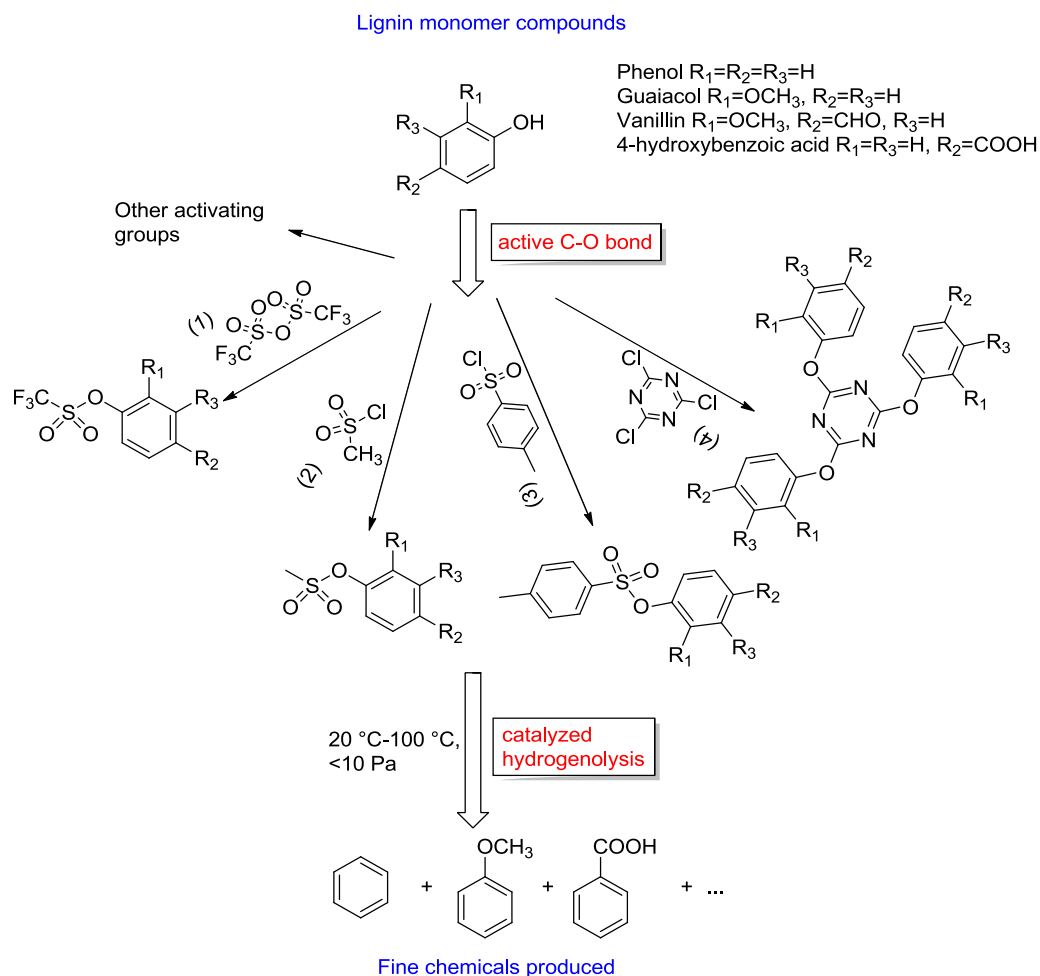


Figure 1.22 Activation routes for the hydroxyl groups in lignin monomer compounds

In Chapter 4, activating $C_{arom}-O$ bonds by other strong electron withdrawing groups, such as tetrazole and triazines, will be studied. The activation will be evaluated via molecular modelling corresponding to the crystal structures of model compounds. The substituent effects of trisubstituted-triazines will be discussed. Additionally, the selectivity of solvents and catalysts will be examined in the earlier hydrogenolysis experiment of tetrazoles.

Hydrogenolysis of trisubstituted triazines will be investigated in Chapter 5. In this chapter, a variety of reaction temperatures, pressures, catalyst types and loading will be revealed and reaction kinetics will also be studied to optimise reaction conditions in batch mode. Hydrodeoxygenation of trisubstituted triazines was initially studied in a batch reactor whilst a continuous stirred tank reactor (CSTR) was investigated to help develop a more commercial viable economical process.

Chapter 6 is an overview of activating phenolic hydroxyl groups and the hydrodeoxygenation processes in batch and continuous flow CSTR systems. Future work will also be discussed.

In Chapter 7, experimental procedures for the synthesis of the chemical compounds, methods of analysis and characterisation are presented.

1.6 References

1. BP, *Energy Outlook 2035*, 2014.
2. U.S. Energy Information Administration, *International Energy Outlook*, **2013**.
3. (a) Ragauskas, A. J.; Williams, C. K.; Davison, B. H.; Britovsek, G.; Cairney, J.; Eckert, C. A.; Frederick, W. J.; Hallett, J. P.; Leak, D. J.; Liotta, C. L.; Mielenz, J. R.; Murphy, R.; Templer, R.; Tschaplinski, T., *Science*, **2006**, *311*, 484-489; (b) Mansouri, N. E.; Salvado, J., *Industrial Crops and Products* **2006**, *24*, 8-16.
4. Lavoie, J. M.; Beauchet, R.; Berberi, V.; Chornet, M., *Biofuel's Engineering Process Technology*, **2011**, 4917-4920.
5. Bozell, J. J., *Clean – Soil, Air, Water*, **2008**, *36*, 641-647.
6. (a) Erickson, B.; Nelson, J. E.; Winters, P., *Biotechnology journal*, **2012**, *7*, 176-185; (b) Elliott, D. C., Chemicals from Biomass, In *Encyclopedia of Energy*, **2004**, *1*, 163-174.
7. (a) Petersen, T. W. A. G., *Top Value Added Chemicals from Biomass: Volume 1—Results of Screening for Potential Candidates from Sugars and Synthesis Gas*; US National Renewable Energy Laboratory: **2004**; (b) Zhang, X. S.; Yang, G. X.; Jiang, H.; Liu, W. J.; Ding, H. S., *Scientific Reports*, **2013**, *3*, 1120-1123.
8. Kumar, D.; Murthy, G. S., *Biotechnology for biofuels*, **2011**, *4*, 27.
9. Huber, G. W.; Iborra, S.; Corma, A., *Chemical. Reviews*, **2006**, *106*, 4044-4098.
10. Pulping: Oxygen and Extended Delignification. Clean Air, Clean Water, Pulp Info Centre. [Online] 2012. [Accessed 12 August 2012]. Available from: <http://www.rfu.org/cacw/basic4KraftPulp.htm>.
11. (a) Kouisni, L.; Fang, Y., Paleologou, M.; Ahvazi, B.; Hawari, J.; Zhang, Y.; Wang, X., *Cellul. Chem. Technol.*, **2011**, *47*, 515-520; (b) Corporation, M. <http://www.meadwestvaco.com/SpecialtyChemicals/Dispersants/MWV002115>.
12. Wahyudiono; Sasaki, M.; Goto, M., *Chem. Eng. Process.: Process Intensification*, **2008**, *47*, 1609-1619.
13. Chakar, F. S.; Ragauskas, A. J., *Industrial Crops and Products*, **2004**, *20*, 131-141.
14. Lignin Institute, *Lignins: A Safe Solution for Roads*. Dialogue/Newsletters, **1992**, *12*, 1.
15. RISI, *World Pulp Annual Historical Data - Excerpt*, **2013**.
16. Hubbe, M. A.; Lucia, L. A., *BioResources* **2007**, *2*, 534-535.

17. Smook, G. A.; Kocurek, M. J., *Handbook for pulp and paper technologists*, Atlanta, GA, U.S.A. : TAPPI ; Montreal, Quebec, Canada : Canadian Pulp and Paper Association, **1982**.
18. Seifer, G. B., *Russian Journal of Coordination Chemistry*, **2002**, 28, 301-324.
19. Yuan, Z.; Cheng, S.; Leitch, M.; Xu, C., *Bioresour. Technol.*, **2010**, 101, 9308-9313.
20. Kadla, J. F.; Kubo, S.; Venditti, R. A.; Gilbert, R. D.; Compere, A. L.; Griffith, W., *Carbon*, **2002**, 40, 2913-2920.
21. Vishtal, A.; Kraslawski, A., *Bioresources*, **2011**, 6, 3569-3584.
22. (a) Lora, J. H.; Glasser, W. G., *Journal of Polymer and the Environment*, **2002**, 10, 39-48; (b) Belgacem, M. N.; Gandini, A., *Monomers, polymers and composites from renewable resources*. Elsevier: Amsterdam ; London, **2008**, 419-431.
23. Kirk, K. T., *Degradation of Lignin*. In *Microbial degradation of organic compounds*. [Online] Gibson, D. T., ed., Ed. New York: Marcel Dekker, Inc.: New York, **1984**, 399-437.
24. Kirk, T. K.; Farrell, R. L., *Annual Review of Microbiology*, **1987**, 41, 465-501.
25. Hatakka, A., *FEMS Microbiology Reviews*, **1994**, 13, 125-135.
26. Bugg, T. D. H.; Ahmad, M.; Hardiman, E. M.; Singh, R., *Current Opinion in Biotechnology*, **2011**, 22, 394-400.
27. Martinez, A. T.; Speranza, M.; Ruiz-Duenas, F. J.; Ferreira, P.; Camarero, S.; Guillen, F.; Martinez, M. J.; Gutierrez, A.; Del-Rio, J. C., *International microbiology*, **2005**, 8, 195-204.
28. (a) Guillen, F.; Gomez-Toribio, V.; Martinez, M. J.; Martinez, A. T., *Archives of Biochemistry and Biophysics*, **2000**, 383, 142-147; (b) Bugg, T. D.; Ahmad, M.; Hardiman, E. M.; Rahmanpour, R., *Natural product reports*, **2011**, 28, 1883-1896.
29. Jönsson, L. J.; Alriksson, B.; Nilvebrant, N. O., *Biotechnology for Biofuels*, **2013**, 6, 16.
30. Thring, R. W.; Chornet, E.; Bouchard, J.; Vidal, P. F.; Overend, R. P., *Canadian Journal of Chemistry*, **1990**, 68, 82-89.
31. Lavoie, J. M.; Baré, W.; Bilodeau, M., *Bioresour. Technol.*, **2011**, 102, 4917-4920.
32. Beauchet, R.; Monteil-Rivera, F.; Lavoie, J. M., *Bioresour. Technol.*, **2012**, 121, 328-334.
33. Thring, R. W., *Biomass and Bioenergy* **1994**, 7, 125-130.
34. Vasile., M. B. C., *Cellul. Chem. Technol.*, **2010**, 44, 353-363.
35. Petrocelli, F. P.; Klein, M. T., *Fuel Sci. Technol. Int.*, **1987**, 5, 25-62.
36. Czernik, S.; Bridgwater, A. V., *Energy Fuels*, **2004**, 18, 590-598.
37. Du, L.; Wang, Z.; Li, S. G.; Song, W. L.; Lin, W. G., *Int. J. Chem. React. Eng.*, **2013**, 11.
38. Alén, R.; Kuoppala, E.; Oesch, P., *J. Anal. Appl. Pyrolysis*, **1996**, 36, 137-148.
39. Nimmanwudipong, T.; Runnebaum, R.; Block, D.; Gates, B., *Catal. Lett.*, **2011**, 141, 779-783.

40. Şenol, O. İ.; Viljava, T. R.; Krause, A. O. I., *Appl. Catal. A*, **2007**, 326, 236-244.
41. Lin, Y. C.; Li, C. L.; Wan, H. P.; Lee, H. T.; Liu, C. F., *Energy Fuels*, **2011**, 25, 890-896.
42. Holladay, J. E.; White, J.; Bozell, J. J.; Johnson, D, *Top Value-Added Chemicals from Biomass-Volume II—Results of Screening for Potential Candidates from Biorefinery Lignin* . Pacific Northwest National Laboratory, Richland, WA.: **2007**.
43. (a) Mansouri, N. E. E.; Yuan, Q.; Huang, F.; *BioResources*, **2011**, 6, 2647-2662; (b) Mansouri, N. E. E.; Pizzi, A.; Salvado, J., *J. Appl. Polym. Sci.*, **2007**, 103, 1690-1699.
44. Danielson, B.; Simonson, R., *J. Adhes. Sci. Technol.*, **1998**, 12, 923-939.
45. U.S. Department of Energy Office of Industrial Technologies, *Energy and Environmental Profile of the U.S. Chemical Industry*, **2000**.
46. Farina, A., What does the future hold for the C6 aromatics chain?A global perspective from a global benzene and styrene producer. In *The 5th Asian Aromatics & Derivatives Conference*, Shell Chemicals: **2011**.
47. Cheng, Y. T.; Wang, Z.; Gilbert, C. J.; Fan, W.; Huber, G. W., *Angew. Chem. Int. Ed*, **2012**, 51, 11097-11100.
48. ICIS pricing. [online]. 2014. [Accessed 11 February 2014]. Available from: <http://www.icispricing.com>.
49. Benner, J. M. V. L.; Harry C., *Identifying breakthrough technologies for the production of basic chemicals: A long term view on the sustainable production of ammonia, olefins and aromatics in the European region*; Delft: **2012**.
50. Sergeev, A. G.; Hartwig, J. F., *Science*, **2011**, 332, 439-443.
51. Wang, Y.; He, T.; Liu, K.; Wu, J.; Fang, Y., *Bioresour. Technol.*, **2012**, 108, 280-284.
52. Gooßen, L. J.; Gooßen, K.; Stanciu, C., *Angew. Chem. Int. Ed.*, **2009**, 48, 3569-3571.
53. Prat, D.; Hayler, J.; Wells, A., *Green Chem.*, **2014**, 16, 4546-4551

Chapter 2 Introduction to upgrading pyrolysis bio-oil to produce lignin derived aromatics and cycloalkanes

Lignin-derived compounds derived from pyrolysis contain a large amount of oxygen in their structure. For upgrading lignin-derived bio oils, there are multiple pathways for removing oxygen functionalities (Figure 2.1).¹

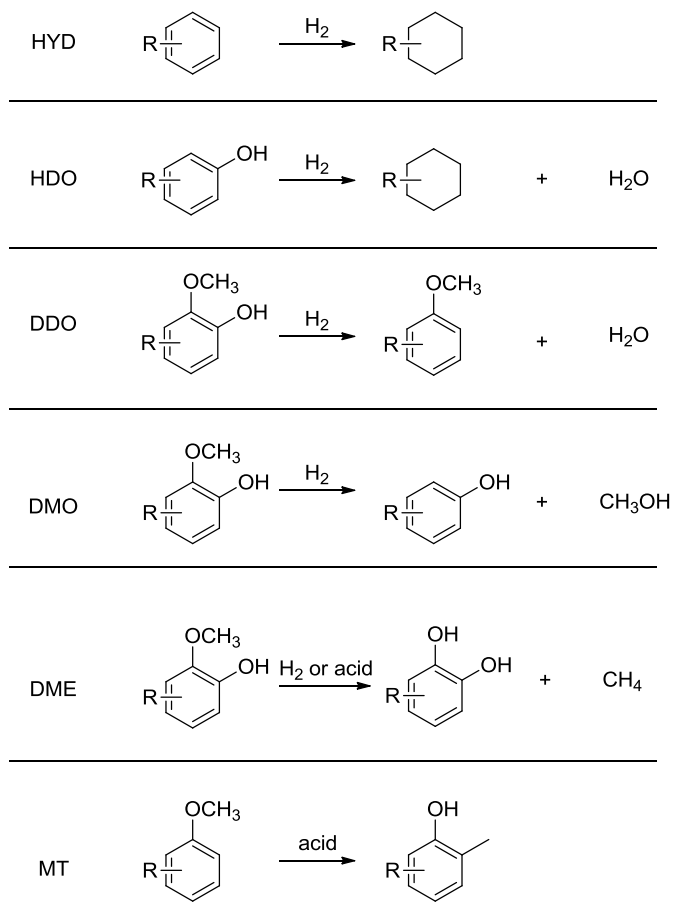


Figure 2.1 Reactions for upgrading lignin-derived compounds

The compounds can be hydrogenated to yield saturated hydrocarbons. An alternative method is deoxygenation that eliminates oxygen without losing any carbon atoms but this needs high temperatures to surmount the activation energy in the transition state. In addition, directly breaking the $\text{C}_{\text{arom}}\text{-O}$ bonds consumes a large amount of reagent, and produces low yields because of their strong bonds, i.e. high bond energies (Table 2.1).²

Table 2.1 Bond dissociation energies (BDE)

Bond type	BDE (kJ/mol)
R-OR	339
Ar-OR	422
R-OH	385
Ar-OH	468

Hydrodeoxygenation (HDO) and direct deoxygenation (DDO) are reactions that remove the oxygen as water, whilst dealkoxylation (DAO) or demethoxylation (DMO) eliminates oxygen by producing alcohols. Nevertheless, the CH₃-OAr bond can be reduced by demethylation (DME) followed by formation of new C-C bonds via transalkylation, in which the methyl transfer (MT) to the aromatic ring occurs. Table 2.2 summarises the properties of pyrolysis oil and its HDO products.³

Table 2.2 Components of pyrolysis oil and its HDO products³

Component	Pyrolysis oil (% w/w)	HDO (% w/w)
Water	15	<5
Oxygen content	50-55	10-15
Organic volatiles (300 °C)	75-80	75-85
Evaporation residue (200 °C)	30-35	25

Guaiacol is a major product (see figure 1.16) from lignin pyrolysis and contains phenolic and methoxy groups, and, because of its chemical simplicity, has attracted attention as a lignin model compound. There are four main reactions of guaiacol degradation with H₂: MT, HYD, HDO and DDO (Figure 2.1).⁴ When co-reacted with H₂, guaiacol is firstly converted to anisole, phenol and catechol, over-hydrogenation then produces benzene, toluene, and *o*-cresol etc. At lower temperatures (100 °C), cyclohexanol is the main products because HYD is the dominant reaction for the guaiacol, whilst HDO is favoured at higher temperature (300 °C), where benzene is the dominant product (Figure 2.2).⁵ However, MT reactions occur when under acidic conditions but it is not a favoured oxygen removal reaction.

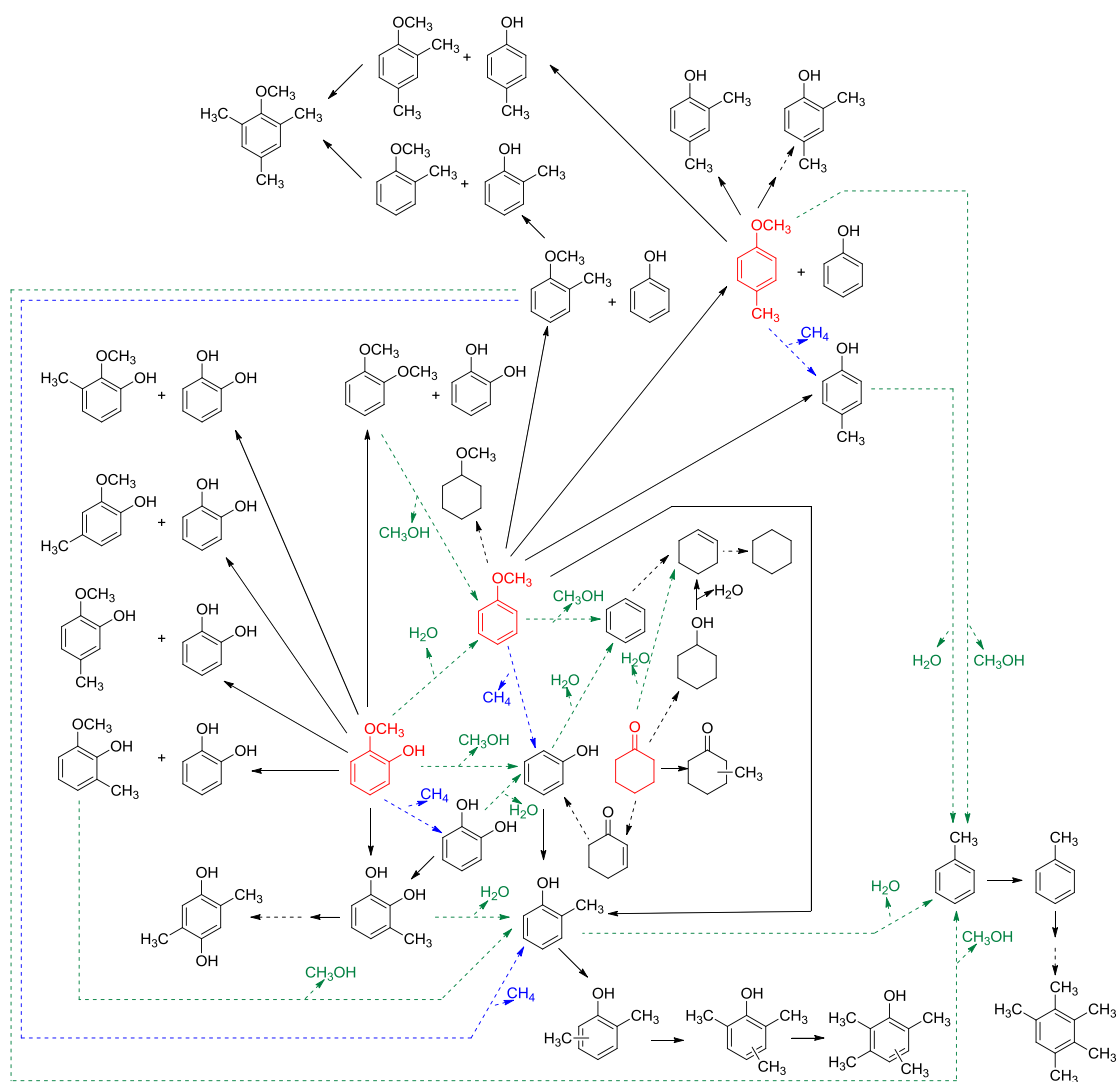


Figure 2.2 Reaction pathway of guaiacol (Solid black arrows represent MT reaction, dash green, blue and black arrows represent HDO, DDO and HYD processes respectively). Drawing modified from reference 5b.^{5b}

The main issue preventing industrial exploration of this chemistry is the low selectivity that produces complex mixtures that make it difficult and expensive to separate pure products. There is a need to develop robust and selective catalysts to avoid product mixtures. Current development on upgrading catalysts has focused on organometallics, noble metals and zeolites. On the other hand, the structure of lignin-derived compounds can be modified to activate the phenolic group so that the cleavage of $C_{\text{arom}}-O$ can be achieved (see Chapter 2, 2.5, p46). In the following section, recent development of catalysts will be discussed.

2.1 Transition metal sulfide (TMS) catalysts

Transition metal sulfide catalysts are widely used in industry.⁶ It has been shown that sulfated molybdenum with cobalt or nickel supported on alumina (CoMo/Al₂O₃ or NiMo/Al₂O₃) has good catalytic activity and is broadly used in hydrotreating of petroleum.⁶ Most of the research has been focused on the deoxygenation of lignin model compounds (e.g. phenol, guaiacol, cresol etc.) with CoMo/Al₂O₃ catalyst. The study of model compounds simplifies the product analysis and provides better insight and deeper understanding of the chemistry of lignin digests. There are two main mechanisms for the degradation of lignin monomer phenolics (Figure 2.3).¹ The HDO pathway forms the intermediate cyclohexanol by hydrogenation of the aromatic ring, followed by dehydration resulting in the by-product water and deoxygenated hydrocarbon. The hydrogenation of cyclohexene then produces the thermodynamically stable cyclohexane product.

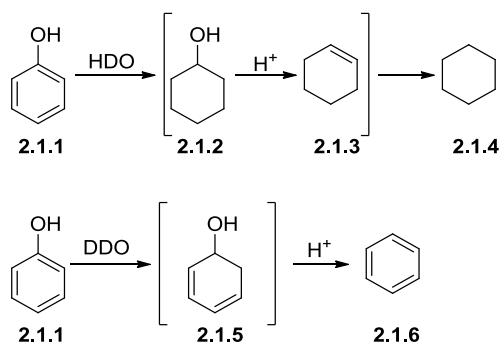
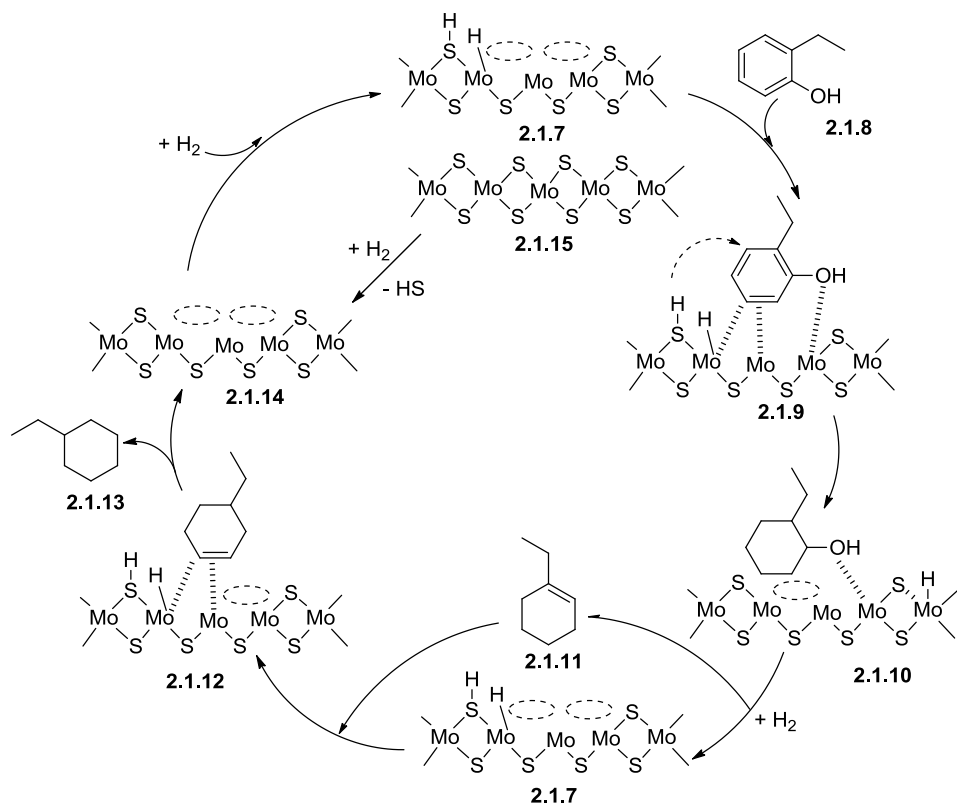
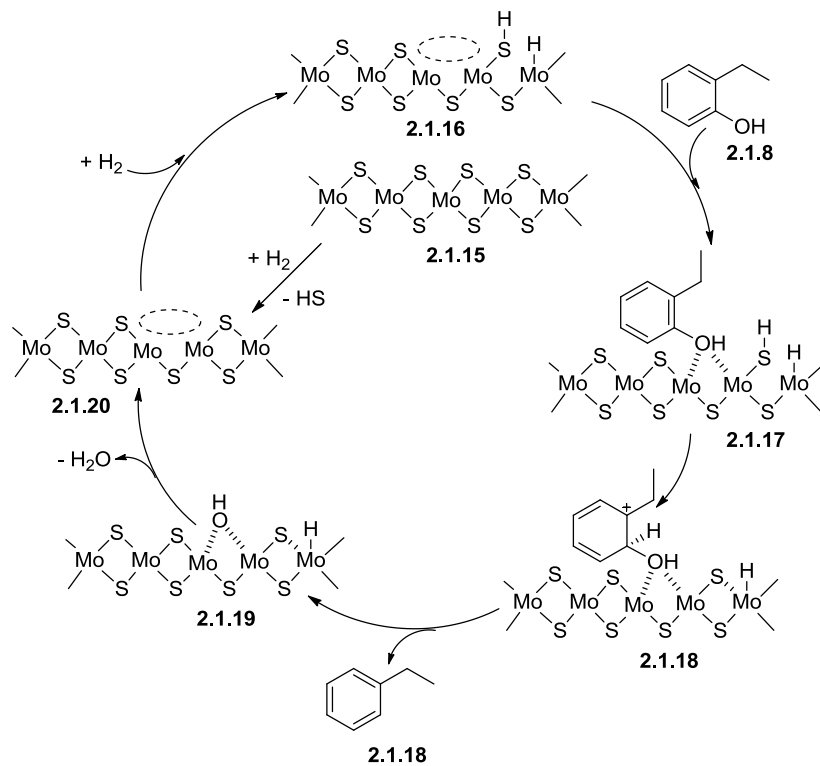


Figure 2.3 Degradation pathways of phenol on TMS catalysts

The second route is DDO, in which the phenolic oxygen adsorbs on the catalyst's unsaturated surface site, perhaps to transiently stabilise the keto, rather than enol tautomer; following reduction to the allylic alcohol, deoxygenation occurs on the edge to eliminate water and reforms the aromatic ring.⁷ The catalytic sites at vacant sulfur atoms act as Lewis acids and coordinate the oxygen's unpaired electrons. Ni or Co atoms are located on the edge of S-Mo-S layers.⁸ The interfaces of Ni-Mo-S and Co-Mo-S structures do not add more vacancies but increase their activity by weakening the S-Mo bond.⁹ The SH group can be treated as a Brønsted acid to provide hydrogen to the adsorbed starting material, and to form a carbocation, followed by deoxygenation (Figure 2.4).



(a)



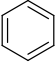
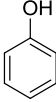
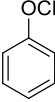
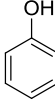
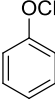
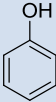
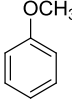
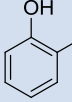
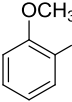
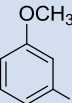
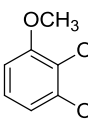
(b)

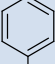
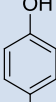
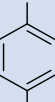
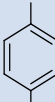
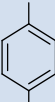
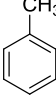
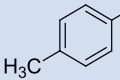
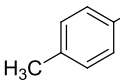
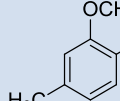
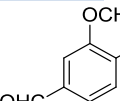
Figure 2.4 (a) mechanism of HDO of 2-ethylphenol with a CoMoS/Al₂O₃ catalyst

(b) mechanism of DDO of 2-ethylphenol with a CoMoS/Al₂O₃ catalyst¹⁰

Other metals have also been studied. The activities of catalysts decrease in the order $\text{Ru} \approx \text{Rh} > \text{Mo} > \text{Pd} > \text{Nb} > \text{Zr}$. Mo is preferred to Ru and Rh due to economic considerations. The steric and electronic effects of the phenolic substituents also affect the reactivity of these reactions. Thus *m*-cresol has a higher reaction rate than *p*-cresol and *o*-cresol.² Jongerius reported that at 300 °C and 50 bar H₂ over a sulfated CoMo/Al₂O₃ catalyst, lignin monomer compounds are selectively converted into deoxygenated products using the three pathways discussed above.⁷ Benzene was the main product formed by deoxygenation of phenol; phenol was produced from anisole; and phenol and catechol were generated from guaiacol (Table 2.3). Additionally, *o*-cresol and *p*-cresol yielded methylated products. The small amount of benzene and toluene present in the overall reactions imply complete deoxygenation, though with low selectivity. In spite of this, under the same conditions, only less than 5% HYD products (such as cyclohexene and cyclohexanol) were obtained and 10% cyclohexane was found after 4 hours conversion of guaiacol.¹¹

Table 2.3 Selective conversion (%) of lignin model compounds on sulfated CoMo/Al₂O₃ catalyst at 50 bar of H₂ and 300 °C for 4 h⁷

Starting Material	Conversion %	Selectivity %				
						
	27	37	n/a	–	–	–
	58	10	64	n/a	–	–
	80	1	36	–	n/a	–
	84	<1	34	3	11	n/a
	78	<1	3	2	–	–
	83	<1	1	<1	3	5

Starting Material	Conversion %	Selectivity %				
						
	23	65	–	–	–	–
	22	60	<1	–	–	–
	85	13	47	n/a	–	–
	89	2	42	–	13	n/a
	53	–	3	–	9	23

A high tolerance of impurities by the TMS catalysts is important in upgrading pyrolysis bio oil. The other advantage of TMS catalysts is the selective reduction of phenols and various other functional groups (such as imines and enamines).¹² Furthermore, deoxygenated products of phenols are produced by DDO so that the H₂ demand can be reduced. The development of large scale manufacturing methods for the production of TMS catalysts has reduced the cost of DDO derived product. However, there are a few drawbacks limiting their applications. Polyphenolic species inhibit the activity of the catalysts by increasing coke formation, and regeneration of the resulting metals release sulfur oxides for which scrubbing systems are necessary to prevent harmful environmental effects. In addition, the deoxygenation over TMS catalysts happens at high pressures and temperatures, requiring high capital cost and large energy requirements. In view of these problems, there is a need for lower energy, more selective catalytic processes.

2.2 Noble metal catalysts

Noble metal catalysts have a higher turnover number compared with sulfide catalysts. It was shown that their higher reactivity and lower energy consumption was due to the avoidance of sulfur stripping and less water sensitivity. Noble metals split hydrogen molecules by adsorbing H₂ on the metal surface, whilst the oxygen containing substrates are adsorbed on the free noble metal sites, or the interface of the supports, and react with the adjacent hydrogen atoms, resulting in the cleavage of C-O bond to form the deoxygenated products. The ability to remove oxygen from pyrolysis bio-oil has been studied by Wildschut.¹³ It was found that the Pt/C catalyst gave the highest yield (58%) of upgraded pyrolysis bio-oil, yet the product contained the most oxygen (28%, Figure 2.5). A desirable catalyst should generate a high yield of oil with low oxygen content. Ru supported TiO₂ and Carbon showed better performance than Ru supported on Al₂O₃ giving both better overall yields and lower oxygen content. Pd/C is a good choice for the HDO process because of the catalyst's availability and consistency, which gave a relatively high yield (43%) and the lowest oxygen content (19%).

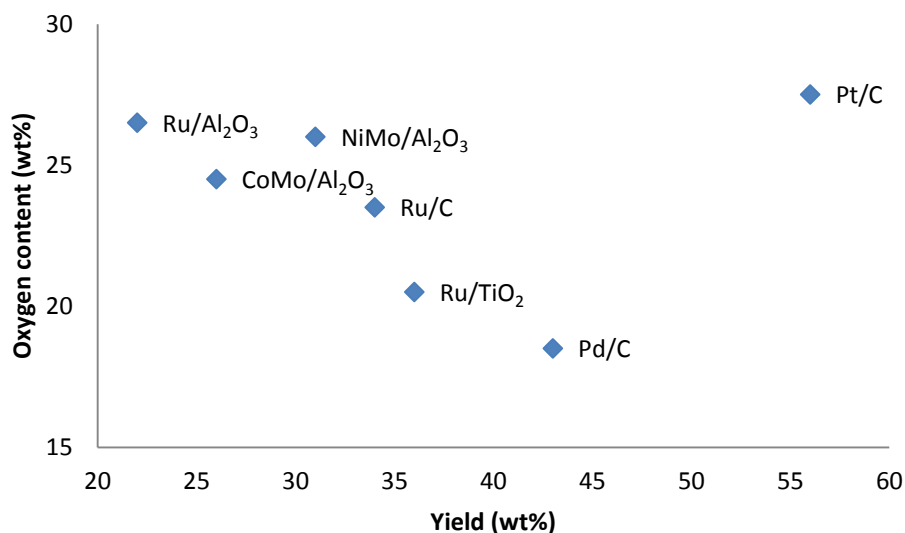


Figure 2.5 Yields of HDO of pyrolysis oil (250 °C, 100 bar, 4 h) by different noble metal catalysts. Data from ref. 13

Supported noble metal catalysts are highly active catalysts for the HDO process. Table 2.4 lists recent research of reduction of bio oil model compounds. Gutierrez et al. investigated HDO reactions at 100 °C and 300 °C.¹⁴ Monometallic catalysts (Pt, Pd, Rh) and bimetallic catalysts (PdPt, RhPt, RhPd) supported on ZrO₂ were examined. The adsorption of H₂ is an exothermic process, so increasing the temperature reduces the H₂ absorbed on the surface of catalysts. The reaction rates of hydrogenation and deoxygenation will therefore be decreased. The results indicated that the ratio of catalytic metals affects the H₂ adsorption. Sajiki et al.¹⁵ examined Pd/C as the catalyst and only Mg powder showed excellent efficiency. There was no effect of Zn, Fe or Al powder. Methanol was used as solvent in the reaction. They reported that addition of ammonium salts (e.g. NH₄OAc) improved the reactivity significantly. Without the addition of NH₄OAc, the reaction took 12 hours while only 0.5 hour was required for the complete reaction with 1.0 equiv of NH₄OAc.

Table 2.4 Recent research into reduction of bio-oil model compounds with noble metal catalysts and hydrogen gas

Catalyst	Reaction conditions	Feed	Conversion (%)	Main product(s)	Reference
Ru/C	443 K, 15 bar	Guaiacol	>99	Cyclohexanol	16
		Catechol	86	Cyclohexanol	
		Phenol	>99	Cyclohexanol	
Ru/C	423 K, 138 bar	Guaiacol	100	2-Methoxycyclohexanol	17
	523 K, 138 bar	Guaiacol	100	Cyclohexanol	
	573 K, 138 bar	Guaiacol	100	Phenol, cresols	
Ru/C	653 K, 40 bar	Phenol	70	Benzene	18
Ru/HZS M-5 (38)	423 K, 50 bar	Phenol	100	Cyclohexane	19
			100	Cyclohexanol	
Ru/CNT*	373 K, 10 bar	Vanillin	100	Vanillyl alcohol	20
	473 K, 10 bar		100	<i>p</i> -Creosol	
Pd/C	H ₂ O-H ₃ PO ₄ , 423 K, 20 bar	Phenol	100	Cyclohexanone	21
	H ₂ O, 423 K, 20 bar		100	Cyclohexanol	
Pd/C	523 K, 138 bar	Guaiacol	80	2-Methoxycyclohexanol	17
	573 K, 138 bar		100	Cyclohexane	
Pd/HZS M-5 (38)	423 K, 50 bar	Phenol	100	Cyclohexane	19
Pd/Al	523 K, 15 bar	Phenol	28	Cyclohexene, cyclohexane	22

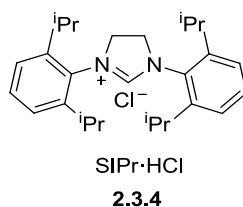
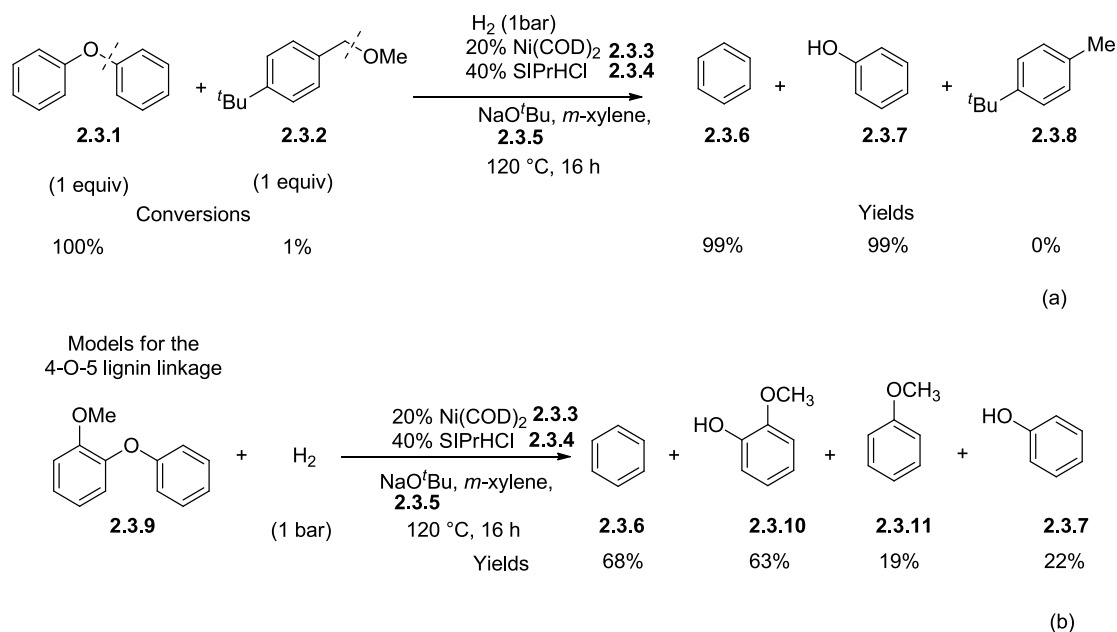
Pd/HY zeolite	623 K, 15 bar	Phenol	35	Bezene	22
Pt/Al₂O₃	473 K, 40 bar	Guaiacol	14	Cyclohexane	23
		Cresol	24	Methylhexane, methylhexanol	
Pt/ZSM-5	473 K, 40 bar	Cresol	93	Methylcyclohexane	23
Pt/γ-Al₂O₃	573 K, 1.4 bar	Guaiacol	8	Phenol, catechol, 3-methylcatechol	24
Pt/HZS M-5 (38)	423 K, 50 bar	Phenol	100	Cyclohexane	19
Pt/MgO	573 K, 1.4 bar	Guaiacol	70	Phenol, catechol	25
Pt/MgO	523 K, 69 bar	Guaiacol	63	Cyclohexanol	26
	523 K, 41 bar		34	Cyclohexanone	

*CNT-carbon nanotube

Although this approach has a number of advantages over conventional methods, it still has some limitations: water is produced along with the hydrocarbons, and when this is not removed, the yield of product is reduced dramatically;²⁷ the high-energy input required makes it uneconomic for large scale industrial operation. Bykova et al. used ionic liquids to replace the aqueous system so that the hydrocarbons and water produced could be separated efficiently.²⁸ They selected appropriate Ni nanoparticles as catalysts improving a one-pot process for the reaction.

2.3 Non noble metal catalysts

Sergeev and Hartwig reported a selective hydrogenolysis of aryl ethers with active nickel catalysts at 80–120 °C with 1 bar of hydrogen to give high yield of phenols and arenes.²⁹ 20 mol% of Ni(COD)₂ (**2.3.3**) combined with SIPr·HCl (**2.3.4**) and NaO^tBu (**2.3.5**) as base were required for high conversions (>95%) of the products.



Scheme 2.3.1 Nickel catalyzed hydrogenolysis of lignin model compounds

The same authors studied the cleavage of lignin linkages, and this approach showed high efficiency and selectivity for breaking the 4-O-5, α -O-4 and β -O-4 bonds (Scheme 2.3.1).

The same nickel catalyst is active in the hydrodeoxygenation of other phenolic monomer compounds.³⁰ Raney[®] Ni and Nafion/SiO₂ catalysts were used to convert phenols into hydrocarbons and methanol with nearly 100% conversion.³¹ Hydrodeoxygenation of guaiacol via nickel catalysts supported on SiO₂ and ZrO₂ has been studied.³² The reaction was carried out at 320 °C and 170 bar H₂ to give hydrodeoxygenation products. However, the products that formed by the hydrogenation of aromatic ring were also found (Figure 2.6). The authors described two pathways for the conversion of guaiacol:

- (1) Reduction of the –OCH₃ group either by demethylation producing catechol and methane, or by demethoxylation forming phenol or methanol;
- (2) Cleavage of C_{arom}-O bond was accompanied by the hydrogenation of the aromatic ring, followed by elimination of phenolic -OH group to produce cyclohexene, and this reduced to cyclohexane.

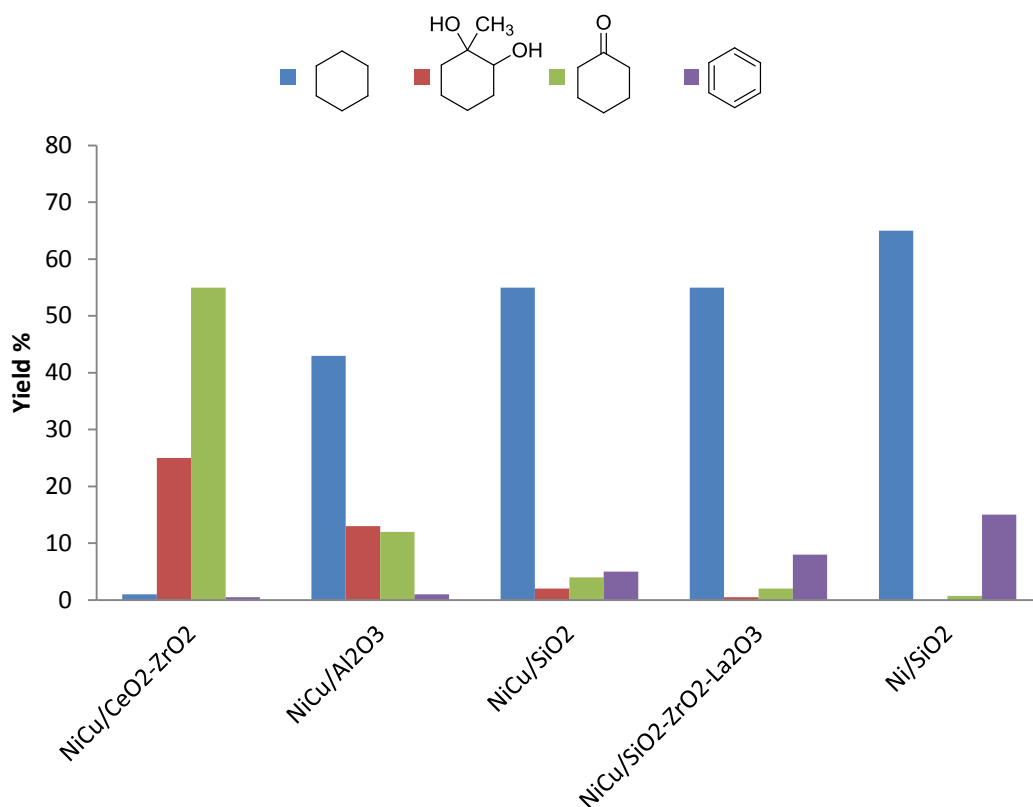


Figure 2.6 The main products of guaiacol HDO over nickel catalysts at 320 °C and 170 bar H₂ for 1 hour

Interest in iron-based catalysts as a potentially cheap and green method to produce aromatic hydrocarbons has been published in pioneering work.³³ The HDO of guaiacol over an Fe/SiO₂ catalyst was carried out at 400 °C in the gas phase (using guaiacol, H₂O, CO, CO₂ and H₂) as a model of hydrotreating a lignin pyrolysis stream.^{33c} Phenol was produced as the main product, and benzene was obtained as the result of reduction of phenol. Cresol was also found in the product mixture, as well as anisole. The cresol could be converted into toluene. The mechanism of Fe/SiO₂ catalysed HDO of guaiacol was explained by Olcese.^{33a} Emmet and Skau showed that no hydrogenation of benzene ring occurred at 400 °C with an Fe catalyst.³⁴

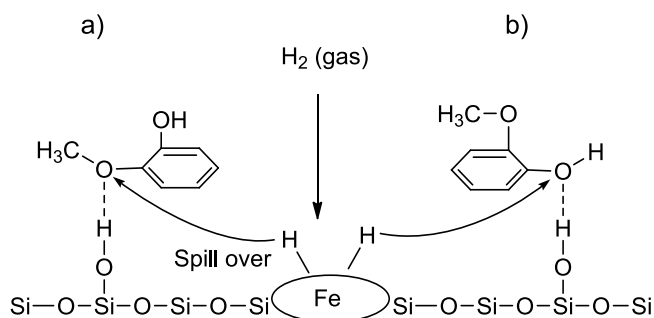


Figure 2.7 Mechanism of Fe/SiO₂ catalysed HDO of guaiacol

There are some issues that limit the application of this method: the recycling of the clean gas; the safety issues of hydrogen gas and the high consumption of H₂; catalyst deactivation caused by coke and oxidation of Fe to Fe₃O₄.^{33c}

Zeolite is a widely used heterogeneous catalyst in the petrochemical industry for upgrading petroleum.³⁵ Although biomass is different from petroleum and new approaches are demanded, zeolite is a promising catalyst for converting biomass to chemical feedstocks.(Figure 2.8).³⁶ A method to upgrade pyrolysis oil using zeolite catalyst has been studied, processes including degradations of phenol and guaiacol were investigated on HZSM-5 zeolite.³⁷ Phenol had very low reactivity with HZSM catalyst and was only transformed to butene and propene partially at 400 °C. It was found that 50 wt% guaiacol thermally decomposed at this reaction temperature, which led to low conversion over HZSM-5 and caused formation of coke.

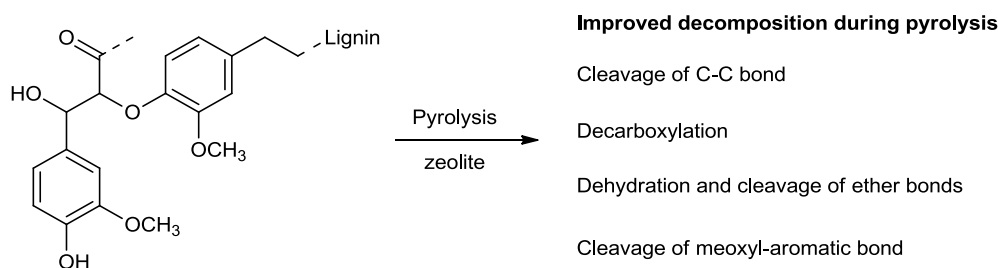


Figure 2.8 Pyrolysis of softwood kraft lignin over zeolite³⁶

2.4 Deactivation of catalysts

The deactivation of catalysts is affected by the reaction compositions and conditions. Furimsky and Massoth demonstrated that the main factors that deactivate catalysts are:³⁸

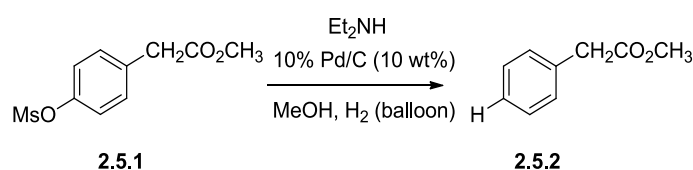
- (1) Catalyst poisoning caused by the feed substances being adsorbed onto the active surface of the catalyst preventing other reactants from being absorbed by the catalyst and decreasing the activity of the catalyst. The most common poisons substances are nitrogen and sulfur containing compounds which strongly adsorb on the catalyst surface.
- (2) Catalyst coking significantly reduces the catalyst's activity by filling the pores on the surface of catalyst and changes the catalyst structure. Coke formation is affected by the properties of the feed, catalyst surface and the reaction conditions. Aromatics compounds and phenols, e.g. phenol, hydroxyphenol and methoxyphenol are important coke precursors.³⁹ It has been found that aromatic

compounds containing more oxygen atoms are more likely to cause coking through polymerization on the catalyst surface.^{11, 39} Further, the more basic the precursor or the more acidic the catalyst surface, the more coking that occurs. Increasing the contact time, reaction temperature and H₂ pressure decreases the amount of coking.⁴⁰

- (3) Changes in the catalyst's structure due to interactions with the reactants, causing further deactivation of the type discussed earlier.³⁸ Temperature, impurities, catalyst type and dispersion, support surface area and porosity affect metal particles reformation and redispersion by affecting sintering rate of supported metals.

2.5 Activation of aryl C–O bonds

Some methods have been reported that convert the phenolic hydroxyl group into its corresponding esters. Clauss and Jensen have published the Pd/C catalysed hydrodeoxygenation of aryl mesylates under mild condition.⁴¹ However, they did not clarify the reaction scales and reaction time. A more developed method has been demonstrated by Sajiki's group: they found that utilisation of diethylamine in a similar reaction to the one Clauss described, could enhance deoxygenation of aryl mesylate.¹⁵ Diethylamine is a basic scavenger for the methanesulfonic acid produced; surprisingly, as an amine, it also promotes the Pd/C-catalysed hydrogenation (Scheme 2.5.1). Despite highly selective hydrogenated products being obtained by this method, most of the reactions had to be carried out for a long reaction time (48 hours).



Scheme 2.5.1

Reduction of other aryl sulfonates has been reported for direct deoxygenation.^{15, 42} Trifluoromethanesulfonate (triflate) is a good leaving group which can increase the leaving ability of phenolic hydroxyl group. Cacchi⁴³ and Kotsuki⁴⁴ showed homogeneous processes (utilising Pd(OAc)₂ and phosphine ligands) for the efficient deoxygenation of phenols *via* their triflates. Triethylammonium formate was used as a hydrogen donor (Scheme 2.5.2).

In contrast to phenol mesylates and triflates, when using aryl toluenesulfonates (tosylates) as substrates, no deoxygenation took place and only the starting material was recovered.⁴⁶ The cleavage of toluenesulfonyl groups would not proceed presumably due to the low electron density of its benzene ring and electron transfer towards the toluenesulfonyl benzene ring rather than the phenyl group (Figure 2.9).⁴⁵⁻⁴⁶

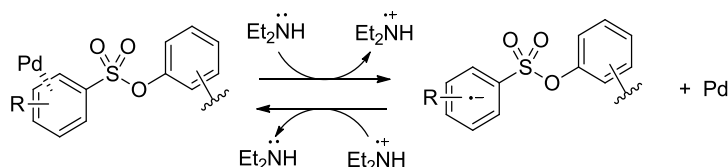
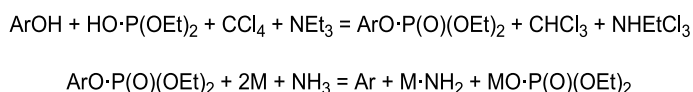


Figure 2.9 Pathway for degradation of aryl toluenesulfonate

In addition, aromatic hydrocarbons could be obtained as a result of reduction of diethyl phosphate esters with alkali metals in liquid ammonia, though this method is unsustainable, being atom inefficient.⁴⁷ A method to prepare aryl diethyl phosphates has been achieved by adding triethylamine into a phenol and diethyl phosphite solution in the banned solvent carbon tetrachloride. Two equivalents of sodium or lithium in liquid ammonia were required for effective deoxygenation (Figure 2.5.4).^{47d}



Scheme 2.5.4

Alternatively, Welch^{47a} reported a high yielding reduction of aryl diethyl phosphites with titanium metal under aprotic conditions. Aromatic hydrocarbons were produced by refluxing in THF for 6-16 hours, followed by quenching with methanol at 5 °C, filtering through a silica plug and removing the solvent. There are a number of issues that make this process industrially unfavourable which are: poor atom efficiency; low reaction temperatures necessitated through the use of liquid ammonia; long reaction times; several reaction steps and chromatographic separation; the titanium phosphate waste which could be environmentally harmful.

2.6 References

1. Ruddy, D. A.; Schaidle, J. A.; Ferrell, J. R.; Wang, J.; Moens, L.; Hensley, J. E., *Green Chem.*, **2014**, *16*, 454-490.
2. Furimsky, E., *Appl. Catal., A*, **2000**, *199*, 147-190.
3. Marsman, J.; Wildschut, J.; Mahfud, F.; Heeres, H., *J. Chromatography A*, **2007**, *1150*, 21-27.

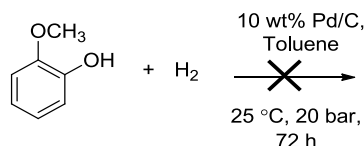
4. Nimmanwudipong, T.; Runnebaum, R.; Block, D.; Gates, B., *Catal. Lett.*, **2011**, *141*, 779-783.
5. (a) Gutierrez, A.; Kaila, R.; Krause, O., In *Hydrodeoxygenation of guaiacol as model compound for pyrolysis oil on noble metal catalysts*, 14th International Congress on Catalysis, Seoul Laboratory of Industrial Chemistry, Helsinki University of Technology: Seoul, **2008**; (b) Runnebaum, R. C.; Nimmanwudipong, T.; Block, D. E.; Gates, B. C., *Catal. Sci. Technol.*, **2012**, *2*, 113-118.
6. Prins, R., In *Handbook of Heterogeneous Catalysis*, Wiley-VCH Verlag GmbH & Co. KGaA: **2008**, 1309-1338.
7. Jongerius, A. L.; Jastrzebski, R.; Bruijninx, P. C. A.; Weckhuysen, B. M., *J. Catal.*, **2012**, *285*, 315-323.
8. Brorson, M.; Carlsson, A.; Topsøe, H., *Catal. Today*, **2007**, *123*, 31-36.
9. He, Z.; Wang, X., *Catalysis for sustainable energy*, **2012**, *1*, 28-52.
10. Romero, Y.; Richard, F.; Brunet, S., *Appl. Catal. B*, **2010**, *98*, 213-223.
11. Hurff, S. J.; Klein, M. T., *Ind. Eng. Chem. Fundam.*, **1983**, *22*, 426-430.
12. Yu, Z.; Jin, W.; Jiang, Q., *Angew. Chem. Int. Ed.*, **2012**, *51*, 6060-6072.
13. Wildschut, J.; Mahfud, F. H.; Venderbosch, R. H.; Heeres, H. J., *Ind. Eng. Chem. Res.*, **2009**, *48*, 10324-10334.
14. Gutierrez, A.; Kaila, R. K.; Honkela, M. L.; Slioor, R.; Krause, A. O. I., *Catal. Today*, **2009**, *147*, 239-246.
15. Sajiki, H.; Mori, A.; Mizusaki, T.; Ikawa, T.; Maegawa, T.; Hirota, K., *ChemInform*, **2006**, *37*, 987-990.
16. Nakagawa, Y.; Ishikawa, M.; Tamura, M.; Tomishige, K., *Green Chem.*, **2014**, *16*, 2197-2203.
17. Elliott, D. C.; Hart, T. R., *Energy Fuels*, **2008**, *23*, 631-637.
18. Chang, J.; Danuthai, T.; Dewiyanti, S.; Wang, C.; Borgna, A., *ChemCatChem*, **2013**, *5*, 3041-3049.
19. Zhang, W.; Chen, J.; Liu, R.; Wang, S.; Chen, L.; Li, K., *ACS Sustain. Chem. Eng.*, **2014**, *2*, 683-691.
20. Yang, X.; Liang, Y.; Cheng, Y.; Song, W.; Wang, X.; Wang, Z.; Qiu, J., *Catal. Commun.*, **2014**, *47*, 28-31.
21. Güvenatam, B.; Kurşun, O.; Heeres, E. H.; Pidko, E. A.; Hensen, E. J., *Catal. Today*, **2014**, *233*, 83-91.
22. Echeandia, S.; Pawelec, B.; Barrio, V. L.; Arias, P. L.; Cambra, J. F.; Loricera, C. V.; Fierro, J. L. G., *Fuel*, **2014**, *117, Part B*, 1061-1073.
23. Wang, Y.; He, T.; Liu, K.; Wu, J.; Fang, Y., *Bioresour. Technol.*, **2012**, *108*, 280-284.
24. Nimmanwudipong, T.; Runnebaum, R. C.; Block, D. E.; Gates, B. C., *Energy Fuels*, **2011**, *25*, 3417-3427.
25. Nimmanwudipong, T.; Aydin, C.; Lu, J.; Runnebaum, R.; Brodwater, K.; Browning, N.; Block, D.; Gates, B., *Catal. Lett.*, **2012**, *142*, 1190-1196.

26. Nimmanwudipong, T.; Runnebaum, R. C.; Brodwater, K.; Heelan, J.; Block, D. E.; Gates, B. C., *Energy Fuels*, **2014**, *28*, 1090-1096.
27. Maggi, R. and Delmon, B., *Stud. Surf. Sci. Catal.*, **1997**, *106*, 99-113.
28. Bykova, M.; Bulavchenko, O.; Ermakov, D.; Lebedev, M.; Yakovlev, V.; Parmon, V., *Catalysis in Industry*, **2011**, *3*, 15-22.
29. Sergeev, A. G.; Hartwig, J. F., *Science*, **2011**, *332*, 439-443.
30. Mortensen, P. M.; Grunwaldt, J. D.; Jensen, P. A.; Jensen, A. D., *ACS Catalysis*, **2013**, *3*, 1774-1785.
31. Zhao, C.; Kou, Y.; Lemonidou, A. A.; Li, X.; Lercher, J. A., *Chem. Commun*, **2010**, *46*, 412-414.
32. Bykova, M. V.; Ermakov, D. Y.; Kaichev, V. V.; Bulavchenko, O. A.; Saraev, A. A.; Lebedev, M. Y.; Yakovlev, V. A., *Appl. Cataly. B.*, **2012**, *113-114*, 296-307.
33. (a) Olcese, R. N.; Bettahar, M.; Petitjean, D.; Malaman, B.; Giovanella, F.; Dufour, A., *Appl. Catal. B*, **2012**, *115-116*, 63-73; (b) Olcese, R.; Bettahar, M. M.; Malaman, B.; Ghanbaja, J.; Tibavizco, L.; Petitjean, D.; Dufour, A., *Appl. Catal. B*, **2013**, *129*, 528-538; (c) Olcese, R. N.; Francois, J.; Bettahar, M. M.; Petitjean, D.; Dufour, A., *Energy & Fuels*, **2013**, *27*, 975-984; (d) Koyama, M., *Bioresour Technol*, **1993**, *44*, 209-215; (e) Koyama, M., *Mokuzai Gakkaishi*, **1995**, *41*, 1017-1021.
34. Emmett, P. H.; Skau, N., *J. Am. Chem. Soc.*, **1943**, *65*, 1029-1035.
35. Degnan Jr, T. F., *Topics in Catalysis*, **2000**, *13*, 349-356.
36. Ben, H.; Ragauskas, A. J., *ACS Sustain. Chem. Eng.*, **2013**, *1*, 316-324.
37. Gayubo, A. G.; Aguayo, A. T.; Atutxa, A.; Aguado, R.; Bilbao, J., *Ind. Eng. Chem. Res.*, **2004**, *43*, 2610-2618.
38. Furimsky, E.; Massoth, F. E., *Catal. Today*, **1999**, *52*, 381-495.
39. Laurent, E.; Delmon, B., *J. Catal.*, **1994**, *146*, 281-291.
40. Oelderik, J.; Sie, S.; Bode, D., *Appl. Catal.*, **1989**, *47*, 1-24.
41. Clauss, K.; Jensen, H., *Angew. Chem. Int. Ed.*, **1973**, *12*, 918-918.
42. (a) Subramanian, L. R.; Martinez, A. G.; Fernandez, A. H.; Alvarez, R. M., *Synthesis*, **1984**, *1984*, 481-485; (b) Saa, J. M.; Dopico, M.; Martorell, G.; Garcia-Raso, A., *J. Org. Chem.*, **1990**, *55*, 991-995; (c) Martinez, A. G.; Alvarez, R. M.; Aguirre, J. A.; Subramanian, L. R., *J. Chem. Soc., Perkin Trans. I*, **1986**, 1595-1598; (d) Subramanian, L.; García Martínez, A.; Herrera Fernandez, A.; Martínez Alvarez, R., *Synthesis*, **1984**, 481-485.
43. Cacchi, S.; Ciattini, P. G.; Morera, E.; Ortar, G., *Tetrahedron Lett.*, **1986**, *27*, 5541-5544.
44. Kotsuki, H.; Datta, P. K.; Suenaga, H., *Synthesis*, **1996**, *1996*, 470-472.
45. Mori, A.; Mizusaki, T.; Ikawa, T.; Maegawa, T.; Monguchi, Y.; Sajiki, H., *Chem Eur. J.*, **2007**, *13*, 1432-1441.
46. Mori, A.; Mizusaki, T.; Ikawa, T.; Maegawa, T.; Monguchi, Y.; Sajiki, H., *Tetrahedron*, **2007**, *63*, 1270-1280.
47. (a) Welch, S. C.; Walters, M. E., *J. Org. Chem.*, **1978**, *43*, 4797-4799; (b) Shono, T.; Matsumura, Y.; Tsubata, K.; Sugihara, Y., *J. Org. Chem.*, **1979**, *44*, 4508-

4511; (c) de Koning, C. B.; Michael, J. P.; van Otterlo, W. A. L., *Tetrahedron Lett.*, **1999**, *40*, 3037-3040; (d) Kenner, G. W.; Williams, N. R., *J. Chem. Soc. (Resumed)*, **1955**, 522-525; (e) Duclos Jr, R. I.; Lu, D.; Guo, J.; Makriyannis, A., *Tetrahedron Lett.* **2008**, *49*, 5587-5589; (f) De Koning, C. B.; Michael, J. P.; van Otterlo, W. A. L., *J. Chem. Soc., Perkin Trans. 1*, **2000**, 799-811.

Chapter 3 Results and Discussion for Activation of C_{arom}-O bonds in Lignin Model Compounds

Direct hydrogenolysis of phenol is difficult, and only achieved at high temperatures using catalysts discussed in chapter 2. As further evidence of this we tested the hydrogenolysis of guaiacol (5.0 g, 40.3 mmol) which was attempted using Pd/C (0.5 g, 10 wt. %) at 25 °C and 20 bar of hydrogen (Scheme 3.0.1). The reaction was operated for 72 hours.



Scheme 3.0.1

The reaction mixture was concentrated *in vacuo* and the crude products were analysed using ¹H and ¹³C NMR spectroscopy, and GC-MS, which indicated no reaction occurred and only starting material was recovered. Surprisingly during the reaction, 1.8 mol of hydrogen was taken-up, however a control reaction without substrate had a similar uptake, indicating that passive adsorption by the Pd/C catalyst the most likely scenario.¹ Based on the literature and our example it is clear that activation of the C_{arom}-O bond is required. Firstly, we looked into the formation and hydrogenolysis of metal phenoxides by reacting the phenol with alkaline metal halide, hydroxide or carbonate. Though potentially very cheap, unfortunately, the process was not successful. So the investigation proceeded to evaluate various activating groups, such as sulfites, sulfates, triflate, mesylates and tosylates that have been widely used for HDO, as described in the previous chapter. Since these methods were either unsuccessful or were expensive, atom inefficient or low yielding we examined tetrazolyl and cyanurate activation methods. The latter method was shown to have good process characteristics and was investigated in more detail. This chapter describes these studies in more detail.

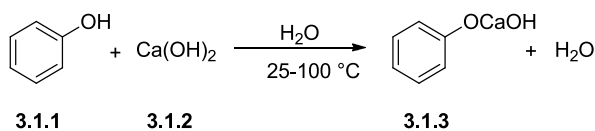
3.1 Metal guaiacolates

3.1.1 Calcium and iron guaiacolate

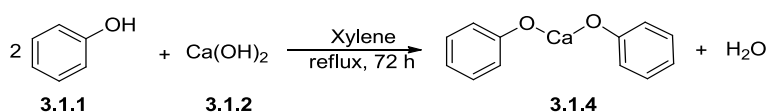
One of the cheapest ways in which to activate the guaiacol would be to make a calcium guaiacolate by reacting it with calcium carbonate (limestone) or calcium hydroxide.

The guaiacol is acidic and might be expected to react with the basic carbonate to generate a dimeric complex and carbon dioxide.

Some calcium phenolates have been prepared, of which hydroxycalcium phenoxide **3.1.3** and calcium diphenoxide **3.1.4** are known compounds reported by Schlosberg (Scheme 3.1.1).²



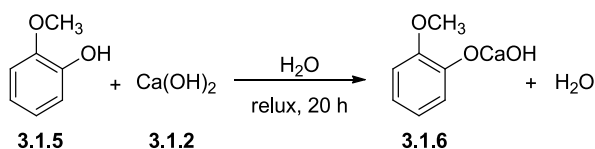
(a)



(b)

Scheme 3.1.1

The hydroxycalcium salt of guaiacol was prepared as shown in Scheme 3.1.2, using water as solvent and giving the product **3.1.6** as pink solid.



Scheme 3.1.2

The infrared (IR) spectrum was used to probe the completion of the reaction. The spectra of calcium hydroxide **3.1.2**, guaiacol and **3.1.6** are shown in Figure 3.1. The IR spectrum of guaiacol **3.1.5** shows a broad absorption at *ca.* 3400 cm⁻¹, characterised as the H-bonded OH group. The calcium hydroxide exhibits a sharp absorption at *ca.* 3600 cm⁻¹, which indicates the free hydroxyl groups. The absent absorption of the expected reaction product **3.1.6** at *ca.* 3400 cm⁻¹ and the appearance of the absorption at *ca.* 3600 cm⁻¹ show that the guaiacol hydroxyl group has been replaced by calcium salt. At the lower frequencies, the absorptions of **3.1.6** are similar to those of guaiacol.

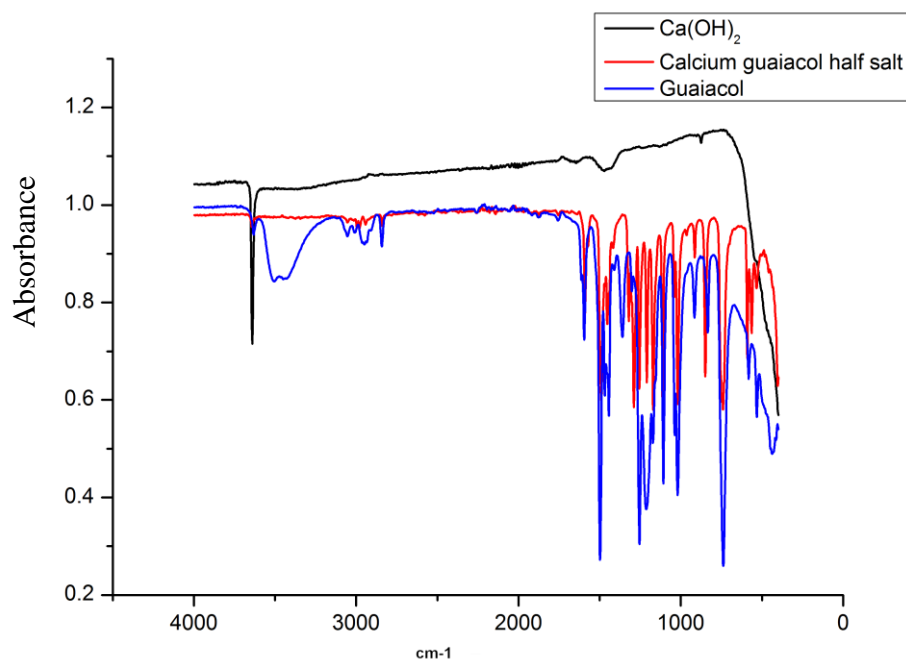
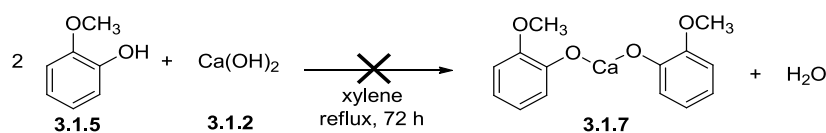
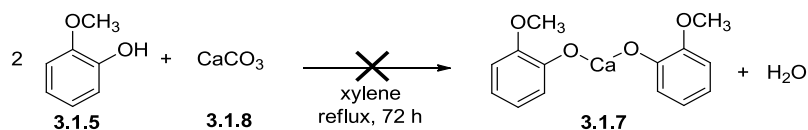


Figure 3.1 IR of calcium guaiacol half salt 3.1.6

The synthesis of calcium diguaiacolate **3.1.7** was attempted in organic media (Scheme 3.1.2a).³ Two equivalent of guaiacol was reacted with calcium hydroxide in refluxing xylenes for 72 hours.



(a)

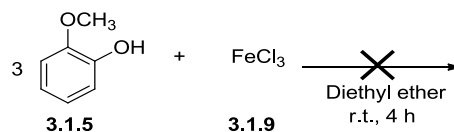


(b)

Scheme 3.1.2

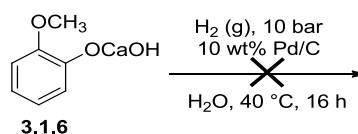
The product was analysed by ¹H NMR spectroscopy. Unfortunately the product was identified as starting material guaiacol **3.1.5** [δ = 7.09 (2H, m, CHAr), 6.92 (2H, m, CHAr), 5.61 (1H, s, OH), 3.85 (3H, s, OCH₃)]. Similarly, when calcium carbonate was reacted with guaiacol under the same conditions, only starting material could be identified as well (Scheme 3.1.2b).

An attempt to make the iron guaiacolate is shown in Scheme 3.1.3, however, guaiacol was recovered and no other products were achieved.



Scheme 3.1.3

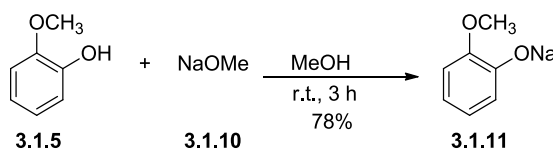
The hydrogenolysis of calcium guaiacolate **3.1.6** was attempted (Scheme 3.1.4), however, no reduction was observed.



Scheme 3.1.4

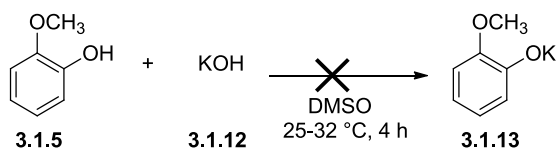
3.1.2 Sodium and potassium guaiacolate

Sodium guaiacolate **3.1.11** and potassium guaiacolate **3.1.13** were prepared as outlined in Scheme 3.1.5 and 3.1.6. Treating guaiacol **3.1.5** with sodium methoxide **3.1.10** gave sodium guaiacolate **3.1.11** as a white solid. ¹H NMR and IR spectroscopy were used to confirm its structure, which showed that the signal of the hydroxyl group had disappeared and gave a yield of with 78%.

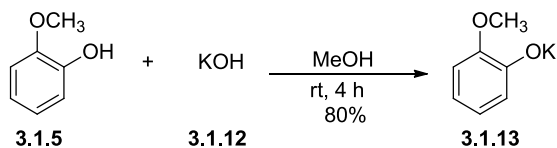


Scheme 3.1.5

The synthesis of potassium guaiacolate **3.1.13** using the procedure that Summerbell reported,⁴ where guaiacol is reacted with KOH in DMSO was unsuccessful, with only brown oily liquid being formed (Scheme 3.1.6a). However, treating a solution of guaiacol in methanol with KOH at room temperature gave the potassium phenolate **3.1.13** as a white solid. ¹H NMR and IR spectroscopy were used to confirm its structure in 80% yield.



(a)

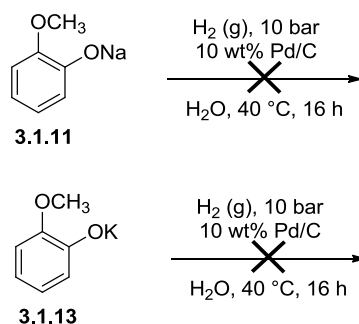


(b)

Scheme 3.1.6

Sodium guaiacolate **3.1.11** and potassium guaiacolate **3.1.13** are soluble in methanol, ethanol and water and insoluble in diethyl ether and petrol. Attempted crystallisation of guaiacولات **3.1.11** and **3.1.13** from methanol and diethyl ether/petrol led to immediate formation of fine white crystals. Better crystals were produced using the anti-solvent diffusion method, dissolving compound **3.1.11** or **3.1.13** (100 mg) in a mixture of methanol and diethyl ether in a 3.5 mL sample vial, itself placed within a second vial containing petrol and the outer tube sealed. After 4 weeks the solvent was removed and the compounds **3.1.11** and **3.1.13** were isolated as fine white needle-like crystals; however, the crystals were too small to get the x-ray structures.

The hydrogenolysis of sodium and potassium guaiacولات were attempted (Scheme 3.1.7), however, no reductions were observed.



Scheme 3.1.7

3.2 Activation of phenols *via* sulfite and sulfate compounds

3.2.1 Synthesis of guaiacol sulfite and sulfate

In Chapter 2, we reviewed the catalytic hydrogenation that removes phenolic hydroxyl groups from their sulfonic esters.⁵ Guan⁶ and Li⁷ have reported that

sulfate is a good leaving group for the activation of phenolic hydroxyl groups (Figure 3.2) and diphenyl sulfite has been made by Suh.⁸ It was hypothesised that the hydrodeoxygenation of diorganosulfates and diorganosulfites would occur resulting in the removal of oxygen from phenols and forming sulfuric acid.

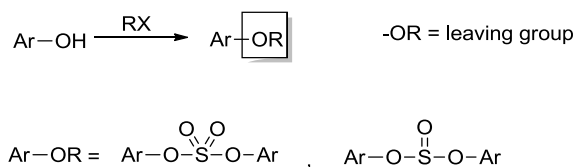
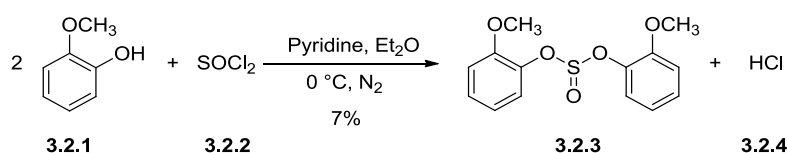


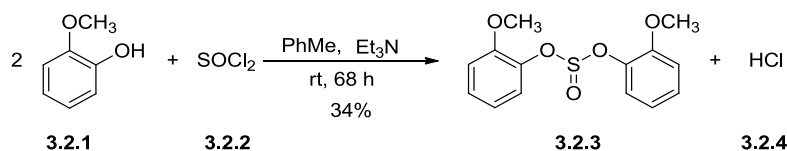
Figure 3.2 Leaving groups for the activation of phenolic hydroxyl group⁶

Using thionyl chloride and diethyl ether as solvent, diguaiacol sulfite **3.2.3** was prepared in a low yield (7%) in Scheme 3.2.1.



Scheme 3.2.1

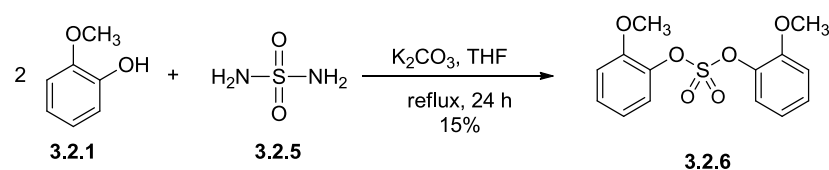
However, by modifying the reaction conditions; using toluene as the solvent and triethylamine (Et₃N) as the base as well as keeping the reaction at room temperature (23 °C), the yield of the desired product **3.2.3** was improved to 34% (Scheme 3.2.2). The reaction was monitored by thin layer chromatography (TLC). ¹H NMR, ¹³C NMR and HRMS spectroscopy were used to confirm the product structure. ¹H NMR (300 MHz, CDCl₃): δ = 7.23–7.17 (m, 4H, C4H/C5H), 6.97–6.90 (m, 4H, C3H/C6H), 3.81 (s, 6H, OCH₃). ¹³C NMR (75 MHz, CDCl₃): δ = 151.78, 137.95, 127.15, 124.21, 120.87, 112.56, 55.97. HRMS (ES+ mode): m/z = 317.0450 [100%, MNa⁺]; calculated for C₁₄H₁₄O₅S [MNa⁺]: m/z = 317.0454.



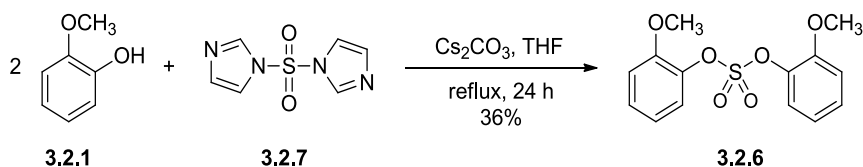
Scheme 3.2.2

Diguaiacol sulfate **3.2.6** was prepared by reacting guaiacol with sulfamide in the presence of potassium carbonate in refluxing THF with the reaction monitored by TLC. The product was obtained as a white solid in a 15% yield (Scheme 3.2.3a). It was found that sulfamide was insufficiently reactive leading to a poor yield, so an

active sulfone, *N,N'*-sulfuryldimidazole **3.2.7** was used.⁹



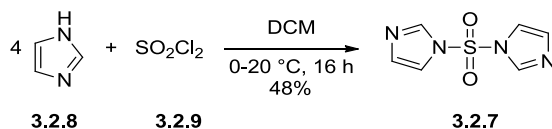
(a)



(b)

Scheme 3.2.3

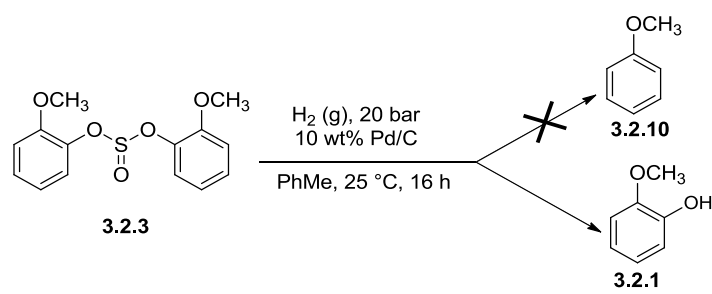
Compound **3.2.7** was prepared from sulfonyl chloride and an excess of imidazole **3.2.8** (Scheme 3.2.4). This method gave white needles in 48% yield. The ¹H NMR spectroscopic data agreed with that reported by Matthews.⁹ When **3.2.7** was reacted with guaiacol and Cs₂CO₃ as base, compound **3.2.6** was isolated with an improved 36% yield (Scheme 3.2.3b).⁶



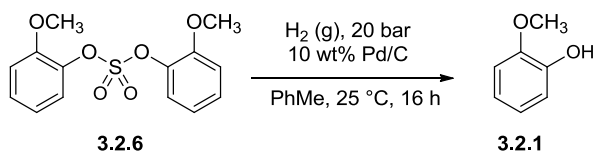
Scheme 3.2.4

3.2.2 Hydrodeoxygenation of guaiacol sulfite

Hydrodeoxygenation of diguaiacol sulfite **3.2.3** (3.00 g, 10.19 mmol) and diguaiacol sulphate **3.2.6** (1.00 g) was attempted over 10% Pd/C (5 wt%) at 25 °C with 20 bar of hydrogen (Scheme 3.2.5). The reaction mixture was concentrated *in vacuo* and the crude product analysed using GC-MS and ¹H NMR spectroscopy. Recovered guaiacol **3.2.1** was observed as the main component of the reaction mixture, indicating the S(O)-O bond is more labile than the Ar-O bond, which was clearly not the desired outcome.



(a)



(b)

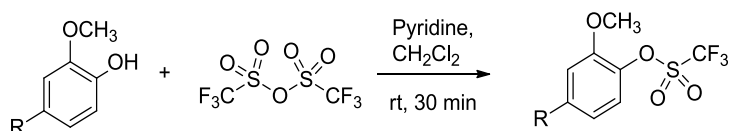
Scheme 3.2.5

3.3 Activation of phenols by sulfonate esters

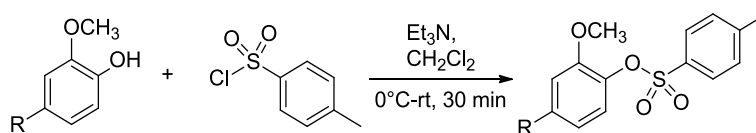
The synthesis and reduction of the guaiacol and vanillin sulfonates will be discussed and the hydrodeoxygenation of these compounds will be studied.

3.3.1 Synthesis of triflates, tosylates, and mesylates

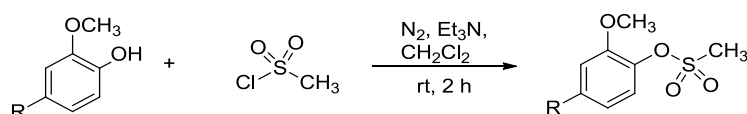
To investigate the hydrodeoxygenation of lignin monomer compounds, guaiacol, vanillin and others were converted into their sulfonates (triflates, tosylates and mesylates, in Scheme **3.3.1**).



(a)



(b)



(c)

Scheme 3.3.1

Table 3.1 Synthesis of aryl sulfonates from lignin monomers

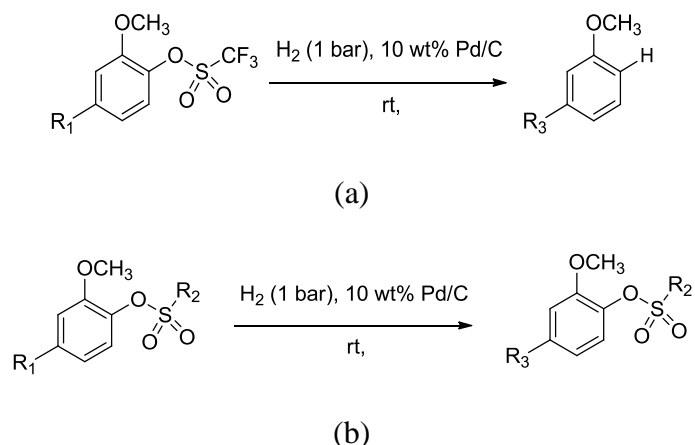
Entry	Compound	R	Yield %
a1	3.3.1	H	95
a2	3.3.2	CHO	60
b1	3.3.3	H	81
b2	3.3.4	CHO	71
c1	3.3.5	H	97
c2	3.3.6	CHO	62

Reaction conditions: lignin monomer (1 equiv.), sulfonate (1 equiv.), Pyridine or Et₃N (1.5–2 equiv.), solvent: DCM, 0 °C–rt, 30 min–2 hour

The guaiacol and vanillin triflates were prepared following Miura's method (Scheme 3.3.2a).¹⁰ Guaiacol and vanillin reacted with trifluoromethanesulfonic anhydride (1.5 equiv.) and pyridine (2 equiv.) in dichloromethane at room temperature respectively. The products were purified by flash column chromatography (petrol: EtOAc = 9:1) to produce 95% of **3.3.1** and 60% of **3.3.2**. Using triethylamine as the base and following the same procedure, guaiacol and vanillin were converted to tosylates and mesylates (compound **3.3.3–3.3.6**) with good yields (Table 3.1).¹¹ The electron-withdrawing effect of the aldehyde group makes the phenol hydroxyl group less nucleophilic, and this may have caused the lower yield of the vanillin sulfonates than that of the guaiacol sulfonates.

3.3.2 Hydrogenolysis of triflate, tosylate and mesylate

For the following catalytic hydrogenolysis, the reaction conditions were kept constant with 10 wt% Pd/C and 1 bar of hydrogen (balloon) at room temperature (Scheme 3.3.3).



Scheme 3.3.3

The cleavage of C–O bonds only occurred successfully in the aryl triflate compounds (Scheme 3.3.3a). Guaiacol triflate **3.3.1** gave 35% of anisole **3.3.7** as a deoxygenation product; the yield and optimal reaction time were determined by gas chromatography (GC) using an internal standard (Table 3.2). It is reported that the activity of aryl triflates hydrodeoxygenation could be reduced by introducing an electron donating group (–OCH₃) on the aromatic ring.¹² After 26 hours, no more anisole was produced in the reaction.

Table 3.2 Pd/C catalysed hydrogenolysis of aryl sulfonates

Entry	Aryl sulfonates	Main hydrogenolysis products	Compound	Yield %	Time (h)
a1	3.3.1	R ₃ =R ₁ =H	3.3.7	35	26
		R ₃ =R ₁ =CHO;	3.3.8	0	
a2	3.3.2	R ₁ =CHO, R ₃ =CH ₂ OH;	3.3.9	30	40
		R ₁ =CHO, R ₃ =CH ₃	3.3.10	70	
b1	3.3.3 (R₂=C₇H₇)	R ₃ =R ₁ =H	3.3.3	60	24
b2	3.3.4 (R₂=C₇H₇)	R ₁ =CHO, R ₃ =CH ₃	3.3.11	53	23
b3	3.3.5 (R₂=CH₃)	R ₃ =R ₁ =H	3.3.5	71	26
b4	3.3.6 (R₂=CH₃)	R ₁ =CHO, R ₃ =CH ₂ OH	3.3.12	81	25

Reaction conditions: aryl sulfonate (1 equiv.), 10 % Pd/C (10 wt%), solvent: EtOAc, rt, 24 hour-40 hour

Vanillin triflate **3.3.2** produced a mixture of hydrogenolysis products as a result of the reduction of the aldehyde, as well as triflate group (Figure 3.3). After 4 hours, less than 1% of 3-anisaldehyde **3.3.8** was produced as most of the benzaldehyde had been converted to 3-methoxybenzyl alcohol **3.3.9** (48%). Also, 3-methylanisole **3.3.10** was formed as determined from the product mixture by quantitative GC with a yield of 38%. These results indicate that cleavage of the C–OTf bonds and the reduction of the aldehyde group occurred at similar rates (route (1) in Scheme 3.3.4).

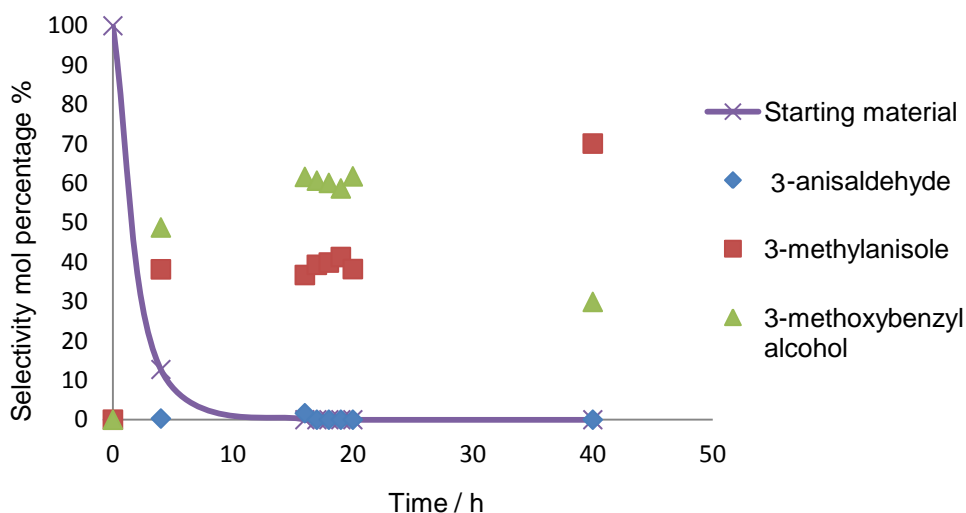
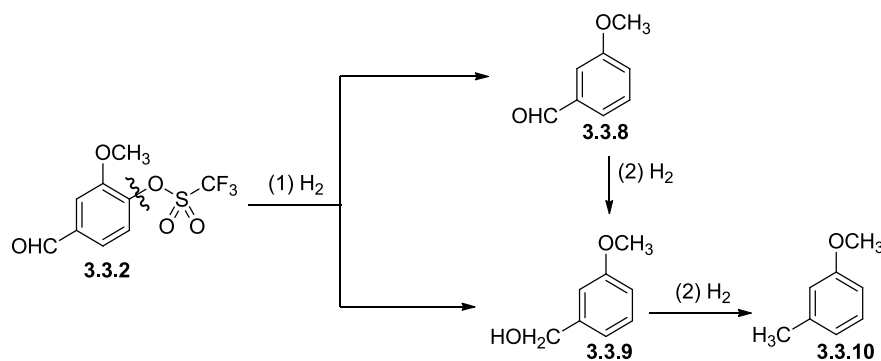


Figure 3.3 Product selectivity of vanillin triflate hydrogenolysis



Scheme 3.3.4 Pathways for the hydrogenolysis of vanillin triflate

After the reaction had been run for 20 hours, compound **3.3.9** was still the major product as the yield increased to 62%, whilst no more compound **3.3.10** was produced and none of compound **3.3.8** was found by GC. Unsurprisingly the benzaldehyde had been completely converted into benzyl alcohol. There are several pathways for the reduction of vanillin triflate **3.3.8**, which involve equilibria between the solution and catalyst surface. Direct formation of 3-methylanisole **3.3.10** may occur with several simultaneous reactions on the catalyst surface, or reactions in which the intermediates

are released from the catalyst into the bulk solution. Since the rates of each of these processes are different, the product compositions vary with time (Table 3.2). The reaction profile may be explained by higher rates of direct hydrogenation of vanillin triflate (**3.3.8**), which produced 38% **3.3.10** in the first 20 hours; and lower rates where the intermediates are released into solution and hydrogenated more slowly. In this way **3.3.2** is hydrodeoxygenated to **3.3.8** that is then reduced more slowly to **3.3.9**. The benzyl alcohol is more stable so accumulates, and is reduced more slowly to **3.3.10**, (route (2) in Figure 3.4). Similar benzaldehyde reduction has been reported by Saddi, Figure 3.4:¹³

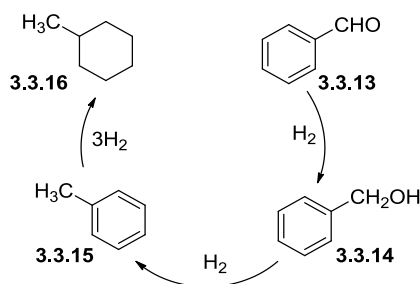
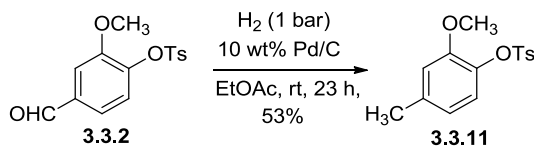


Figure 3.4 Hydrogenolysis of benzaldehyde over nickel catalysts supported on Al_2O_3 ¹³

The $\text{C}_{\text{arom}}\text{-O}$ bonds of aryl tosylates and mesylates are much stronger than the aryl triflates, with much less hydrogenolysis occurring under the same conditions (rt, 24 hour and 1 atmosphere of H_2). After hydrogenating the guaiacol sulfonates for 24 hours, no hydrogenated products were found by GC. By evaporating the solvent and analysing the residue using ^1H NMR spectroscopy, the following starting materials were recovered: guaiacol tosylates **3.3.3** (60%) and guaiacol mesylate **3.3.5** (71%). The remaining mass was unaccounted for.

^1H NMR and ^{13}C NMR spectroscopy indicate the hydrogenation of the aryl aldehyde to tolyl group. Evidence for this is the absence of an aldehyde group (^1H NMR $\delta = 9.97$ (s, 1H, CHO), ^{13}C NMR $\delta = 192.03$, (CHO)) and a new methyl group being formed (^1H NMR $\delta = 3.54$ (s, 3H, CH_3); ^{13}C NMR $\delta = 21.46$, CH_3), indicating the product **3.3.11** in 53% yield (Scheme 3.3.5).



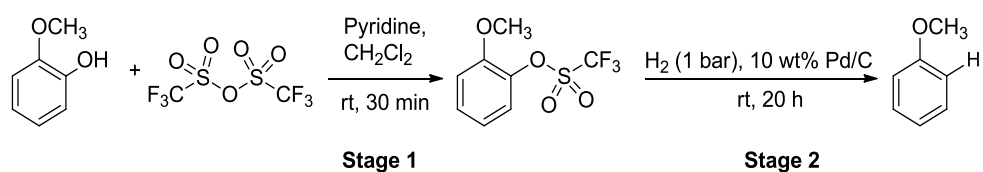
Scheme 3.3.5

Importantly no tosylate hydrogenolysis has occurred. In Chapter 2, we suggested that the unsuccessful reduction of aryl tosylate was due to the electron transfer from Pd(0) to the toluenesulfonyl benzene ring rather than the vanillin benzene ring.¹⁴

3.4 Conclusions

We have carried out experiments to investigate the reduction of guaiacol metal and sulfonate derivatives, and these were unsuccessful. Whilst guaiacol disulfite and guaiacol disulfate compounds were made, hydrodeoxygenation reaction occurred at 25 °C and 20 bar H₂ for 16 hours. Lignin monomer compounds were then transformed to a range of corresponding sulfonate derivatives and subjected to hydrodeoxygenation, with 10 wt% Pd/C at room temperature and 1 atmosphere of H₂. It was found that neither aryl tosylates nor mesylates could remove the phenolic hydroxyl group effectively and only aryl triflates afforded deoxygenated products. For example anisole was generated from guaiacol triflates in 35% yield and 3-methylanisole is the main product of vanillin triflate hydrogenolysis. Despite the triflate activation of C_{arom}-O bonds, this process is inefficient with low yields and low atom economy of 44%. Moreover, the bulk cost of trifluoromethanesulfonic anhydride is prohibitively high for industrial application, >£45/kg. A rough material cost was estimated in Table 3.3.

Table 3.3 Estimated material cost for the hydrogenolysis of guaiacol triflate



Stage 1

Yield %	95.00					
Material	M Wt	% w/w Strength	m/m	Usage Kg/Kg of stage	Price £/Kg	Cost per Kg Stage
Guaiacol	124.00	100.00	1.00	0.51	1.00	0.51
Trifluoromethanesulfonic anhydride	282.00	100.00	1.50	1.74	45.00	78.27
Pyridine	79.00	100.00	2.00	0.65	3.00	1.95
Effluent				1.90	0.20	0.38
Product RMM =	256.00				Total	81.11

Stage 2:

Yield %	35.00					
Material	M Wt	% w/w Strength	m/m	Usage Kg/Kg of stage	Price £/Kg	Cost per Kg Stage
Stage 1	256.00	100.00	1.00	6.77	81.11	549.30
Pd/C	106.40	100.00	0.04	0.12	40.00	4.73
hydrogen	2.00	100.00	10.00	0.53	0.10	0.05
Effluent				6.42	0.20	1.28
Product RMM =	108.00				Total	555.37

The price of anisole is extremely high, which makes this process unfavourable. Table 3.3 shows that most of the cost is caused by the step of activating hydroxyl group. Therefore, more economic and greener processes needed to be found.

3.5 References

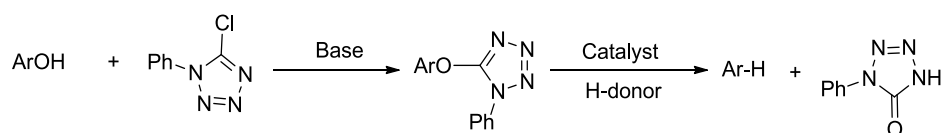
1. Simnick, J. J.; Sebastian, H. M.; Lin, H. M.; Chao, K. C., *J. Chem. Eng. Data*, **1978**, *23*, 339-340.
2. Schlosberg, R. H.; Scouten, C. G., *Energy Fuels*, **1988**, *2*, 582-585.
3. Gooßen, L. J.; Gooßen, K.; Stanciu, C., *Angew. Chem. Int. Ed.*, **2009**, *48*, 3569-3571.
4. Summerbell, L. J., *J. Chem. Soc.*, **1934**, 992-996.
5. Clauss, K.; Jensen, H., *Angew. Chem. Int. Ed.*, **1973**, *12*, 918-918.
6. Guan, B.; Lu, X.; Zheng, Y.; Yu, D.; Wu, T.; Li, K. I.; Li, B.; Shi, Z., *Org. Lett.*, **2009**, *12*, 396-399.
7. Li, B. J.; Yu, D. G.; Sun, C. L.; Shi, Z. J., *Chem. Eur. J.*, **2011**, *17*, 1728-1759.
8. Suh, J.; Koh, D.; Min, C., *J. Org. Chem.*, **1988**, *53*, 1147-1153.
9. Macielag, M. J.; Matthews, J. M.; McNally, J. J.; Xia, M., Imidazo [1, 2-a] pyridine sulfonamides as trpm8 modulators, Patent WO2012078994 A1, **2012**.
10. Miura, M.; Koike, T.; Ishihara, T.; Hirayama, F.; Sakamoto, S.; Okada, M.; Ohta, M.; Tsukamoto, S. I., *Synth. Commun.*, **2006**, *36*, 3809-3820.
11. (a) Wan, W.; Wang, P.; Jiang, H. Z.; Hao, J., *Mol. Cryst. Liq. Cryst.*, **2008**, *482*, 42-56; (b) Fujikawa, N.; Ohta, T.; Yamaguchi, T.; Fukuda, T.; Ishibashi, F.; Iwao, M., *Tetrahedron*, **2006**, *62*, 594-604.
12. Sajiki, H.; Mori, A.; Mizusaki, T.; Ikawa, T.; Maegawa, T.; Hirota, K., *ChemInform*, **2006**, *37*, 987-990.
13. Saadi, A.; Merabti, R.; Rassoul, Z.; Bettahar, M. M., *J. Mol. Catal. A: Chem.*, **2006**, *253*, 79-85.
14. Mori, A.; Mizusaki, T.; Ikawa, T.; Maegawa, T.; Monguchi, Y.; Sajiki, H., *Chem. Eur. J.*, **2007**, *13*, 1432-1441.

Chapter 4 Removing phenolic hydroxyl groups with strong electron-withdrawing groups

Chapter 4 explores the use of heterocyclic compounds to activate the phenolic hydroxide group in guaiacol towards hydrodeoxygenation. It was expected that the reductive cleavage of the C_{arom}-O bond in the heterocyclic ethers would be more favourable. This is due to the ability of the heterocyclic system to delocalize the oxygen lone-pair electrons of the phenol group and, hence, reduce the electron density of the guaiacol aromatic ring.

4.1 Synthesis and hydrogenolysis of tetrazoles

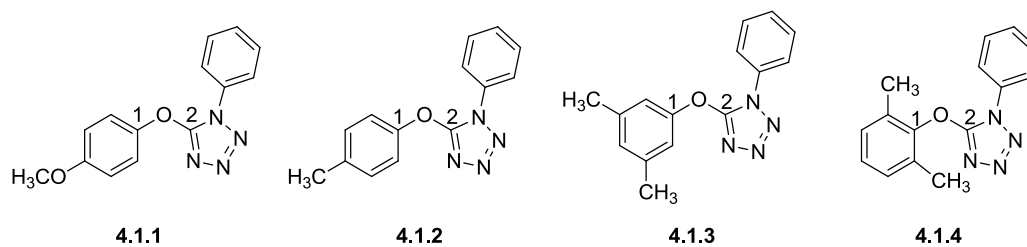
Alkoxy and benzyloxy derivatives of tetrazoles have been shown to be effective derivatives for the removal of phenolic hydroxide groups *via* catalytic hydrogenolysis (Scheme 4.1.1).¹ However this system has not been applied to phenolic compounds derived from lignin such as guaiacol or vanillin.



Scheme 4.1.1

The bond length of the phenolic C–O bond is 1.37 Å, which is shorter than an aliphatic single C–O bond (1.43 Å), but it is longer than a C=O double bond (1.23 Å).^{1b} The electron-withdrawing effect of tetrazole can weaken the aromatic C–O bond, encouraging its cleavage. Alves examined the changes of the bond lengths and bond angles of the tetrazole compounds using X-ray crystallography.^{1b} The studies showed that by converting phenols into 5-aryloxy-1-phenyltetrazole ethers, the original aromatic C–O bond length increased from 1.33 Å to 1.42 Å, whereas, the C–O bond length between the tetrazole carbon and the ether oxygen is shorter (*ca.* 1.33 Å). The bond energy of the phenolic C–O bond was decreased from 460 kJ·mol⁻¹ to 350 kJ·mol⁻¹ by coupling with the strong electron-withdrawing tetrazolyl group so that the phenolic C-O bond is expected to be broken easily.

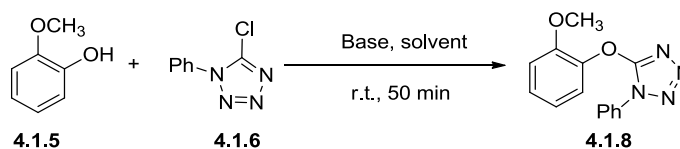
Table 4.1 Bond lengths and bond angles of some 5-aryloxy-1-phenyltetrazole ethers^{1b}



Ether	C ¹ -O bond length / Å	C ² -O bond length / Å	C ¹ -O-C ² bond angles / °
4.1.1	1.434	1.335	116.4
4.1.2	1.415	1.329	122.2
4.1.3	1.423	1.331	117.8
4.1.4	1.428	1.333	116.5

4.1.1 Synthesis of 5-(2-methoxy-phenoxy)-1-phenyl-1*H*-tetrazole

The 5-(2-methoxy-phenoxy)-1-phenyl-1*H*-tetrazole **4.1.8** was prepared for further investigations towards a catalysed hydrogenolysis process of guaiacol **4.1.5**. Guaiacol **4.1.5** was reacted with 5-chloro-1-phenyl-1*H*-tetrazole **4.1.6** in the presence of potassium *tert*-butoxide **4.1.7** in DMF using the procedure which has been reported by Entwistle and gave ether **4.1.8** in a poor 32% yield.^{1a} Switching to xylene as the solvent did not improve the yield. However, using K₂CO₃ as the base and the greener solvent acetone as the solvent gave the ether **4.1.8** in an improved yield (75%).² ¹H NMR spectroscopy was used to confirm its structure.²

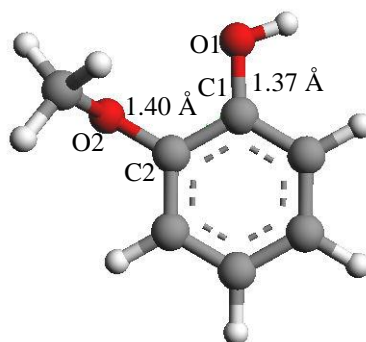


Scheme 4.1.2^{1a, 2}

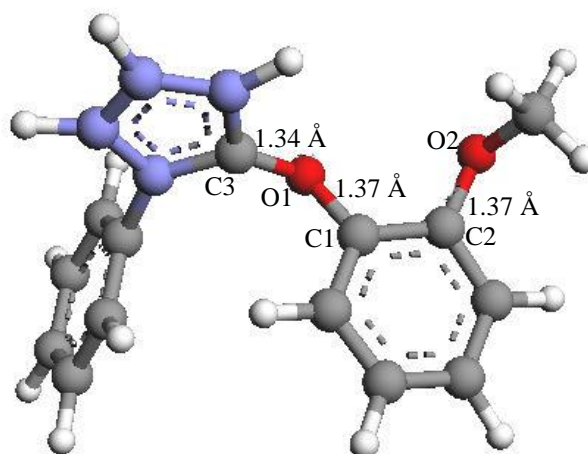
Table 4.2 Reaction conditions for synthesis of tetrazole compound

Entry	Base	Solvent	Yield %
1	t BuOK	DMF	32
2	K ₂ CO ₃	Acetone	75

The bond lengths of guaiacol **4.1.5** and tetrazole **4.1.8** were calculated using ‘ArgusLab’ software (Figure 4.1). The model showed that the phenyltetrazolyl ether bond is stronger (bond length 1.34 Å) than the aromatic C–O bond (bond length 1.37 Å). We envisaged that the presence of the electron-withdrawing tetrazole in **4.1.8** would facilitate the hydrogenolysis of guaiacol.



(a) guaiacol 4.1.5



(b) tetrazole compound 4.1.8

Figure 4.1 Molecular modelling of guaiacol and 5-(2-methoxy-phenoxy)-1-phenyl-1*H*-tetrazole 4.1.8

Also, compound **4.1.8** was made by the method described earlier (Scheme 4.1.2) and the crystals obtained were used to determine molecular structure (Figure 4.2), which corresponds to the modelling results.

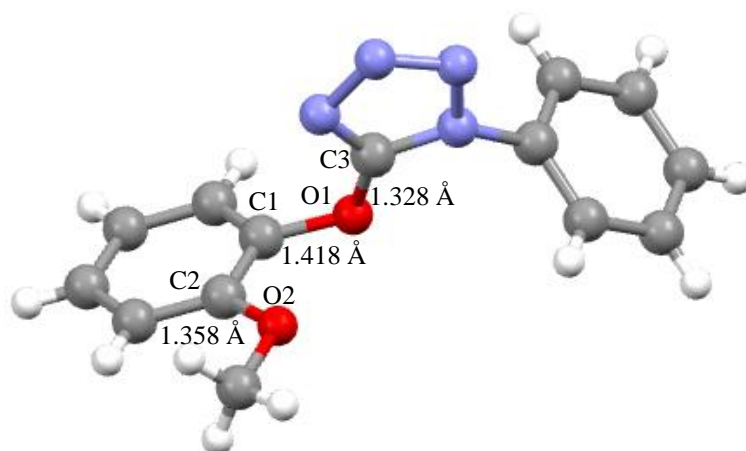
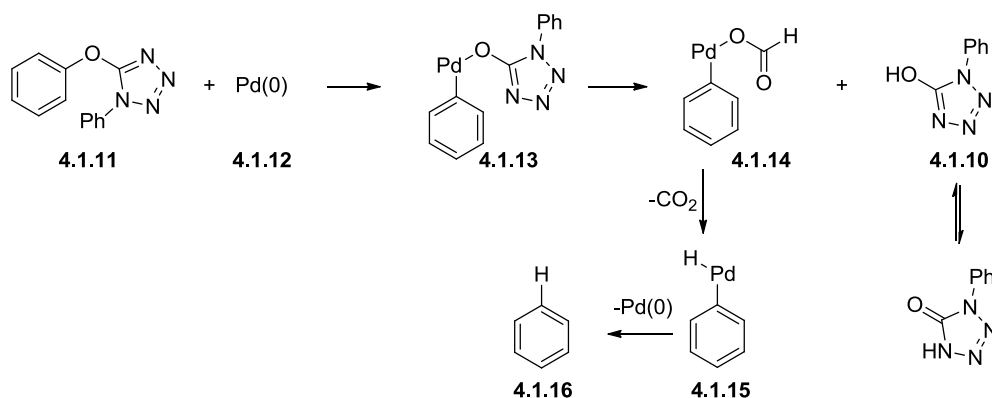


Figure 4.2 X-ray structure of 5-(2-methoxy-phenoxy)-1-phenyl-1H-tetrazole 4.1.8

4.1.2 Catalytic hydrogenolysis of 5-(2-methoxy-phenoxy)-1-phenyl-1H-tetrazole

4.1.2.1 Hydrogen transfer hydrogenolysis

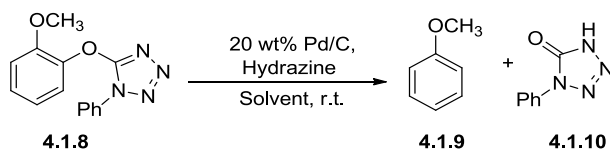
In transfer hydrogenolysis the molecular hydrogen was replaced by a hydrogen donor, which showed a selective and rapid approach in converting phenols to arenes. The mechanism of catalytic transfer hydrogenolysis of phenol is shown below:



Scheme 4.1.3³

We investigated the catalytic transfer hydrogenation of tetrazole **4.1.8** using the general procedure with hydrazine as the reductant (Scheme 4.1.4).² The effects of the different kinds of solvents were examined (Table 4.3). The reactivity of various hydrogen donors, catalyst type and catalyst amounts were also investigated (Table 4.4). The products were analysed by GC-MS, however, compared to a quantitative standard anisole, the peak areas were very small indicating < 5% yields. Furthermore a

trace of anisole was detected in the xylene solvent used for this reaction, indicating even the low level of anisole found may not be due to hydrogenolysis of the tetrazole **4.1.8**. When hydrazine was replaced by sodium phosphinate as the hydrogen donor, only the starting material **4.1.9** was found as the main component in the reaction mixture by TLC and ^1H NMR.



Scheme 4.1.4

Table 4.3 Solvent effects on the production

Entry	Solvent	Product yield (%)
1	Xylene	n/a
2	Acetone	<5%
3	C ₇ H ₈ /EtOH/H ₂ O (7:3:2)	<5%
4	C ₆ H ₅ OH/EtOH/H ₂ O (7:3:2)	<5%

No hydrogenolysis occurred when xylene was used as the solvent. Although tetrazole **4.1.8** is very soluble in xylene, since most hydrogen donors are water soluble either a water miscible solvent was employed to make it a single-phase or an aqueous-organic bi-phase was used. In either case the product can be readily separated from reaction mixture by simple extraction.

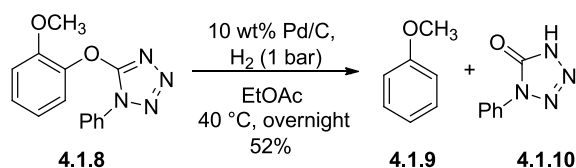
Table 4.4 Transfer hydrogenation of tetrazole with different hydrogen donor and catalysts

Entry	Hydrogen donor	Catalyst (wt%)	Yield %
1	Hydrazine	Pd/C (10%)	0
2	Hydrazine	Pd/C (20%)	<5
3	Hydrazine	Pt/C (10%)	0
4	Hydrazine	Pt/C (20%)	0
5	Sodium phosphinate	Pd/C (10%)	0
6	Sodium phosphinate	Pd/C (20%)	0
7	Sodium phosphinate	Pt/C (10%)	0
8	Sodium phosphinate	Pt/C (20%)	0

Reaction conditions: tetrazole (1 equiv.), hydrogen donors (3 equiv.), solvent: C₆H₅OH/EtOH/H₂O (7:3:2), rt, overnight.

Hydrazine and sodium phosphinate were examined as hydrogen donors. The only indication of any transfer reduction was with hydrazine using 20 wt% Pd/C catalyst. Entwistle has shown that palladium is the only active heterogeneous catalyst in the transfer hydrogenation of phenol using formate.^{1a}

4.1.2.2 H₂ (gas) hydrogenolysis



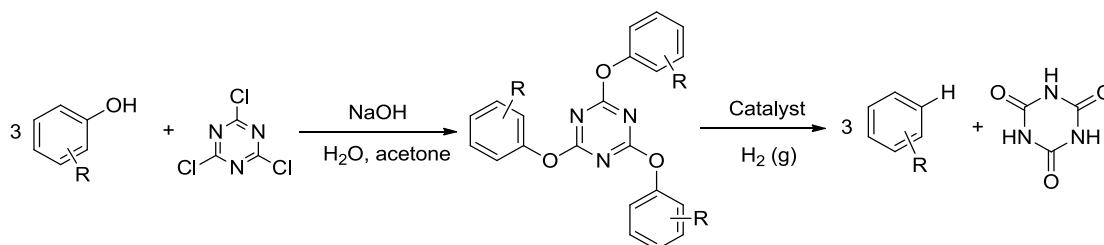
Scheme 4.1.5

In our work we tested the use of 10 wt% of Pd/C and hydrogen gas at atmospheric pressure with guaiacol tetrazole **4.1.8** (Scheme 4.1.5). The product was analysed by quantitative GC with an internal standard: anisole **4.1.9** was obtained in a 52% yield after an overnight hydrogenation. Unreacted starting material was recovered (40 %) after separating the product and evaporating the solvent. The conclusion of these experiments is that this process is not industrially viable because of the low yields

(<5%), unsuitable reductants (hydrazine, sodium phosphinate), high atom inefficiency (42%), and high cost of 5-chloro-1-phenyl-1*H*-tetrazole (£4,000/ kg).

4.2 Synthesis of tri-substituted triazines from lignin monomer compounds

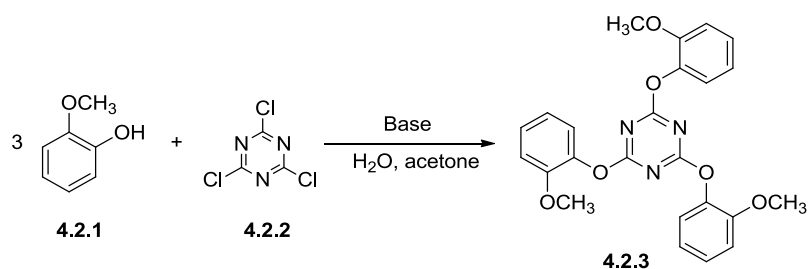
Another heterocyclic compound, cyanuric chloride, has the potential to overcome the limitations exhibited by tetrazole. High yields of 2,4,6-triaryloxy-1,3,5-triazines have been obtained *via* reaction of cyanuric chloride and phenols in water/actone.⁴ Cyanuric chloride is a far cheaper reagent (£1/kg in bulk) than the tetrazole. It is made by trimerisation of cyanogen chloride made from chlorine and hydrogen cyanide. Furthermore only one third of an equivalent of cyanuric chloride is needed for one equivalent of guaiacol. The atom efficiency of phenol hydrogenolysis to benzene done this way is 50%. If the cyanuric acid by-product can be recycled this increases to 76% (Scheme 4.2.1).



Scheme 4.2.1

4.2.1 Synthesis of guaiacolate-cyanurate complex (1,3,5-triazines)

2,4,6-*tris*(2-methoxyphenoxy)-1,3,5-triazine **4.2.3** was synthesised by using the procedure Forbes reported, in which guaiacol **4.2.1** (3 equivalents) was reacted with cyanuric chloride **4.2.2** (1 equivalent) in the presence of base (Scheme 4.2.2).⁵ A mixture of water/acetone was used as the solvent. The formed guaiacol salt was soluble in water. Acetone was used to introduce cyanuric chloride into the aqueous phase. The reaction was dependent on the pH and temperature. High pH was more effective than the lower pH solutions. Owing to the exothermic reaction, the reaction temperature was controlled at 0–5 °C in the method demonstrated by Forbes.⁵ However, a higher yield of product could be obtained by running the reaction at 25 °C (see Table 4.5). The product was analysed by ¹H NMR and ¹³C NMR spectroscopy and HRMS.



Scheme 4.2.2

Table 4.5 pH and temperature influence on the effectiveness of cyanuric chloride reaction

Entry	Base	pH	Temperature / °C	Time / h	Yield%
1	NaOH	14	0-5	5	80
2	NaOH	14	25	5	86
3	Na ₂ CO ₃	10.5	0-5	5	67
4	Na ₂ CO ₃	10.5	25	5	77

The bond length of 2,4,6-tris(2-methoxyphenoxy)-1,3,5-triazine **4.2.3** was modelled by ‘ArgusLab’ software (Figure 4.3). The aromatic C–O bond length increased from 1.37 Å (Figure 4.1a) to 1.41 Å for all three bonds. The C–O bond to the central heterocyclic ring is 1.35 Å as well as is symmetric for all three groups (i.e. the structure is symmetric).

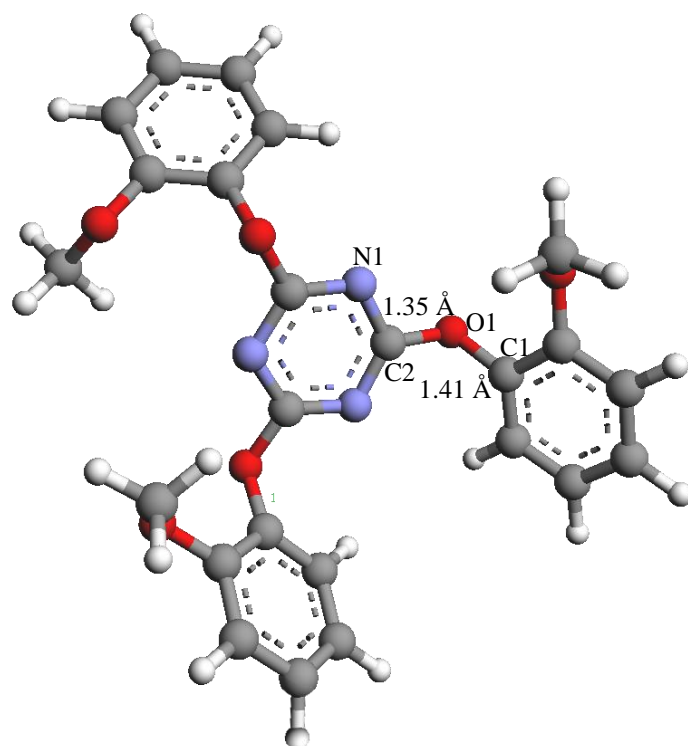


Figure 4.3 Molecular modeling of 2,4,6-*tris*(2-methoxyphenoxy)-1,3,5-triazine (4.2.3)

The crystal structure and C–O bond length of compound **4.2.3** was determined and is shown in Figure 4.4. The bond lengths of **4.2.3** correspond to the modelling prediction (in Figure 4.3). The crystal structure illustrates that the aromatic C–O bond is weaker than the heterocyclic ether bond, which means that it should subsequently be cleaved using our hydrogenolysis process.

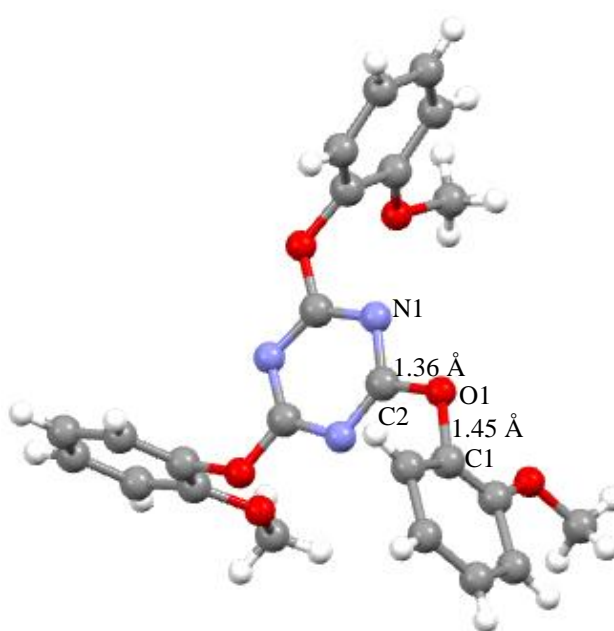


Figure 4.4 X-ray structure of 2,4,6-*tris*(2-methoxyphenoxy)-1,3,5-triazine 4.2.3

4.2.2 Synthesis of trisubstituted-1,3,5-triazines by lignin monomers

A range of 2,4,6-trisubstituted-1,3,5-triazine derivatives were prepared using the following procedure: 1 equivalent of cyanuric chloride (**4.2.2**) in acetone was reacted with 3 equivalents of the sodium salts of phenols in aqueous acetone at room temperature for 3 hours.⁶ Using this method, lignin monomer compounds were converted into the desired trisubstituted-1,3,5-triazine derivatives in moderate to good yields (Table 4.5). The products were analysed by ¹H NMR, ¹³C NMR spectroscopy and HRMS.

Steric effects

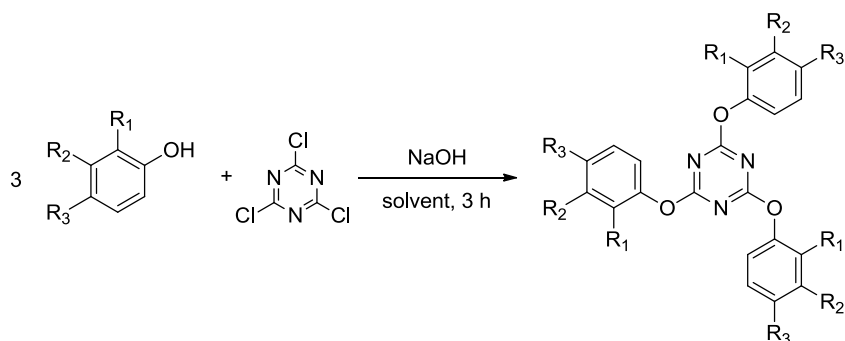
The reactions of 2-methoxy substituted phenols ($R_2 = \text{OCH}_3$) **4.2.1**, **4.2.12**, **4.2.16** and **4.2.20** gave lower yields than those that have no *ortho*-methoxy group (**4.2.4**, **4.2.10**, **4.2.14** and **4.2.18**, see table 4.6), which indicates that the steric effects are operating.^{6a} The steric hindrance in the synthesis of triaryloxy-1,3,5-triazines (**4.2.7** and **4.2.9**) is relieved when the methoxy group is *para* (**4.2.8**) or *meta* (**4.2.6**) in the attacking phenolate and 92% yields were achieved with either regioisomer. The reaction occurs by the $\text{S}_{\text{N}}\text{Ar}$ mechanism and the tetrahedral intermediate may be crowded with the *ortho*-substituent making this higher energy and product formation less favourable.

Electronic effects

It was found that electronic effects are minor when there is a methoxy substituent in the *para* or *meta* position of phenol. However an electronic effect may be in operation when the reaction yield of phenol is compared with the substituted phenolates. Methoxy is a strongly electron donating group, that back-donates electrons from its lone pairs into the aromatic ring, which makes the phenolate a strong nucleophile. On the contrary, electron withdrawing groups (e.g. CHO, CO₂CH₃ and CO₂H) reduce the electron density on the oxygen atom, which results in poorer nucleophilic substitution. This might account for the lower yields. Good yields of the triazines were achieved 4-hydroxybenzaldehyde (**4.2.10**), vanillin (**4.2.12**), and 4-hydroxybenzoate (**4.2.18**).

The esters methyl 4-hydroxybenzoate (**4.2.14**) and methyl vanillate (**4.2.16**) were insoluble in water and when dissolved in THF with NaOH, the base caused ester hydrolysis. Using an excess of DIPEA base in THF at reflux resulted in poor yields of **4.2.15** and **4.2.17** were achieved, 66% and 33% respectively. Again, the electron withdrawing effects of the CO₂H and CO₂CH₃ groups may reduce the nucleophilicity

of the phenol anion and therefore reducing its participation in the desired S_NAr reaction.⁷



Scheme 4.2.3

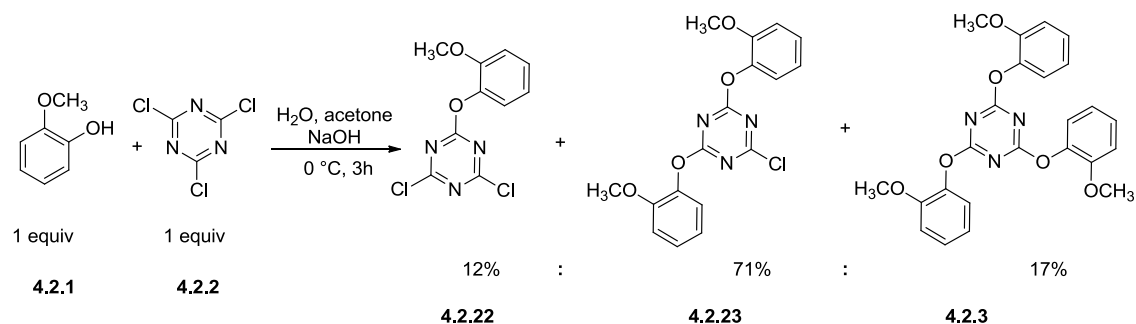
Table 4.6 Synthesis of trisubstituted-1,3,5-triazines by lignin monomers

Entry	Compound	R ₁	R ₂	R ₃	Base	Solvent	Condition	Yield %	Product
1	4.2.4	H	H	H	NaOH, 3 equiv	H ₂ O/acetone	rt, 3h	89	4.2.5
2	4.2.1	OCH ₃	H	H	NaOH, 3 equiv	H ₂ O/acetone	rt, 3h	86	4.2.3
3	4.2.6	H	OCH ₃	H	NaOH, 3 equiv	H ₂ O/ acetone	rt, 3h	92	4.2.7
4	4.2.8	H	H	OCH ₃	NaOH, 3 equiv	H ₂ O/ acetone	rt, 3h	92	4.2.9
5	4.2.10	H	H	CHO	NaOH, 3 equiv	H ₂ O/ acetone	rt, 3h	85	4.2.11
6	4.2.12	OCH ₃	H	CHO	NaOH, 3 equiv	H ₂ O/ acetone	rt, 3h	62	4.2.13
7	4.2.14	H	H	COOCH ₃	DIPEA, 3 equiv	THF	reflux, 5h	66	4.2.15
8	4.2.16	OCH ₃	H	COOCH ₃	DIPEA, 3 equiv	THF	reflux, 5h	33	4.2.17
9	4.2.18	H	H	COOH	NaOH, 6 equiv	H ₂ O/ acetone	rt, 3h	76	4.2.19
10	4.2.20	OCH ₃	H	COOH	NaOH, 6 equiv	H ₂ O/ acetone	rt, 3h	71	4.2.21

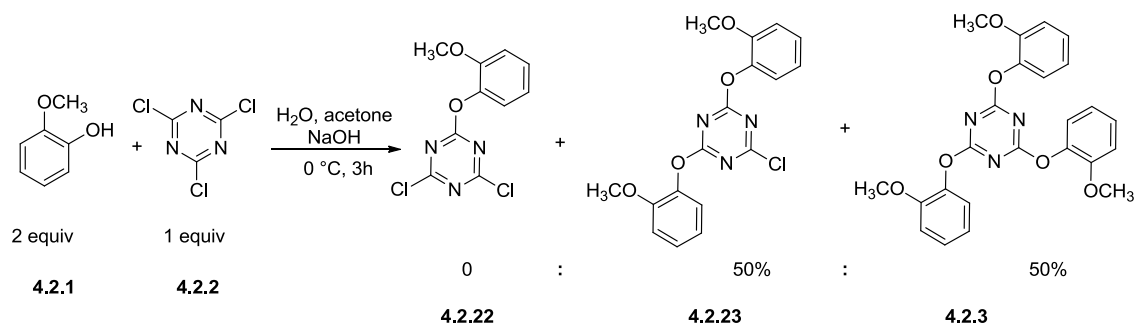
4.2.3 Reaction mechanism

Since formation of the tri-substituted cyanurate must involve formation of first the singly then doubly-substituted species, we wanted to understand why they were not

observed and therefore their rates of formation. Reactions of cyanuric chloride were carried out with 1 equivalent and 2 equivalents guaiacol (Scheme 4.2.4). A similar procedure to that for tri-substitution was employed: the reaction mixture was stirred at 0 °C for three hours. The products were analysed by ^1H , ^{13}C NMR and LC-MS. We tried to monitor the reaction by on-line Raman spectroscopy, however significant peak changes were too difficult to identify.



(a)



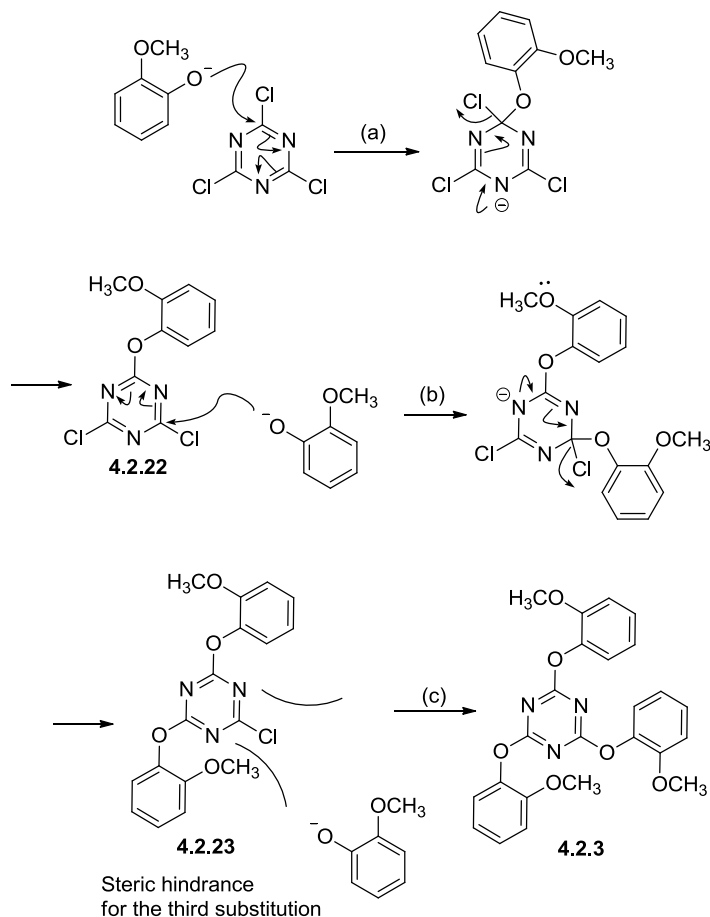
(b)

Scheme 4.2.4 Reactions of cyanuric chloride react with 1 equivalent and 2 equivalents guaiacol

The obtained products in Scheme 4.2.4a were analysed by LC-MS. Only 12% of product **4.2.22** was determined in the product mixture. On the other hand, disubstitutions contributed to the dominant product (**4.2.23**, 71%) in this reaction as well as small amount of trisubstituted product (**4.2.3**, 17%). As with the NMR results, a mixture of products was also shown to occur in both reactions, however, we were unable to identify these three products because of their comparable structures. After 2 equivalents of guaiacol were mixed with the cyanuric chloride solution at 0 °C for three hours, di- and trisubstituted products (**4.2.23** and **4.2.3**) were formed in the

reaction (50% and 50% respectively), without producing any mono substituted product **4.2.22**.

The steric effect does not seem to impact upon the second substitution. However, when the third substitution occurred, the steric hindrance affects the formation of the product (Scheme 4.2.5).



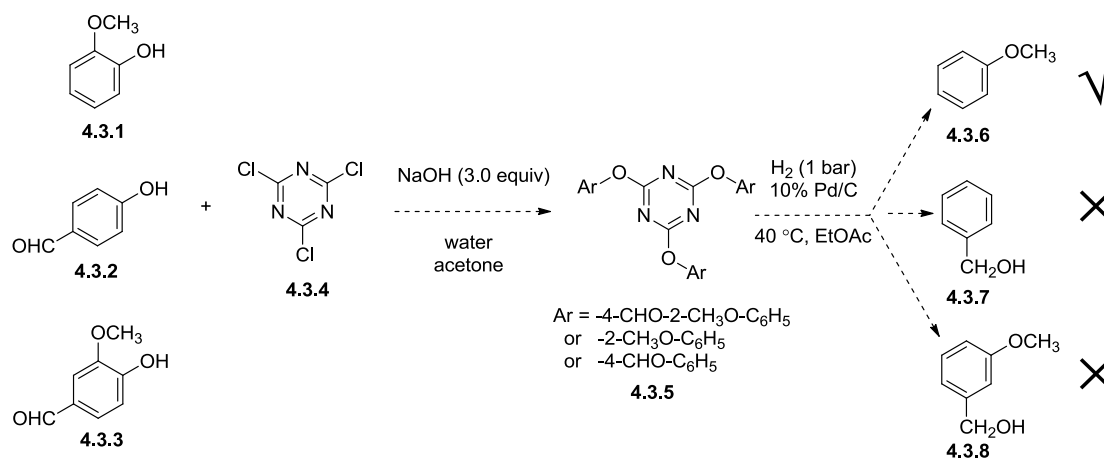
Scheme 4.2.5 Possible mechanism for the formation of trisubstituted triazines

When the first substitution occurs the methoxy group on the phenol can donate electrons into the triazine ring thereby diminishing its electrophilicity and hence diminishing the rate of the second nucleophilic addition. The rate of the third nucleophilic substitution is determined by the even lower electrophilicity of the disubstituted product **4.2.23** together with an increased steric hindrance. Only if > 2 equivalents guaiacol is added does the triply-substituted product **4.2.3** form as the main product. Therefore, reaction (c) is the rate limiting step (Scheme 4.2.5).

4.3 Mixed phenol addition – “the lignin soup model”

Pyrolysis oil or residual lignin from the Kraft cooking process is made up of a complex mixture of hydroxyl-substituted aromatic compounds. We investigated our two step

derivatisation-hydrogenolysis process on a synthetic mixture of monomers likely to come from lignin digestion from the Kraft pulping process, which we called ‘lignin soup’.



Scheme 4.3.1

A mixture of lignin monomer compounds, guaiacol **4.3.1** (1 equiv.), 4-hydroxybenzaldehyde **4.3.2** (1 equiv.) and vanillin **4.3.3** (1 equiv.) were reacted with cyanuric chloride (1 equiv.). The crude product was analysed by ¹H NMR spectroscopy and TLC. A mixture of the products was produced as a result of different activities of the three substrates. As we have discussed earlier (page 75 and 76), steric hindrance and electronic effects have a significant influence on this reaction and these impacted upon the complex mixture observed.

Without separating the mixture it was subjected directly to hydrogenolysis. The mixed product was analysed by TLC, GC-MS, ¹H NMR and ¹³C NMR spectroscopy. Based on the TLC results it could be seen that new compounds were formed, and a trace of anisole was found by GC-MS but none of the other desired products (**4.3.7**, **4.3.8** or other hydrogenated products produced by the reduction of vanillic triazine and 4-hydroxybenzaldehyde triazine) were present. Unfortunately, this mixture of products was difficult to separate and characterise by NMR spectroscopy. It would be worthwhile carrying out further work, as this approach is likely to be close to an industrial bio-refinery process.

4.4 Conclusions

The use of heterocycles as activating agents for the hydrodeoxygenation of guaiacol was investigated. A guaiacol adduct of tetrazole **4.1.8** was produced by reacting guaiacol and tetrazolyl chloride. The crystal structure and molecular modelling of this

compound provided evidence that the C_{arom}-O bond could be activated by the strongly electron-withdrawing group (tetrazolyl group). Only Pd/C catalyst was active in the hydrogenolysis of compound **4.1.8** via hydrogen transfer and H₂ gas, and produced only a small amount anisole. The process using 5-chloro-1-phenyl-1*H*-tetrazole is unsuitable for an industrial process because of its high cost, low atom efficiency and low yielding reaction. Therefore the triazine moiety was considered as an alternative electron-withdrawing group to activate the phenols. Cyanuric chloride is cheap and potentially cost effective (1/3 mole equiv. required). It reacts readily with a variety of phenoxides to form the 2,4,6-trisubstituted-1,3,5-triazines. Compared with the tetrazole derivatives, hydrogenolysis of tri-substituted triazines is a much more atom efficient process, as one equivalent triazine compound will reduce to three equivalents of deoxygenated aromatic. A variety of compounds that can be derived from lignin were converted into the corresponding 2,4,6-trisubstituted-1,3,5-triazine derivatives in moderate to good yields. The methoxy group *ortho* to the phenol was found to limit the yield of the product due to steric effects, whilst methoxy in the *para* and *meta*-positions substituents had less effect. Electronic effects become more prominent when comparing molecules that have similar steric effects. The methoxy electron donating group enriches the aromatic electron density making it a stronger nucleophile to attack cyanuric chloride. In contrast, if there is an electron withdrawing group on the phenol (-CHO, -CO₂H), this reduces the electron density on the oxygen anion which make it a weaker nucleophile and may explain the lower product yield. The bond lengths from the crystal structure of 2,4,6-*tris*(2-methoxyphenoxy)-1,3,5-triazine **4.2.3** corresponded well with those of modelling the structure. This showed the C_{arom}-O bond was longer, activated by the triazine ring, and therefore weaker helping facilitate hydrogenolysis.

4.5 References

1. (a) Entwistle, I. D.; Hussey, B. J.; Johnstone, R. A. W., *Tetrahedron Lett.*, **1980**, *21*, 4747-4748; (b) Alves, A. C. J.; Barkley, V. J.; Brigas, F. A.; Johnstone, A. W. R., *J. Chem. Soc., Perkin Trans. 2*, **1997**, 669-678; (c) Cristiano, M. L. S.; Johnstone, R. A. W.; Price, P. J., *J. Chem. Soc., Perkin Trans. 1*, **1996**, 1453-1459; (d) Johnstone, R. A. W.; Price, P. J., *J. Chem. Soc., Perkin Trans. 1*, **1987**, 1069-1076.
2. Musliner, W. J.; Gates, J. W. J., *Org. Synth.*, **1988**, *6*, 150.
3. Hussey, B. J.; Johnstone, R. A. W.; Entwistle, J. D., *Tetrahedron*, **1982**, *38*, 3775-3781.
4. Sagar, A. D.; Patil, D. S.; Bandgar, B. P., *Synth. Commun.*, **2000**, *30*, 1719-1723.
5. Psotta, K., *Holzforschung*, **1984**, *38*, 43-46.

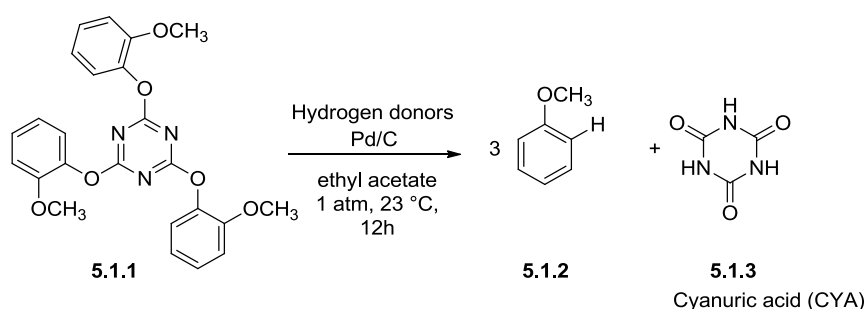
6. (a) Allan, F. J.; Allan, G. G.; Mattila, T.; Mauranen, P., *Acta Chem. Scand.*, **1969**, *23*, 1903-1910; (b) Van Muijlwijk, A. W.; Kieboom, A. P. G.; Van Bekkum, H., *Recueil des Travaux Chimiques des Pays-Bas*, **1974**, *93*, 204-206.
7. Sawyer, J. S.; Schmittling, E. A.; Palkowitz, J. A.; Smith, W. J., *J. Org. Chem.*, **1998**, *63*, 6338-6343.

Chapter 5 Hydrogenolysis of lignin monomer compounds

In this chapter, hydrodeoxygenation of trisubstituted-1,3,5-triazines containing lignin monomer compounds will be discussed. The processes were carried out in both a batch reactor and a continuous stirred tank reactor (CSTR). Hydrogen transfer reagents and hydrogen gas were applied to the reaction as hydrogen sources and, a variety of catalysts were evaluated to determine their efficiency for hydrogenolysis. The reaction kinetics were studied to help optimise the reaction conditions.

5.1 Hydrogenolysis of 2,4,6-*tris*(aryloxy)-1,3,5-triazine derivatives in batch

5.1.1 Transfer hydrogenolysis



Scheme 5.1.1

The transfer hydrogenolysis of 2,4,6-*tris*(2-methoxyphenoxy)-1,3,5-triazine (TMPT) **5.1.1** was studied at 23 °C over 12 hours (Scheme 5.1.1). When using hydrazine hydrate as hydrogen donor, the only material recovered was guaiacol in 80% yield by GC area% analysis. Other hydrogen donors, sodium phosphinate, 2-propanol and glucose were also examined with no reaction observed. The recovered 2,4,6-*tris*(2-methoxyphenoxy)-1,3,5-triazine **5.1.1** was analysed by TLC and ¹H NMR spectroscopy.

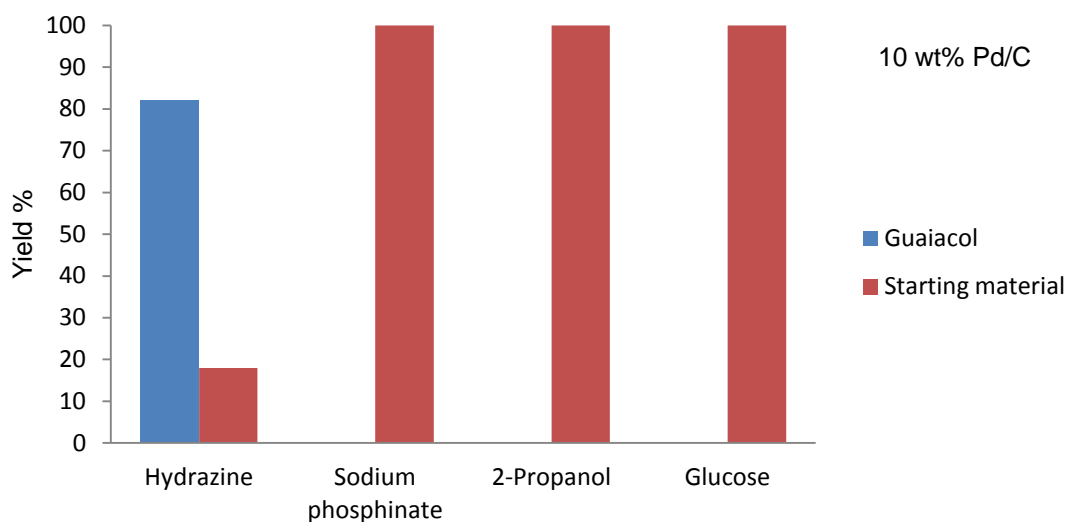


Figure 5.1 Hydrogen donors for the transfer hydrogenolysis of 2,4,6-*tris*(2-methoxyphenoxy)-1,3,5-triazine 5.1.1

The effect of hydrazine was to act as a good nucleophile in the S_NAr reaction to liberate guaiacol, rather than act as a reductant.¹ The likely mechanism of this is shown in Figure 5.2. Unfortunately the trihydrazinyl triazine could not be isolated. In a similar way ammonium acetate was also shown to react with the triazine **5.1.1**, to liberate guaiacol. These reactions show the sensitivity of the triaryloxytriazine to even weak nucleophiles

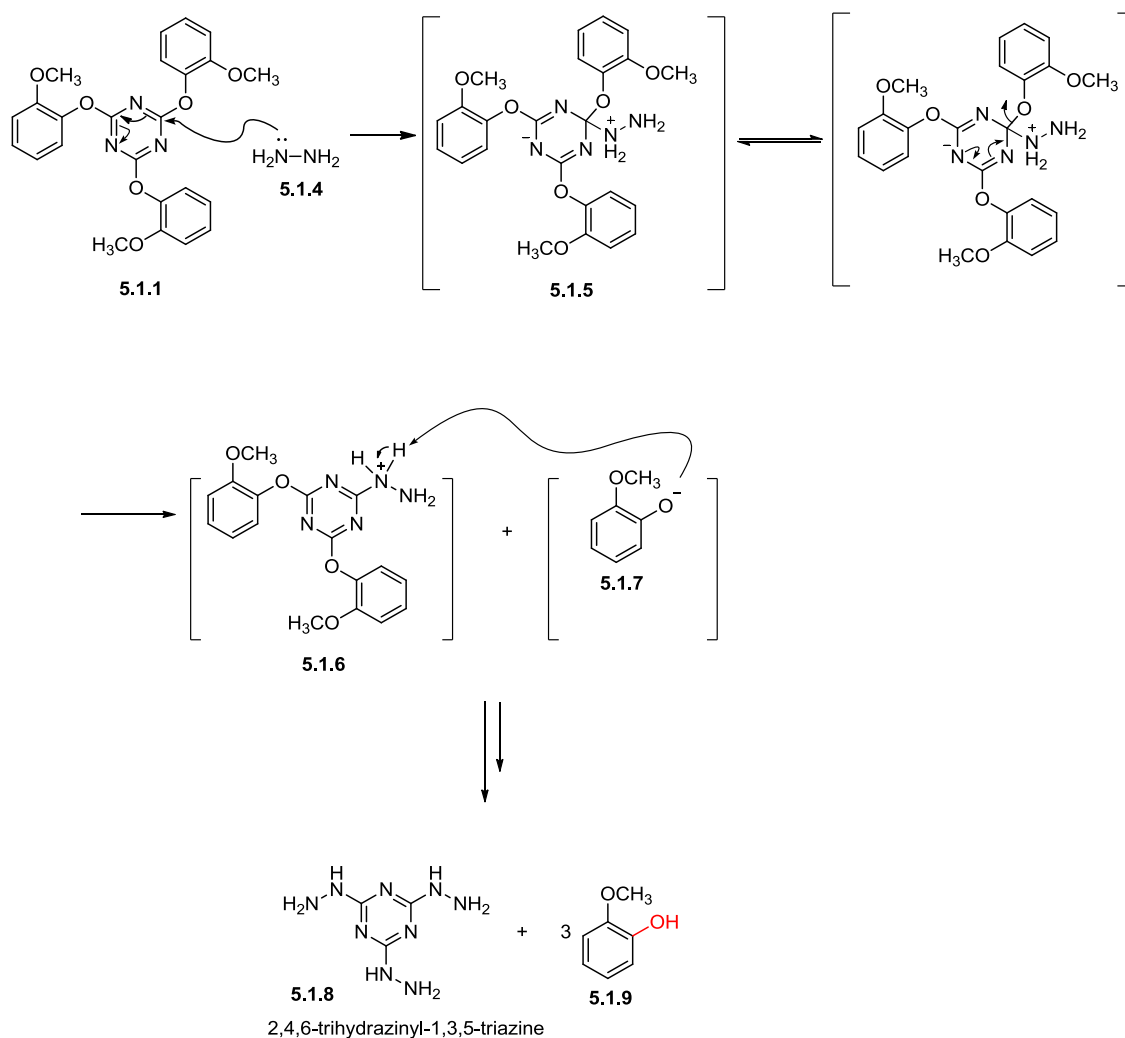


Figure 5.2 Possible mechanism of hydrazine reaction with TMPT 5.1.1 to produce guaiacol

5.1.2 Catalytic hydrogenation using hydrogen gas

To investigate the catalytic hydrogenolysis of triazine compound **5.1.1**, hydrogen gas was introduced in the presence of a variety of catalysts (Table 5.1). The reaction conditions were kept constant: 1 atmosphere of hydrogen (balloon) in EtOAc at room temperature for 12 h.

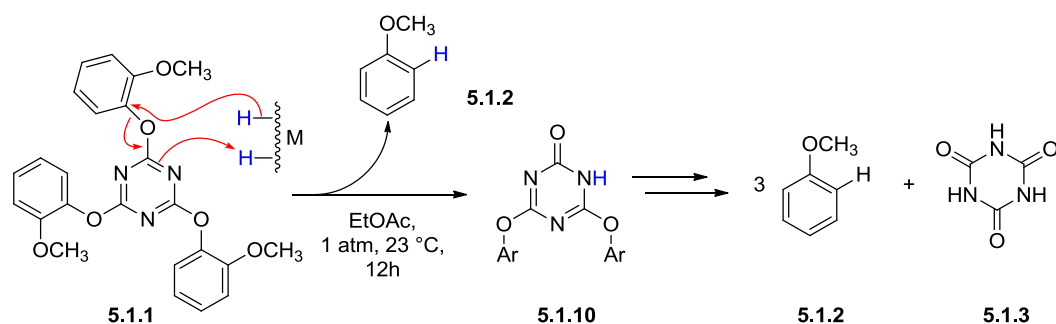


Table 5.1 Catalysts used hydrogenolysis reactions of 2,4,6-tris(2-methoxyphenoxy)-1,3,5-triazine

Entry	Catalyst	Anisole Yield (%)	TOF (min ⁻¹)
1	5 wt% Pd/C	0	n/a
2	10 wt% Pd/C	58	0.58
3	10 wt% Pt/C	12	0.13
4	10 wt% Ru/C	11	0.08
5	10 wt% Ni/Al	0	n/a

Reaction conditions: rt, 1 bar H₂, solvent: EtOAc, 12 hour.

Using 10% Pd/C (10 wt% loading) as the catalyst yielded 58% anisole **5.1.2** (calculated by quantitative GC results from the crude reaction mixture). Whereas, no reduction occurred with 5 wt% Pd/C and only starting material **5.1.1** was recovered. Both 10 wt% Pt/C and Ru/C were ineffective in the hydrogenolysis reaction with only 11–12% anisole obtained. However, based on GC retention time *vs.* an authentic standard a similar quantity of cresol as anisole was produced (Figure 5.3). As in some heterogeneous reactions discussed in Chapter 2, it would appear that these catalysts encourage rearrangement of the methyl group. The mechanism of this is unknown.

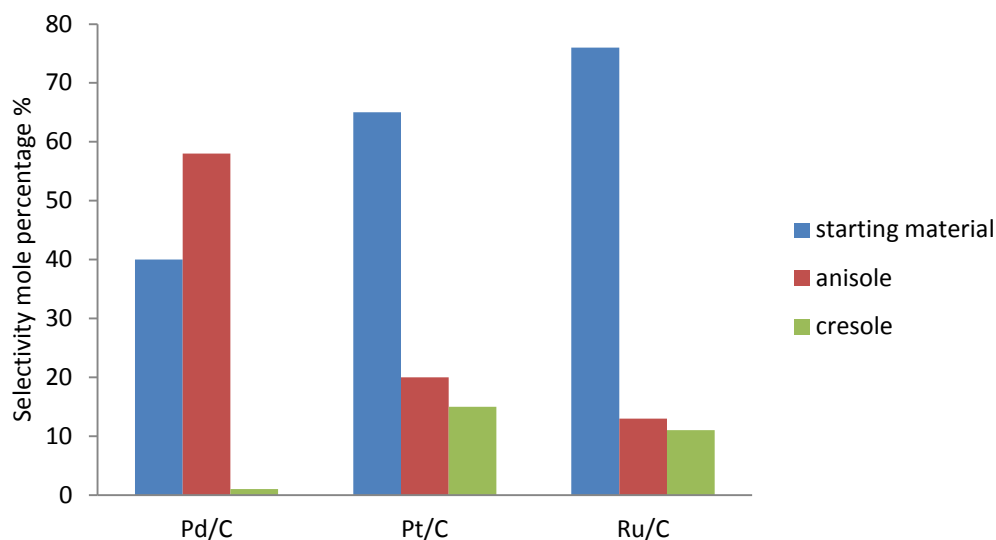
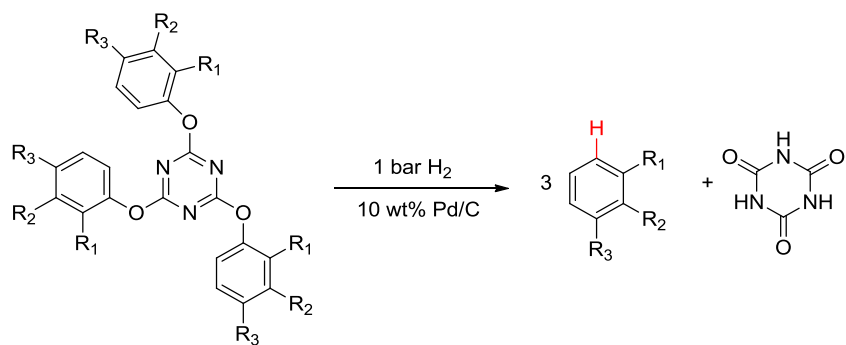


Figure 5.3 Hydrogenolysis of 2,4,6-*tris*(2-methoxyphenoxy)-1,3,5-triazine over 10 wt% Pt/C and 10 wt% Ru/C

Hydrogenolysis with 10 wt% Ni/Al was unsuccessful. As a result of this study, Pd/C has the highest hydrogenolysis activity, and 10 wt% catalyst is the minimum effective amount of palladium for hydrogenolysis.

Application of the successful Pd/C catalysed hydrogenolysis to the 2,4,6-*tris*(aryloxy)-1,3,5-triazine derivatives was studied with results shown in Table 5.2. Phenol triazine **5.1.11** was converted into benzene (**5.1.12**) with 10% yield as determined ascertained by quantitative GC analysis of the reaction mixture. At room temperature, low yields of anisole **5.1.2** were obtained from guaiacol (**5.1.1**) and 3-methoxyphenol (**5.1.13**) in 56% and 20% yield respectively. Increasing the reaction temperature to 40 °C, the reaction yields were significantly improved at 78% and 68% respectively. However, compounds **5.1.15** and **5.1.17** gave lower yields even with temperatures up to 50 °C, albeit they were done in water as their solubility allowed this. The presence of the electron-withdrawing substituents on the aromatic ring deactivates the hydrogenolysis of the C_{arom}-O bond of those compounds. Benzoic acid was obtained in 21% yield from the hydrogenolysis of compound **5.1.15**, while 58% of 3-methoxybenzoic acid was recovered from compound **5.1.17**. It was also found that by adding the base in the heterogeneous solution, the reaction could be accelerated.



Scheme 5.1.3

Table 5.2 Hydrogenolysis of 2,4,6-*tris*(aryloxy)-1,3,5-triazines

Entry	Compound	R ₁	R ₂	R ₃	Base	Solvent	Temperature °C	Yield %	Product
1	5.1.11	H	H	H	n/a	EtOAc	23	10	5.1.12
2	5.1.1	OCH ₃	H	H	n/a	EtOAc	23	56	5.1.2
3	5.1.1	OCH ₃	H	H	n/a	EtOAc	40	78	5.1.2
4	5.1.1	OCH ₃	H	H	Et ₃ N	EtOAc	40	86	5.1.2
5	5.1.13	H	OCH ₃	H	Et ₃ N	EtOAc	23	20	5.1.2
6	5.1.13	H	OCH ₃	H	Et ₃ N	EtOAc	40	68	5.1.2
7	5.1.14	H	H	OCH ₃	Et ₃ N	EtOAc	40	68	5.1.2
8	5.1.15	H	H	COOH	n/a	H ₂ O	50	21	5.1.16
9	5.1.17	OCH ₃	H	COOH	n/a	H ₂ O	50	58	5.1.18

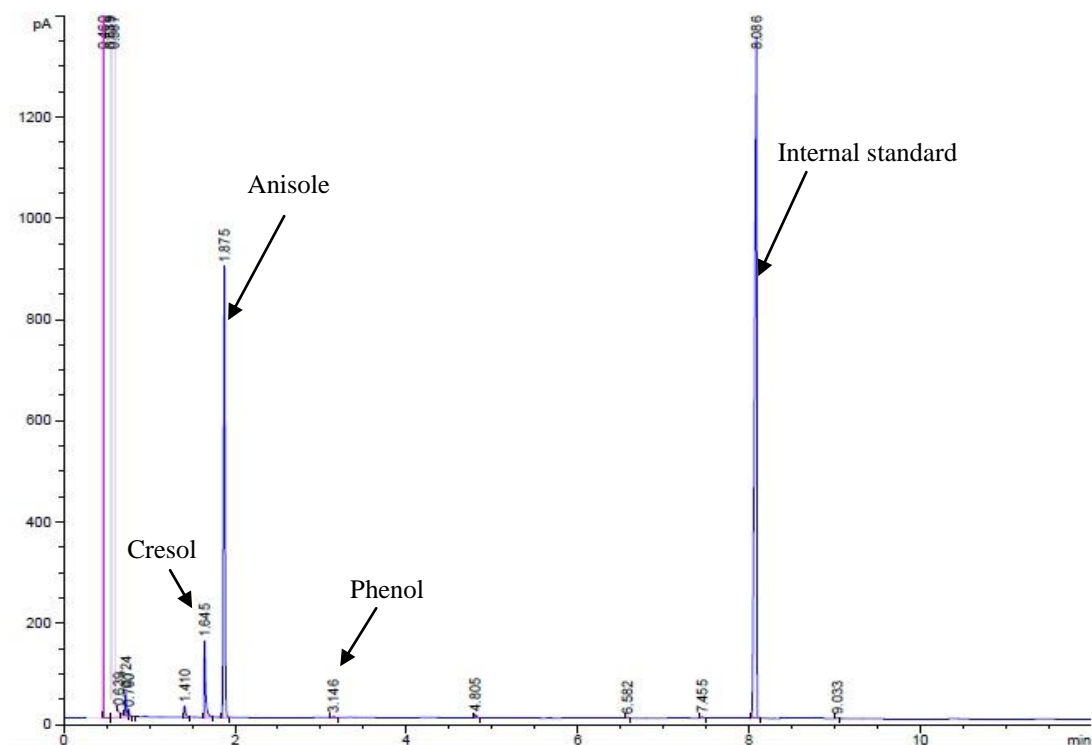


Figure 5.4 Hydrogenolysis of 5.1.1 to produce anisole over 10 wt% Pd/C and 1 bar of H₂ at 40 °C, 25 h

Surprisingly the by-product of the hydrogenolysis reaction was difficult to find in the work-up residues. It was found that cyanuric acid **5.1.3** is insoluble in ethyl acetate, and that it was adsorbed on the catalyst surface, which may have retarded the hydrogenolysis. Cyanuric acid has poor solubility in most solvents. After separating the ethyl acetate solution, the residual palladium on carbon was grey. Washing the catalyst with distilled water, a white solid was still found coated on the surface, which was suspected of being cyanuric acid. Separating the cyanuric acid **5.1.3** from the catalyst directly was difficult, but washing with sodium hydroxide solution to form a sodium salt gave 2% recovery of the theoretical amount.

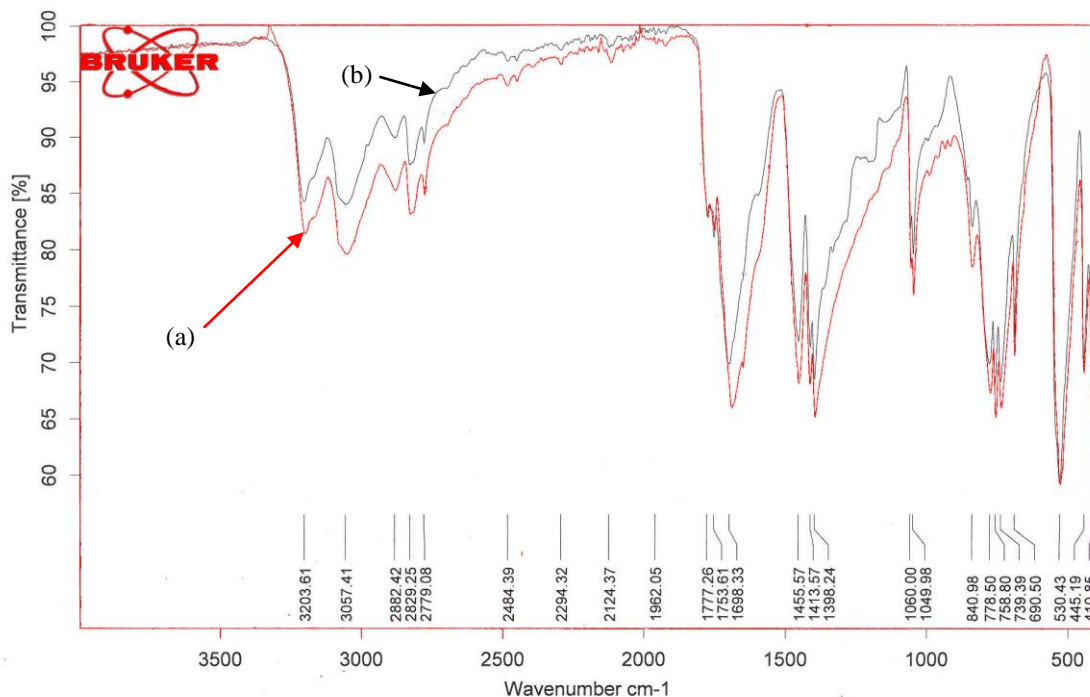


Figure 5.5 IR of (a) recovered CYA (5.1.3) after hydrogenolysis; (b) commercial CYA (5.1.3) 98%, Aldrich

The evidence of the recovered cyanuric acid is shown from the IR spectrum (Figure 5.5), which the peaks of the recovered (re-acidified) material from catalyst surface are consistent with those of a commercial cyanuric acid sample. Therefore, cyanuric acid was formed as a by-product in the hydrogenolysis process.

To improve the reaction efficiency, we had considered recovery and recycle of the cyanuric acid (5.1.3). However, the low recoveries suggest that it was found reported in the literature that it can decompose to isocyanic acid or ammonia and CO₂ gas (Figure 5.6) as reported in the literature.²

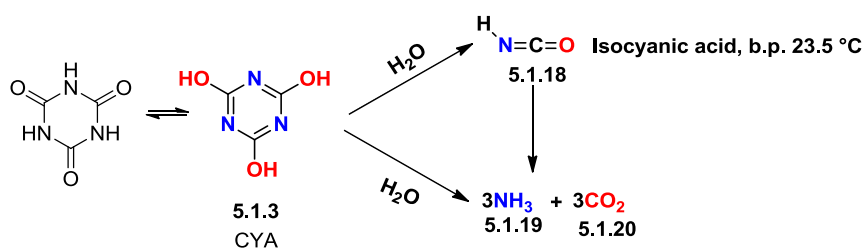


Figure 5.6 Decomposition of cyanuric acid 5.1.3²

A control reaction, reduction of cyanuric acid, was carried under same reaction hydrodeoxygenation conditions. Cyanuric acid was dissolved in H₂O and mixed with 10% Pd/C, stirring this heterogeneous mixture at 50 °C over 1 bar of H₂ for 12 hours.

The catalyst was filtered-off and only 60% of the cyanuric acid mass was recovered. No cyanuric acid was recovered from the catalyst surface, thus 40% of cyanuric acid was decomposed. Increasing the pressure to 5 bar, 21% of cyanuric acid was recovered from water while 17% was retrieved from catalyst surface.

5.1.3 Reaction kinetic study of hydrogenolysis of triazine compound in a batch reactor

The kinetics of the hydrogenolysis of triazine compound **5.1.1** were studied. Three different concentrations of compound **5.1.1** in EtOAc were prepared, 10 wt% Pd/C was employed with 1 atmosphere of H₂ from a balloon, and the temperature was controlled at 40 °C.

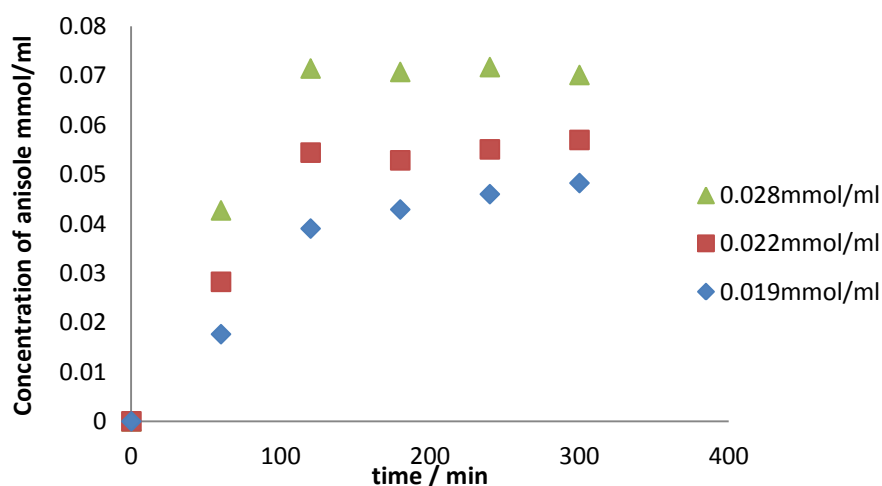


Figure 5.7 Hydrogenolysis of **5.1.1** at different concentrations in EtOAc

The poor solubility of **5.1.1** limited the concentration of solutions that could be used. At room temperature, 1 g can be dissolved in 80 mL (0.028 mmol/mL) EtOAc, but at 50 °C 1 g/ 50 mL (0.045 mmol/mL). Unfortunately maintaining this temperature whilst pumping the material during a flow process is difficult as it can crystallise and block the lines. All the reactions go to 100% conversion. The higher the concentration of **5.1.1**, the higher the rate of anisole produced (Figure 5.7). Despite this, the turnover frequency (TOF) of these three reactions was calculated and the catalyst showed same activity for all reactions (Table 5.3).

Table 5.3 TOF of hydrogenolysis of compound 5.1.1

Reaction	TOF (min ⁻¹)
0.028 mmol/mL	0.52
0.022 mmol/mL	0.52
0.019 mmol/mL	0.53

Reaction conditions: triazine (8.06 mmol), 10% Pd/C (10 wt% loading), solvent EtOAc, 40 °C, 5 hour, 1 bar H₂

Therefore, the reaction rate is independent of the concentration of the starting material. The rate of formation of anisole was studied over a period of 0–120 min, which the concentration shows almost straight lines; after 120 minutes, the reaction was almost completed (Figure 5.7). The reaction is considered as a zero-order reaction, the rate law of the overall reaction is as follows:

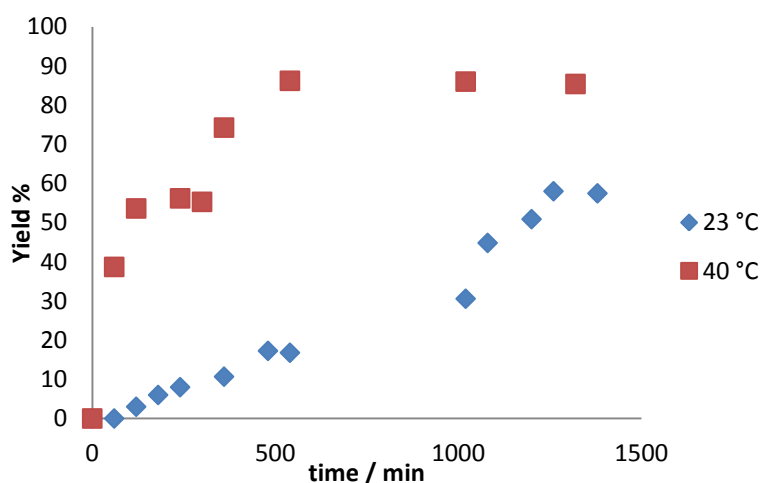
$$rate = k_{obs} \quad \text{Equation 5.1}$$

where k_{obs} was determined as $6.00 \times 10^{-7} \text{ mol} \cdot \text{mL}^{-1} \cdot \text{min}^{-1}$.

However, Figure 5.8 shows that increasing the reaction temperature increases the reaction rate. This indicated that the reaction rate is affected by the concentration of hydrogen, and the rate law of the reaction can be rearranged as:

$$rate = k[\text{H}_2] \quad \text{Equation 5.2}$$

where the concentration of H₂ in ethyl acetate at 40 °C and 1 bar was calculated as $3.83 \times 10^{-6} \text{ mol} \cdot \text{mL}^{-1}$, therefore, the rate constant k is 0.16 min^{-1} .

**Figure 5.8 Temperature effect of the hydrogenolysis reaction**

5.2 Process development for the hydrogenolysis of trisubstituted triazines in a continuous stirred-tank reactor

Figure 5.9 shows the CSTR equipment used to investigate the hydrogenolysis process. The starting material, 2,4,6-*tris*(2-methoxyphenoxy)-1,3,5-triazine (**5.1.1**) in EtOAc was fed into the reactor with an ultra-compact high pressure pump (AZURA P 4.1S). This pump provides a wide range of flow rates from 0.01 to 50 mL/min with a maximum pressure of 150 bar. The solution was mixed with pressurised H₂, and a back-pressure regulator was connected to allow the product to be continuously collected.

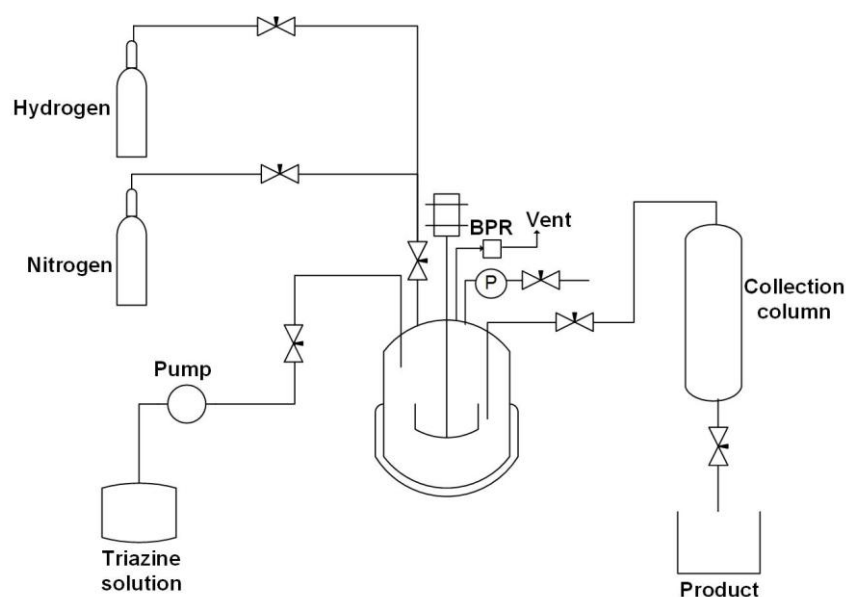


Figure 5.9 Line diagram of the CSTR set-up used in the catalytic hydrogenolysis

5.2.1 Optimisation of flow hydrogenolysis with CSTR

Two flow methods were designed with the CSTR system. Method A involved 4 mol% Pd/C loaded into the reactor over hydrogen but without any liquid; the starting material in EtOAc was fed to the reactor and hydrogen introduced under pressure; the product was collected once the feed time equalled the residence time. Method B involved 4 mol% Pd/C loaded in the reactor along with starting material in EtOAc and filled to reach the over-flow volume, the product was collected at same time as feeding the starting material, though at least 2 residence time volumes are required to reach steady-state.

With method A, as the reactor fills the ratio of substrate to catalyst (S/C) decreases until the liquid over-flows and the reaction can the start to reach steady state. Since the average residence time of the starting material is longer than at steady-state and the

initial S/C ratio small, it is expected that a higher anisole concentration will be observed. Indeed the product concentration was observed to fall. The residence time (τ [min]) was calculated as:

$$\tau = \frac{V}{v} \quad \text{Equation 5.3}$$

Where V is the residence volume of reactor [mL]; v is volumetric flow rate [mL/min].

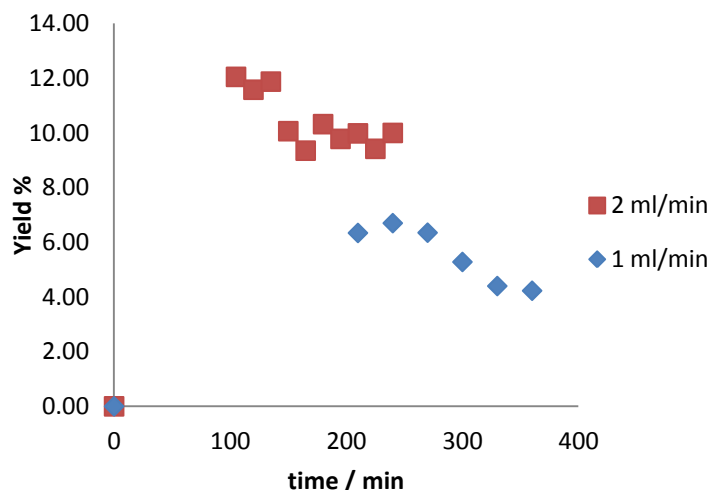


Figure 5.10 Yield of anisole produced by catalytic hydrogenolysis in a continuous flow CSTR (method A) at different flow rates

At a flow rate of 1 mL/min the yield of anisole falls from 8% to 4.5% at steady state. The residence time of 210 min takes a further 120 min to reach steady state. Increasing the flow rate to 2 mL/min, the residence time was halved and the yield of anisole was enhanced as well. Shorter residence times are needed for a viable industrial process. After feeding the starting material for 105 min, 12% anisole was observed and dropped to a steady-state 10% at 150 min. The lower anisole yield from the low flow rate may be caused by the longer residence time leading to poisoning of the catalyst; which we have shown earlier cokes the catalyst surface and reduces the catalyst activity. Method B was expected to minimise this effect.

To reduce the residence time, we can either increase the flow rate or reduce the reaction volume. In method B a smaller volume (30mL) was achieved by adjusting the length of the dip-tube, see Figure 5.8. The hydrogenolysis was investigated with flow rate 4 mL/min over 10 bar of H₂ at 50 °C (Figure 5.11).

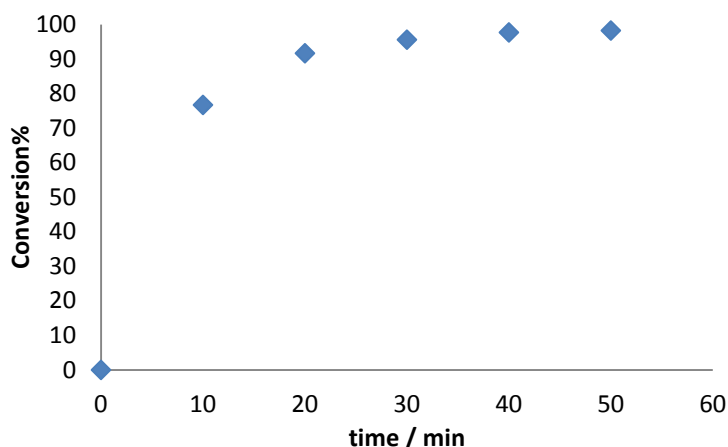


Figure 5.11 CSTR hydrogenolysis with flow rate 4 mL/min over 10 bar H₂ at 50 °C with 30 mL reactor volume

The first sample was collected at 0 min, then samples taken every 15 min. The yield of the product increased until it reached steady-state. At this higher flow rate (4 mL/min), more anisole was produced (70%) than by method A and the starting material was fully converted. Moreover, the residence time was reduced to 8 min.

In batch hydrogenolysis the yield could be enhanced by adding base to the starting solution to remove cyanuric acid from catalyst surface. Accordingly triethylamine was added to the CSTR hydrogenolysis. In this experiment 2,4,6-*tris*(2-methoxyphenoxy)-1,3,5-triazine was dissolved in the solvent EtOAc along with 3 equivalents of triethylamine. The mixture was fed into the reactor using method B with flow rate 4 mL/min and heated at 50 °C, and 10 bar of hydrogen was supplied. Surprisingly little increase in yield was found. After 30 min, the yields with triethylamine were slightly higher than without, which might support the hypothesis of cyanurate removal from the catalyst surface. The downside of adding base is that it increases the process costs, not only the material, but also the capital due to corrosion, and waste through either disposal or recycling.

As discussed in Chapter 2, a lot of lignin phenolic hydrodeoxygenation processes have been studied under conditions that are not industrially viable (eg. high pressure, temperature) and may cause safety and cost issues.³ Here we sought an industrial process using low pressures and temperatures. Figure 5.12 shows that lower H₂ pressures (5 bar) had little effect on the rate of starting material conversion. As with most hydrogenations it is likely that the hydrogen mass transfer rate controls the reaction rate. The solubility of hydrogen is low and the gas-liquid mixing determines

the rate. The mass transfer coefficient for this pressure reactor has not been determined. Unfortunately to test this requires a variable impeller speed that is not available on the pressure equipment use.

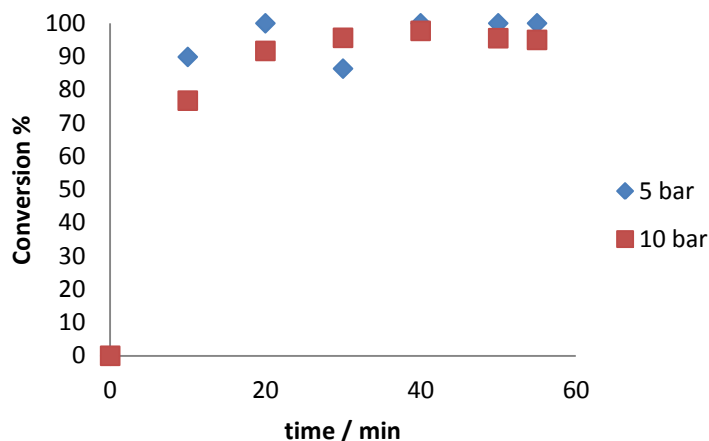


Figure 5.12 Hydrogen pressure effect on the catalytic hydrogenolysis of 5.1.1 in the CSTR

The degradation of anisole during hydrogenolysis has been reported previously and phenol, benzene and cresol were the main products derived from the hydrogenolysis of anisole using Ni or Mo catalyst.⁴ We decided to evaluate the products generated in our reaction in more detail.

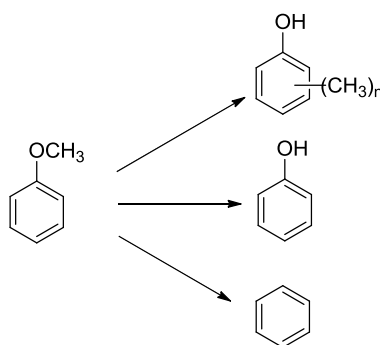
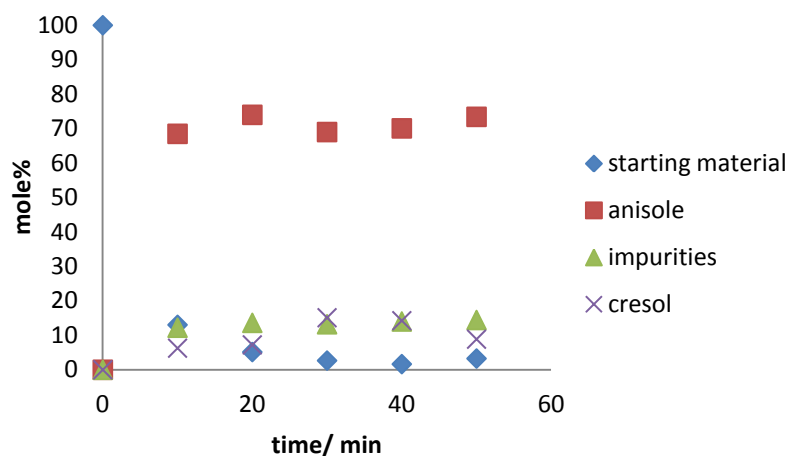
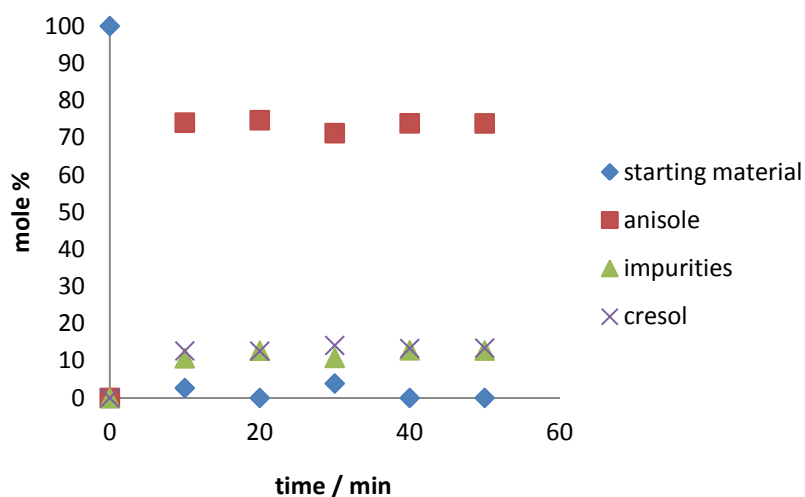


Figure 5.13 Reported reduction of anisole to give a mixture of aromatic products^{4c}

The retention times of authentic standards of benzene, phenol and cresol were determined by GC, and compared with our continuously produced product (Figure 5.14a) at 10 bar H_2 and 5.14b at 5 bar H_2 . The retention time of *ortho*-cresol was 4.80 min and this was found in our product at up to 15 mol% under both conditions. Some small peaks were also present, which could not be identified by GC or GCMS.



(a)



(b)

Figure 5.14 Selectivity of hydrogenolysis products produced in CSTR (a) 4mL/min, 10 bar; (b) 4 mL/min, 5 bar

To try and improve the process a higher flow rate also was investigated. Twice the flow rate (8 mL/min) gave a lower anisole productivity. At steady-state, the starting material was incompletely reduced, and the conversion of the starting material was only about 60% (Figure 5.15).

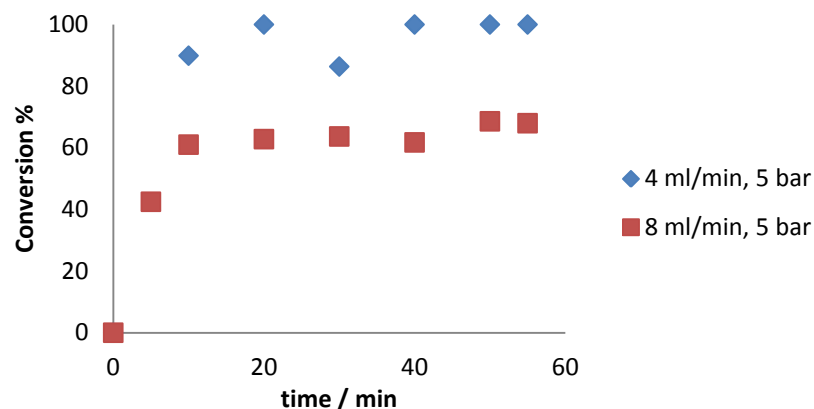


Figure 5.15 Conversion of CSTR hydrogenolysis with 4 mL/min and 8 mL/min flow rate

To test the robustness, after 1 hour continuous flow at 5 bar and 4 mL/min, the pumps were stopped and the heterogeneous solution left to settle overnight. The following morning the catalyst was filtered-off and reused in the next hydrogenolysis reaction. Figure 5.16 shows that after one recycle the catalyst activity decreased. The yield of anisole was reduced from 73% to 44% and the conversion was only 50%. The differences between the active and deactivated catalyst were studied, and these are discussed in 5.2.2

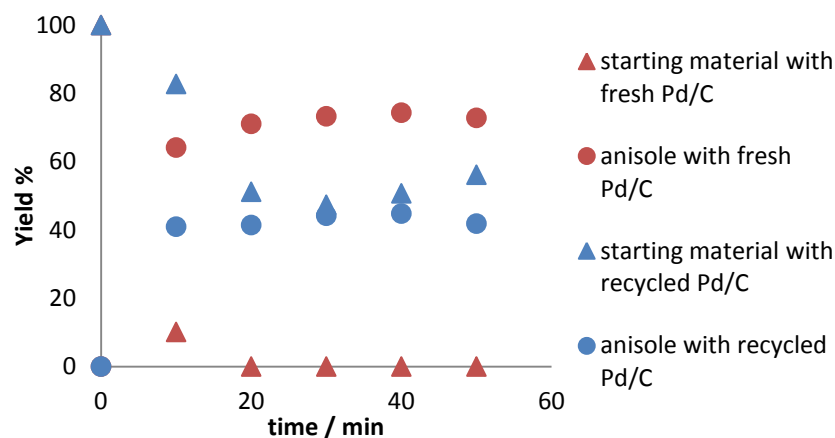


Figure 5.16 Hydrogenolysis over Pd/C and recycled Pd/C

5.2.2 Characterisation of Pd/C catalyst

The physical properties of the catalyst were analysed by scanning electron microscopy (SEM). After hydrogenolysis, the catalyst was collected and dispersed in a small amount of water. In Figure 5.17, it is observable that the appearance of the fresh catalyst (Figure 5.17a) and the used catalysts (used once Figure 5.17b and used twice Figure 5.17d) has little effect on the surface appearance. The catalyst that has changed

most is that in which triethylamine was used, Figure 5.17c. The particles had all clustered and no longer granular in shape. The particle size distribution for each catalyst is displayed in Figure 5.18.

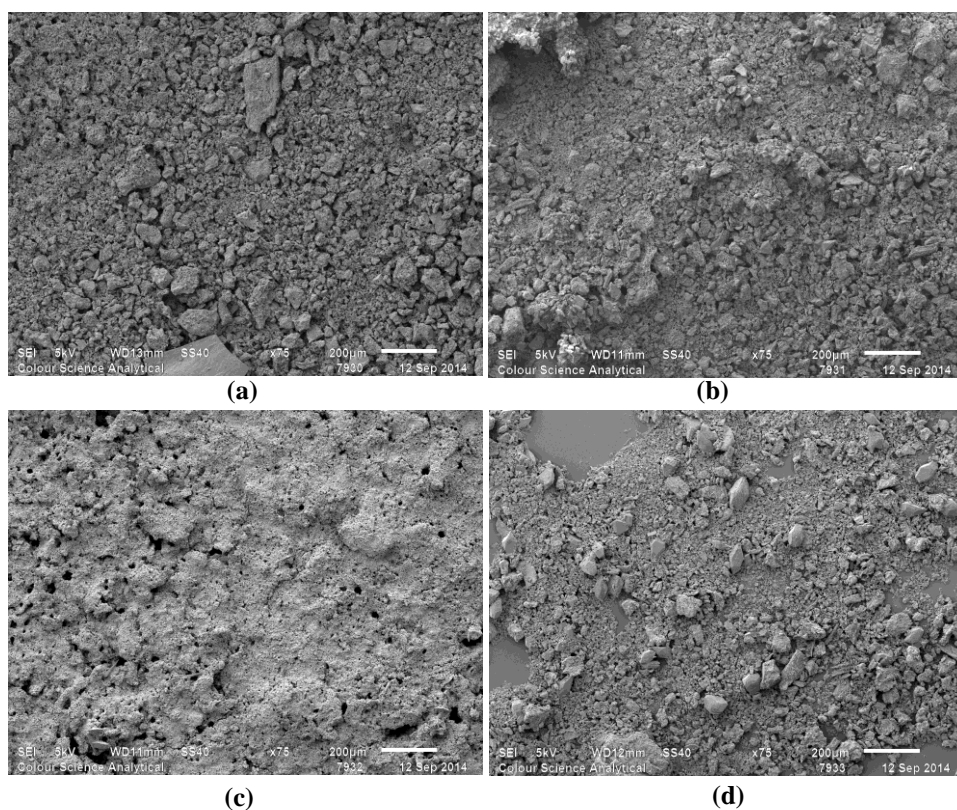


Figure 5.17 (a) 5% Pd/C (Johnson Matthey 87L); (b) Pd/C collected from a CSTR hydrogenolysis over 10 bar H_2 and flow rate 4 mL/min for 1 hour; (c) Pd/C collected from a CSTR hydrogenolysis with Et_3N over 10 bar H_2 and flow rate 4 mL/min for 1 hour; (d) One-time recycled Pd/C collected from a CSTR hydrogenolysis over 10 bar H_2 and flow rate 4 mL/min for 1 hour.

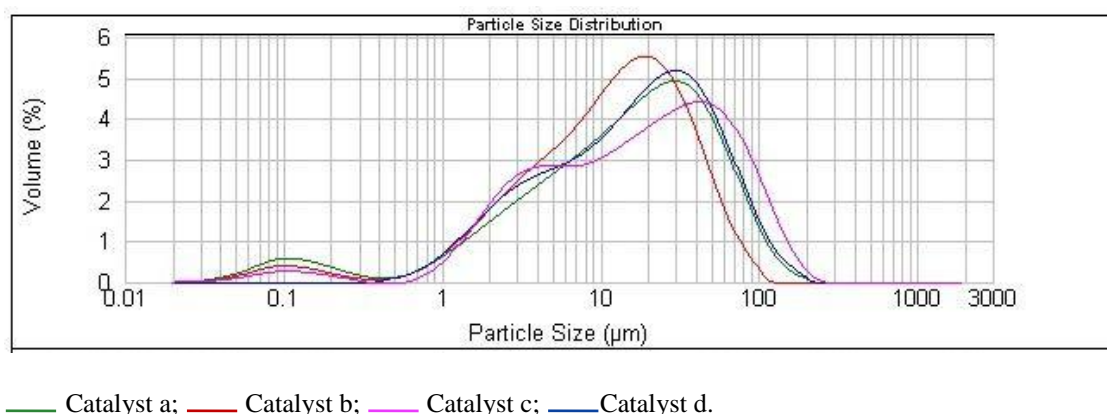


Figure 5.18 Particle size distribution of Pd/C catalysts

The percentages of carbon and palladium were detected by a coupled energy-dispersive X-ray spectroscopy (EDS) system (Table 5.4).

Table 5.4 Wt% and Wt ratio of carbon and palladium from catalysts: a. fresh, b. after 1 use, c. with triethylamine, d. second use (see Figure 5.16)

Pd/C	C (wt %)	Pd (wt %)	N (wt %)	Ratio Pd/C
Catalyst a	79	11	0	0.14
Catalyst b	53	5	22	0.09
Catalyst c	73	11	6	0.15
Catalyst d	52	4	23	0.08

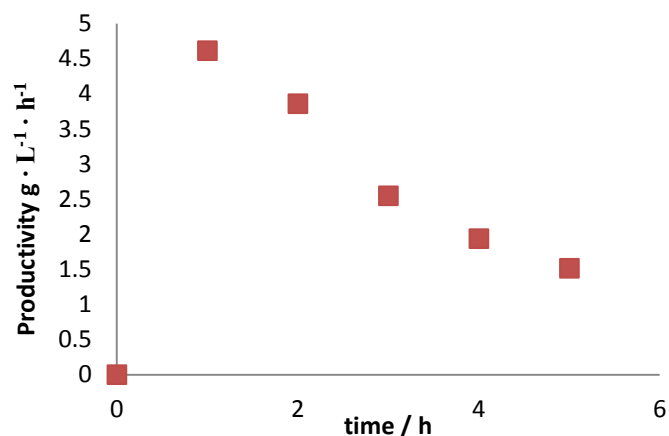
The X-ray analysis illustrates that the hydrogenolysis with triethylamine had little effect on palladium leaching (catalyst c compared to catalyst a); however, its activity was the same as catalyst b, in which almost half the palladium has been lost. This is because the hydrogenolysis is limited by the hydrogen mass transfer. Furthermore the amount of palladium in the recycled catalyst d had a similar level to used once catalyst b, despite its activity being very low (*c.a.* 50% conversion). It is clear that none of these analytical techniques are able to determine surface modification i.e. coking of the catalyst. The X-ray map of catalyst b shows the low wt% of carbon was due to the nitrogen atom replacement which was 22 wt %, and may be due to cyanuric acid absorbed on the catalyst surface.

However, accuracy of the X-ray mapping technique can be affected by many factors, such as signal convolution and the nature of the sample. In our case, uneven sample distribution can reduce the accuracy of the results.

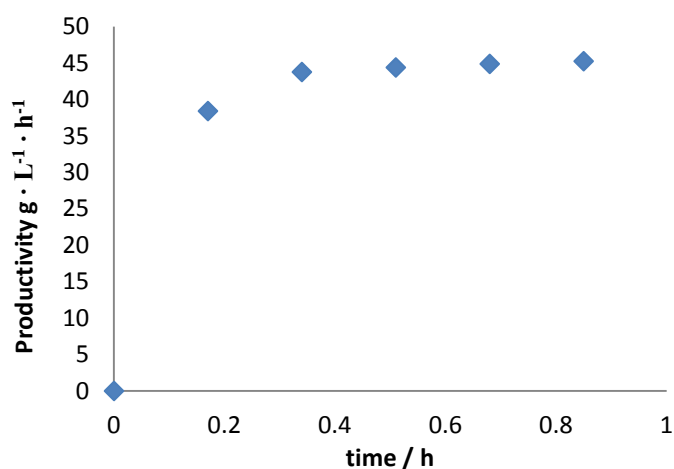
5.3 Economic evaluation

5.3.1 Comparison of batch and CSTR productivity

In the batch reactor, the hydrogenolysis to produce anisole decreased with time; the mean productivity in 5 hours was $2.4 \text{ g}\cdot\text{L}^{-1}\cdot\text{h}^{-1}$ (Figure 5.19a), whereas in the CSTR system the productivity at steady state was $45 \text{ g}\cdot\text{L}^{-1}\cdot\text{h}^{-1}$ (Figure 5.19b).



(a)



(b)

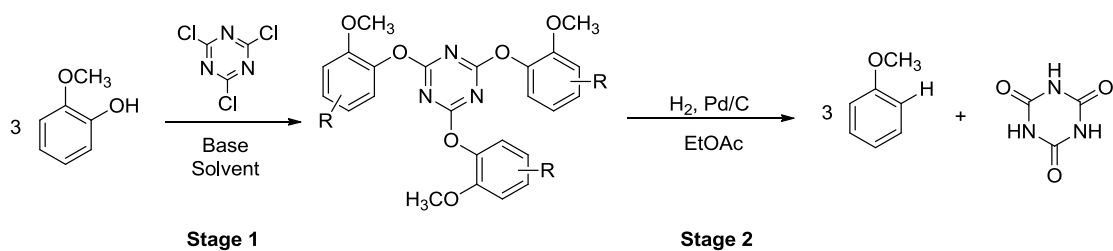
Figure 5.19 Anisole productivity of (a) batch reactor, 1 bar and (b) CSTR system, 5 bar, 4 mL/min

5.3.2 Process cost estimation

Estimating the cost of an industrial process requires evaluating the raw material, operating and capital costs. At lab scale only rough estimations can be made, and the more the process is defined the better the data and the more accurate the estimate of the manufacturing cost.

A rough estimate of the raw material costs in a bulk manufacture of anisole based on the two-step process developed, including continuous hydrogenolysis, are calculated as follows:

Table 5.5 Raw material cost estimation of anisole production



Stage 1

Yield %	86.00					
Material	M Wt	% w/w Strength	m/m	Usage Kg/Kg of stage	Price £/Kg	Cost per Kg Stage
Guaiacol	124.00	100.00	3.00	0.97	1.00	0.97
Cyanuric chloride	184.00	100.00	1.00	0.48	1.50	0.72
Effluent				0.45	0.20	0.09
Product RMM =	447.00				Total	1.80

Stage 2:

*Yield %	252.00					
Material	M Wt	% w/w Strength	m/m	Usage Kg/Kg of stage	Price £/Kg	Cost per Kg Stage
Stage 1	447.00	100.00	1.00	1.60	1.80	2.90
Pd/C	106.00	100.00	0.04	0.02	40.00	0.66
hydrogen	2.00	100.00	10.00	0.07	0.10	0.01
Effluent				0.73	0.20	0.15
Product RMM =	108.00				Total	3.70

* In stage 2, the overall yield was calculated as 3 mol of anisole produce from 1 mol intermediate of stage 1.

** Assumes 90% palladium recovery or 10 catalyst recycles

The raw material cost of producing anisole using our process, assuming 90% Pd recovery, is £3.7/kg. Another assumption is that digested lignin can produce lignin for £1/kg, which is not yet possible. A further assumption is that no solvent is used in stage 1, and solvent is water (zero cost) or efficiently recycled in stage 2. The cost will of course be higher when adding capital and operating costs. For bulk production these might be 50% of the raw material cost, and of course the flow hydrogenation process should reduce the capital requirement. Overall a production cost of <£5/kg may be possible. The current market price of petrochemically produced anisole is about £8/kg, showing the potential commercial viability of this process. Nevertheless the productivity in both stage 1 and 2 needs to be improved. The costing shows where development work should be directed and this includes solvent, catalyst use and yield.

5.4 Conclusions

In this chapter the results of catalytic hydrodeoxygenation of trisubstituted triazine derivatives in both batch and CSTR reactors have been discussed. Using a batch reactor, a variety of catalysts were investigated and 10 wt% Pd/C showed the highest catalytic activity in breaking the C_{arom}-O bond. Low conversions were observed with 10 wt% Pt/C and Ru/C, and no reduction occurs with 10 wt% Ni/Al. When hydrogen was replaced with hydrogen donors, no cleavage of the aromatic C-O bonds was observed. However, when hydrazine was used as the hydrogen source, guaiacol was found as the main product showing an S_NAr reaction rather than reduction.

The reaction conditions were optimised in a batch reactor. At 1 atmosphere hydrogen, increasing the temperature from 25 °C to 50 °C, the yield of the hydrogenolysis increased greatly. Cyanuric acid was produced as the by-product and seems to coat the catalyst surface, with increasing concentrations gradually deactivating the catalyst. Base was shown to remove it as cyanurate, whilst adding triethylamine the yield was only slightly increased from 78% to 86%. The reaction was completed in 3 hours and the reaction rate was independent of the concentration of the triazine solution, but it was limited by hydrogen mass transfer.

The hydrogenolysis was carried out by continuous flow process using a CSTR and residence time was varied by changing volume and flow rate. A large volume (210 mL) and slow flow rate (1 mL/min and 2 mL/min) gave a low yield of anisole, which may be a result of the degradation of catalyst. Whereas, when the flow rate was adjusted to 4 mL/min and residence volume to 30 mL, the system reached steady-state

in 10 min and gave the highest yield of anisole (80%) at $45 \text{ g}\cdot\text{L}^{-1}\cdot\text{h}^{-1}$. The Pd/C catalyst was recycled; however, only half the conversion of triazine was obtained (50%) and anisole was produced with the yield of 45%. None of the different methods used to analyse the catalyst identified surface changes that might be caused by cyanuric acid; they did however indicate palladium leaching.

An economic evaluation of the hydrogenolysis process was carried out. With assumptions around the bulk cost of guaiacol from lignin, solvent and palladium recovery, the raw material cost to produce anisole is estimated at £3.7/kg.

5.5 References

1. (a) Koppes, W. M.; Forohar, F.; Moran, J.; Rosenberg, D. M.; Mannion, J. D.; Vos, B. W., High-energy 1,3,5-triazinyl diazenes, and process thereof, Patent US 7399841 B1, **2008**; (b) Camden, J. B.; Dabek, R. A., Cancer treatment, Patent US 6384049 B1, **2002**.
2. Bernhard, A. M.; Peitz, D.; Elsener, M.; Wokaun, A.; Kröcher, O., *Appl. Catal. B*, **2012**, *115–116*, 129-137.
3. (a) Boudart, M., *Chem. Rev.*, **1995**, *95*, 661-666; (b) Güvenatam, B.; Kurşun, O.; Heeres, E. H.; Pidko, E. A.; Hensen, E. J., *Catal Today*, **2013**; (c) Wang, Y.; He, T.; Liu, K.; Wu, J.; Fang, Y., *Bioresour. Technol.*, **2012**, *108*, 280-284.
4. (a) Zhu, X.; Mallinson, R. G.; Resasco, D. E., *Applied Catalysis A: General*, **2010**, *379*, 172-181; (b) Kallury, R.; Tidwell, T.; Boocock, D.; Chow, D., *Can. J. Chem.*, **1984**, *62*, 2540-2545; (c) Huuska, M., *Polyhedron*, **1986**, *5*, 233-236.

Chapter 6 Conclusion and future work

Novel approaches for transforming lignin monomers into more useful materials *via* hydrodeoxygenation are presented in this work. A new process that has commercial potential has been developed. In contrast to the high energy processes reported in the literature that involve direct cleavage of the aromatic C–O bond accompanied by a complex mixture of products, our method employs low temperature and pressure catalytic hydrodeoxygenation by firstly activating the C_{arom}–O bond by a urea analogue. Guaiacol was chosen as the lignin monomer for most development work as this constitutes around 40% of the digested lignin mass. This was converted selectively into anisole in up to 80% yield and with a productivity of 45 g·L·h⁻¹ using Pd/C and hydrogen. The catalytic hydrodeoxygenation of other lignin related monomer compounds, such as vanillin and vanillic acid was also achieved with satisfactory yields.

Calcium, sulfonyl and phosphoryl derivatives of guaiacol were initially considered as an economic means to remove the phenolic hydroxyl group; however, the hydrogenolysis resulted in regeneration of the starting material rather than cleavage of the C_{arom}–O bond. Despite 35% anisole being converted from guaiacol triflate, the high cost of the starting material (trifluoromethanesulfonic anhydride) lead to a non-economic and wasteful process. Whilst activation through the tetrazolyl heterocycle gave poor hydrodeoxygenation, use of cyanuric chloride to give triaryloxytriazine gave much better results.

Molecular modelling and x-ray structural data illustrated that the strong electron-withdrawing effect of the heterocyclic ring contributes to the delocalisation of the lone-pair electrons on the oxygen which reduce its donation into the phenol ring and lengthens the C_{arom}-O bond.

Cyanuric chloride was reacted with a variety of phenolic lignin monomer compounds to obtain their corresponding 2,4,6-trisubstituted-1,3,5-triazine derivatives. The formation of these trisubstituted triazines is affected by the electronic effects of the phenyl ring substituents as well as the steric environment. Both the formyl and carboxyl electron-withdrawing groups on some of the monomers reduce the electron density on the oxygen anion, resulting in a weaker nucleophile and lower yield of the product. In contrast, the methoxy electron donating group donates electrons to the hydroxyl oxygen anion and enhances the product yield. Nevertheless, when the

methoxy group is *ortho* to the hydroxyl group, the steric effect is the dominant factor limiting the reaction yield whereas, *para* and *meta* substituents have less steric effect.

The hydrogenolysis of 2,4,6-*tris*(2-methoxyphenoxy)-1,3,5-triazine over a variety of catalysts was investigated in a batch reactor. No conversion was observed with a Ni/Al catalyst, whilst only 10% anisole was produced using 10 wt% Pt/C or Ru/C as catalysts. It was found that 10 wt% Pd/C had the greatest activity in the hydrogenolysis process, which converted the triaryl triazine into anisole in a 58% yield at room temperature and 1 atmosphere of H₂. By increasing the temperature to 40 °C, the yield improved to 78% over 3 hours. Cyanuric acid was seen in the product mixture, but the recycling of it proved impossible because it was partially absorbed on the catalyst surface. To reduce the catalyst degradation caused by cyanuric acid, triethylamine was employed in the system. The yield of anisole was increased to 86% however the catalyst was found to retain more palladium to help recycle, though the cost and separation of the base is undesirable. The reaction kinetics were studied to try to understand the reaction bottleneck; the low solubility of triaryltriazine in EtOAc lead to a long reaction time and the reaction is also likely to be limited by the mass transfer of hydrogen.

The application of continuous flow process is essential for manufacture of bulk material such as anisole. A CSTR was found to be the most appropriate reactor for the hydrogenolysis due to the multiphasic reaction; and a process was developed and optimised. Steady-state operation was achieved with a short residence time of 10 min and gave a satisfactory 80% anisole yield. When the catalyst was recycled, the activity decreased and only half the amount of triaryltriazine was converted to anisole. SEM results, it was shown that the residual cyanuric acid was coated on the catalyst surface. Significant palladium leaching was seen as its ratio with carbon was much lower than unused catalyst. Compared with batch, the CSTR hydrogenolysis system improved the productivity greatly. A project raw material costing of anisole (£3.70/kg) shows that the process has the potential to be economic at around £5/kg, however a number of assumptions need to be tested. These include the price of lignin derived guaiacol at £1/kg, use of water, or efficient solvent recycle and >90% palladium recovery. Whilst the production rate is good for lab (45 g·L⁻¹·h⁻¹), this needs to be several-fold higher for a commercial process.

Future work for the continuous hydrogenolysis of lignin monomer compounds should focus on:

- Continuous hydrogenolysis of lignin mixtures ‘the lignin soup’ model. Activation of phenolic hydroxyl groups in a mixture of lignin monomer compounds via their trisubstituted triazine derivatives.
- Removal of oxygen from pyrolysis oil since it is the most abundant product from lignin waste.
- Further investigation of the catalyst and its degradation is recommended to improve the product yields.
- In respect of the current kinetics studies, the model should test hydrogen mass transfer and be developed to apply different (mixed) feedstocks to help predict their formation.

Chapter 7 Experimental

Compounds numbered in this Chapter are shown in the following table:

Chapter 7 Compound Number	Chapter Compound Number	Chapter 7 Compound Number	Chapter Compound Number
7.2.1	3.1.5	7.6.3	4.2.3
7.2.2	3.1.10	7.6.4	4.2.11
7.2.3	3.1.11	7.6.5	4.2.7
7.2.4	3.1.12	7.6.6	4.2.13
7.2.5	3.1.13	7.6.7	4.2.9
7.3.1	3.1.5, 3.2.1, 7.2.1	7.6.8	4.2.15
7.3.2	3.2.2	7.6.12	4.2.17
7.3.3	3.2.3	7.6.15	4.2.19
7.3.4	3.2.4	7.6.16	4.2.21
7.3.5	3.2.5	7.7.1	3.3.1, 7.4.2
7.3.6	3.2.6	7.7.2	3.3.3, 7.4.5
7.3.7	3.2.7	7.7.3	3.3.5, 7.4.8
7.3.8	3.2.8	7.7.4	3.3.2, 7.4.3
7.3.9	3.2.9	7.7.5	3.3.4, 7.4.6
7.4.2	3.3.1	7.7.6	3.3.6, 7.4.9
7.4.3	3.3.2	7.7.8	5.1.1, 4.2.3, 7.6.3
7.4.5	3.3.3	7.7.9	5.1.2
7.4.6	3.3.4	7.7.10	5.1.3
7.4.8	3.3.5	7.7.11	4.2.7, 7.6.5
7.4.9	3.3.6	7.7.12	4.2.9, 7.6.7
7.5.1	3.1.5, 3.2.1, 4.1.5, 7.2.1, 7.3.1	7.7.13	4.2.3, 7.6.3
7.5.2	4.1.6	7.7.14	4.2.5, 7.6.2
7.5.3	4.1.8	7.7.15	4.2.11, 7.6.4
7.6.1	4.2.2	7.7.16	4.2.13, 7.6.6
7.6.2	4.2.5		

7.1 General Procedures

All reagents and solvents were obtained from commercial suppliers and used as supplied unless stated otherwise. Where appropriate, solvents and reagents were dried by standard methods i.e. distillation from the usual drying agent under nitrogen atmosphere prior to use: THF and Et₂O from sodium benzophenone; CH₂Cl₂, MeCN, and PhMe from CaH₂. Petrol refers to distilled light petroleum (b.p. 40–60 °C).

All reactions were magnetically stirred under an atmosphere of nitrogen unless stated otherwise and monitored by TLC using 0.25 mm E. Merck pre-coated silica gel plates visualised with UV light followed by phosphomolybdic acid (PMA) unless stated otherwise. All organic extracts were dried over magnesium sulfate (MgSO₄), or through azeotropic drying with toluene and concentrated *in vacuo* using a Büchi rotary evaporator. All yields refer to chromatographically and spectroscopically pure products unless stated otherwise.

All NMR spectra were recorded on Bruker DPX-300 and DRX-500 spectrometers in the solvents specified. Chemical shifts (δ) are reported in ppm relative to the residual signals of chloroform (CDCl₃, $\delta_{\text{H}} = 7.27$, $\delta_{\text{C}} = 77.2$) or dimethyl sulfoxide (DMSO-d₆, $\delta_{\text{H}} = 7.37$, $\delta_{\text{C}} = 128.4$) unless stated otherwise. Coupling constants (J) are reported in Hertz (Hz) with multiplicities described using the following abbreviations: s = singlet, d = doublet, t = triplet, q = quartet, quint = quintet, sext = sextet, sept = septet, m = multiplet, br s = broad singlet.

Infrared spectra were recorded neat on NaCl plates or as a solid on a diamond transmission accessory using a Perkin Elmer FT-IR spectrometer; details are reported as ν_{max} in cm⁻¹.

Mass spectra analysis was carried out by Tanya Marinko-Covell at the Mass Spectra service, Department of Chemistry, University of Leeds using a Micromass LCT (ES mode), Bruker Daltonic (ES mode) and Waters GCT Premier (EI and FI mode) apparatus and are reported as values in atomic mass units followed by the peak intensity relative to the base peak (100%).

Elemental analysis was carried out by Martin Huscroft and Ian Blakeley at the Microanalytical Laboratory, Department of Chemistry, University of Leeds, using a Carlo Erba 1108 Elemental Analyser apparatus.

Crystal and molecular structures were determined using single crystal X-ray diffraction carried out by Michael Hardie and Christopher Pask at the X-Ray Crystallography Facility, Department of Chemistry, University of Leeds, using Nonius KappaCCD and Bruker-Nonius FR591/X8Apex apparatus.

Melting points were measured using a Griffin melting point apparatus and are uncorrected.

Raman spectra were collected by a RamanRxn1™ fitted with a fiber-optical probe which supplies illumination at 785 nm, and the data were analysed by iC Raman™ software.

Gas chromatographic (GC) analyses of the hydrodeoxygenation reactions were performed on an Agilent HP6890 chromatograph, using a capillary column HP-5 (5% phenyl methyl siloxane) HP 19091J-413; dimensions: 30 m × 320 μm × 0.25 μm; pressure: 4.3 psi; nominal initial flow: 1.6 mL/min; average velocity: 33 cm/sec; equilibration time: 3; injection volume: 1 μL; oven: initial temperature: 60 °C; ramp: 20 °C/min to 250 °C; hold for 3 min; total run time = 21 min; inlet:mode: split ratio 10.7:1; temperature: 250 °C; split flow: 17.5 mL/min; total flow: 28.3 mL/min; gas saver: 20 mL/min; detector: temp: 250 °C; mode: constant flow; H₂ flow: 30 mL/min; air flow: 300.0 mL/min; makeup flow: 10 mL/Min (N₂). Quantitative product analysis was calculated using the following method: a 0.10 mL solution of biphenyl (10 mg/L) containing a standard of the specific compound of interest (0.05 mL) in MeOH (1.00 mL) was prepared and the internal response factor (F) was determined using following equation:

$$F = \frac{area_{IS} amount_{SC}}{area_{SC} amount_{IS}}$$

IS = internal standard (biphenyl); SC = standard specific compound of interest

During hydrogenations 0.05 mL of reaction mixture was taken every hour with 0.10 mL solution of biphenyl (10 mg/L) in MeOH (1.0 mL). The average peak areas of the analytes were measured and the amount of the hydrogenolysis products calculated using following equation:

$$amount\ of\ specific\ compound = \frac{amount_{IS} area_{SC}}{area_{IS}} \times F$$

IS = internal standard; SC = specific compound of interest; F = internal response factor

By following the standard GC method, the GC retention times of commercial standards or pure products are obtained (Table 7.1).

Table 7.1 The GC retention time of commercial standards or pure products

GC standard	Retention time (min)
anisole	2.00
benzene	0.63
phenol	3.28
cresol	4.80
toluene	1.13
3-methylanisole	5.8
3-methoxybenzyl alcohol	8.96
3-methoxybenzaldehyde	8.09
2,4,6-tris(2-methoxyphenoxy)-1,3,5-triazine	19.86

The hydrogenation reactors used in the high pressure batch and continuous stirred tank reactors are two fully-automated 0.6 L Parr reactors of Hastelloy[®] construction. In continuous mode the two reactors are connected together by 3mm high pressure tubing, whilst in batch mode only a single reactor was used. The reactors are pressure rated to 100 bar (70 bar working pressure) and the operation temperature range is 0 – 300 °C. Batch or flow mode can be switched by setting the software ‘SpectView 32 849’.



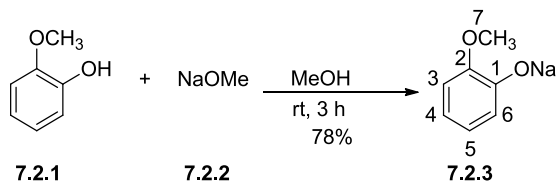
Figure 7.1 Two-stage cascade pressure CSTR, automated Parr reactors

Scanning electron microscopy (SEM) was performed on a Jeol JSM-6610LV model coupled with an Oxford Instruments INCA X-Max^N 80 with energy dispersive X-ray spectroscopy (EDS) system. The preparation of sample involved drying a representative amount of Pd/C catalyst under atmosphere condition on a glass plate surface. The sample was then coated with gold using a Quorum Q150R S sputter coater. The sample was examined under the electron microscope over the magnification range of x 5 to 300,000, using an accelerating voltage range from 300 V through to 30 kV. SEM with EDS is the most widely used for surface analytical technique and elements mapping. EDS is used to map and analyse the elemental distribution of a sample. By scanning a high energy electron beam and measuring X-ray emission, high resolution images of element distribution can be generated.

The instrument used for particle size analysis was a Malvern Mastersizer 2000. The particle sizes were measured by means of laser diffraction. Prior to running the samples, they were briefly exposed to ultrasound in an ultrasonic bath to try to break-up any aggregated particles. The sample was then added to the Hydro 2000G water tank (containing distilled water) and then pumped through to the flow cell, where the sample is exposed to the laser beam.

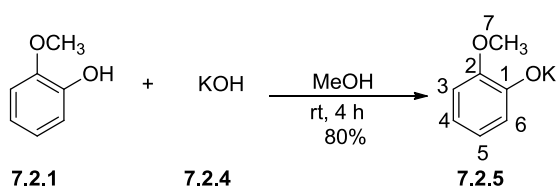
7.2 Synthesis of metal guaiacolate

7.2.1 Synthesis of sodium guaiacolate¹



Sodium methoxide (2.20 g, 40.74 mmol) was added to a solution of guaiacol (5.00 mL, 40.32 mmol) in methanol (100 mL) and the reaction mixture was stirred at room temperature for 2 h forming a purple solution. The reaction mixture was filtered and the filtrate concentrated *in vacuo* to give a white solid that was recrystallised from methanol/Et₂O/petrol to give the title compound as colourless needles (4.60 g, 31.50 mmol, 78%). ¹H NMR (300 MHz, D₂O): δ = 6.90–6.69 (m, 2H, C4H/C5H), 6.65–6.41 (m, 2H, C3H/C6H), 3.70 (s, 3H, OCH₃). ¹³C NMR (75 MHz, D₂O) δ = 156.43, 151.01, 122.49, 118.75, 113.91, 113.24, 56.12. IR ν_{max}/ cm⁻¹ (film): 3052, 2938, 2835, 2560, 1649, 1582, 1485, 1210, 1172, 725. LC-MS (ES+ mode): m/z = 146.20; calculated for C₇H₇NaO₂ requires [M⁺]: m/z = 146.12. Mpt. 115–117 °C; Lit¹ Mpt. 120°C.

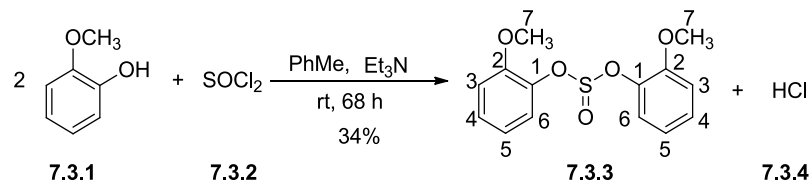
7.2.2 Synthesis of potassium guaiacolate²



Guaiacol (5.00 mL, 40.32 mmol) was added dropwise to a solution of KOH (2.30 g, 41.07 mmol) in methanol (100 mL) and the reaction mixture was stirred at room temperature for 12 h forming a pink suspension. The solid was collected by suction filtration and recrystallised from methanol/Et₂O/petrol to afford the title compound as white needles (5.20 g, 32.10 mmol, 80%). ¹H NMR (300 MHz, CDCl₃): δ = 6.90–6.70 (m, 2H, C4H/C5H), 6.64–6.41 (m, 1H, C3H/C6H), 3.70 (s, 3H, OCH₃). ¹³C NMR (75 MHz, D₂O) δ = 156.40, 151.00, 122.49, 118.73, 113.93, 113.24, 56.12. IR ν_{max}/ cm⁻¹ (film): 3047, 2987, 2833, 2563, 1654, 1580, 1487, 1208, 1176, 733. LC-MS (ES+ mode): m/z = 162.10; calculated for C₇H₇KO₂ requires [M+]: m/z = 162.23. Mpt. 163–165 °C; Lit² Mpt.167 °C.

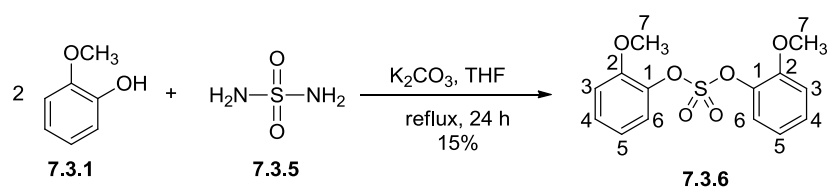
7.3 Synthesis of diguaiacol sulfite and sulfate

7.3.1 Synthesis of diguaiacol sulfite

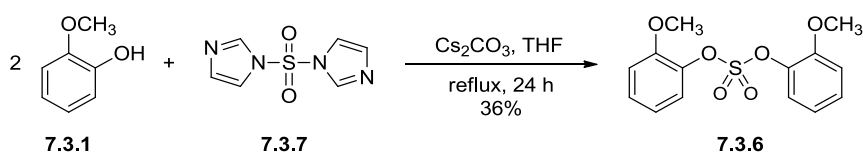


A mixture of guaiacol (10.00 g, 80.65 mmol) and Et₃N (11.20 mL, 80.30 mmol) was added dropwise to a solution of SOCl₂ (4.40 mL, 59.17 mmol) in toluene (100 mL) at room temperature. The resulting brown mixture was stirred at room temperature for 68 h. The reaction mixture was filtered and the filtrate concentrated *in vacuo* to give a yellow solid that was recrystallised from Et₂O/petrol to give the title compound as a white solid (4.00 g, 13.60 mmol, 34%). ¹H NMR (300 MHz, CDCl₃): δ = 7.23–7.17 (m, 4H, C4H/C5H), 6.97–6.90 (m, 4H, C3H/C6H), 3.81 (s, 6H, OCH₃). ¹³C NMR (75 MHz, CDCl₃): δ = 151.78, 137.95, 127.15, 124.21, 120.87, 112.56, 55.97. IR ν_{max}/ cm⁻¹ (film): 3071, 2943, 2841, 2557, 2159, 2025, 1602, 1458. HRMS (ES+ mode): m/z = 317.0450 [100%, MNa⁺]; calculated for C₁₄H₁₄O₅S [MNa⁺]: m/z = 317.0454. Mpt. (Et₂O/petrol) 70–71 °C.

7.3.2 Synthesis of diguaiacol sulfate³



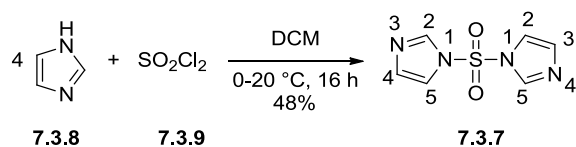
A mixture of guaiacol (2.20 g, 17.74 mmol), K₂CO₃ (1.20 g, 8.70 mmol) and sulfamide (0.85 g, 8.85 mmol) in THF (5 mL) was heated at reflux for 24 h. The mixture was allowed to cool to room temperature and then filtered through a short plug of silica eluting with Et₂O. The filtrate was concentrated *in vacuo* to give a solid that was then recrystallised from Et₂O/petrol to give the title compound as a white solid (0.4 g, 1.29 mmol, 15 %). ¹H NMR (300 MHz, CDCl₃): δ = 7.26–6.93 (m, 4H, C4H/C5H), 6.88 (d, 2H, C6H), 6.80 (t, 2H, C3H), 3.86 (s, 6H, OCH₃). ¹³C NMR (75 MHz, CDCl₃): δ = 150.74, 137.92, 127.11, 124.25, 120.87, 112.51, 55.97. LC-MS (ES+ mode): m/z = 333.0 [MNa⁺]; calculated for C₁₄H₁₄NaO₆S requires [MNa⁺]: m/z = 333.0. IR ν_{max}/ cm⁻¹ (film): 3072, 2943, 2842, 2025, 1777, 1599, 1467, 1196. Mpt. 53–54 °C; Lit.³ Mpt. (ethanol) 54°C.



A mixture of guaiacol (5.50 g, 44.35 mmol), Cs₂CO₃ (4.90 g, 15.04 mmol) and N,N'-sulfuryldiimidazole (3.00 g, 15.15 mmol) in THF (15 mL) was heated at reflux for 24 h. The reaction mixture was cooled to room temperature and then filtered through a short plug of silica eluting with Et₂O. The filtrate was concentrated *in vacuo* to give a solid that was recrystallised from Et₂O/petrol to give the title compound as a white solid (1.69 g, 5.45 mmol, 36%).

Spectroscopic data identical as those reported above.

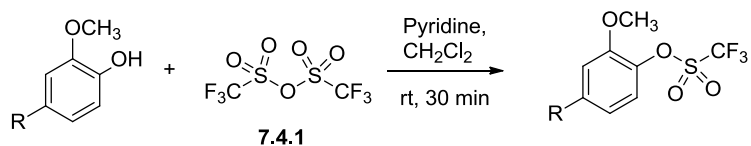
N,N'-sulfuryldiimidazole⁴



A solution of imidazole (20.00 g, 293.77 mmol) in CH₂Cl₂ (210 mL) was cooled to 0 °C and added dropwise to a solution of sulfuryl chloride (5.00 mL, 61.87 mmol) in CH₂Cl₂ (28 mL) at 0 °C. The reaction mixture was warmed to room temperature and stirred at room temperature for 16 h. The reaction mixture was filtered and the filtrate concentrated *in vacuo* to give a white solid that was recrystallised from isopropyl alcohol (100 mL) to give the title compound as white needles (7.11 g, 35.88 mmol, 48%). ¹H NMR (300 MHz, CDCl₃): δ = 8.42 (d, *J* = 2.2 Hz, 2H, C2H), 7.68 (s, 2H, C5H), 6.99 (d, *J* = 1.5 Hz, 2H, C4H). Lit⁴ ¹H NMR (400 MHz, DMSO-d₆): δ = 8.51 (s, 2H), 7.92 (s, 2H), 7.24 (s, 2H). ¹³C NMR (75 MHz, CDCl₃): δ = 136.55, 132.51, 117.40. Lit⁴ ¹³C NMR (100 MHz, d₆-DMSO): δ = 118.4, 131.9, 137.6. HRMS (ES+ mode): *m/z* = 199.0279 [100%, MH⁺]; calculated for C₆H₆N₄O₂S requires [MH⁺]: *m/z* = 199.0290.

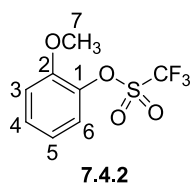
7.4 Synthesis of aryl sulfonates

7.4.1 General procedure for synthesis of aryl triflates



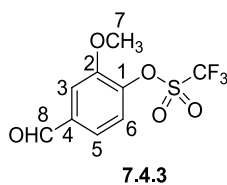
To a solution of phenol (1.00 equiv.) in dichloromethane (1.67 % (w/v)) at ambient temperature was added trifluoromethanesulfonic anhydride (1.50 equiv.) and pyridine (2.00 equiv.). The reaction mixture was stirred for 30 min then quenched with water (1 × 20 mL), the organic phase separated and washed twice more with water (2 × 20 mL). The organic layer was dried over MgSO₄, filtered and concentrated *in vacuo*. The residue was purified by chromatography (petrol:ethyl acetate, 9:1).

Guaiacol triflate⁶



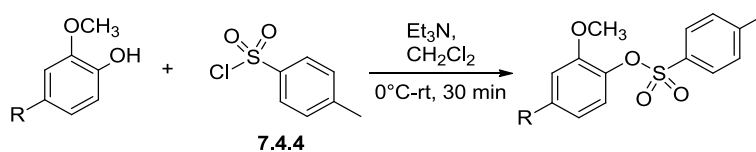
To a solution of guaiacol (1.10 g, 8.06 mmol) in CH_2Cl_2 was added trifluoromethanesulfonic anhydride (3.40 g, 12.09 mmol) and pyridine (1.30 mL, 16.12 mmol) in dichloromethane (1.67 % (w/v)) at ambient temperature. The reaction mixture was stirred for 30 min then quenched with water (1×20 mL), the organic layer was separated, washed twice more with water (2×20 mL), dried over MgSO_4 , filtered and concentrated *in vacuo*. The residue was purified by chromatography (petrol: ethyl acetate, 9:1) to give the title product (1.97 g, 7.69 mmol, 95%) as a yellow oil that required no further purification. ^1H NMR (501 MHz, CDCl_3): $\delta = 7.32$ (ddd, $J = 8.3, 1.6, 1$ Hz, 1H, C5H), 7.22 (dd, $J = 8.2, 1.6$ Hz, 1H, C4H), 7.04 (dd, $J = 8.3, 1.5$ Hz, 1H, C6H), 6.99–6.94 (m, 1H, C3H), 3.91 (s, 3H, OCH_3). Lit⁵ ^1H NMR (400 MHz, CDCl_3): $\delta = 7.33$ (ddd, $J = 8.4, 8.0, 1.6$ Hz, 1H), 7.22 (dd, $J = 8.0, 1.6$ Hz, 1H), 7.04 (dd, $J = 8.4, 1.4$ Hz, 1H), 6.98 (dd, $J = 8.0, 1.4$ Hz, 1H), 3.92 (s, 3H). ^{13}C NMR (126 MHz, CDCl_3): $\delta = 151.44, 138.81, 129.21, 122.44, 120.87, 117.48$ (CF_3), 113.19, 56.11. Lit⁶ ^{13}C NMR (CDCl_3): $\delta = 151.6, 139.0, 129.5, 122.6, 121.0, 119.0$ (q, $J_{\text{C-F}} = 321$ Hz), 113.36, 56.2.

Vanillin triflate⁷



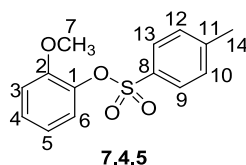
To a solution of vanillin (0.80 g, 6.45 mmole) in CH_2Cl_2 was added trifluoromethanesulfonic anhydride (2.72 g, 9.68 mmol) and pyridine (1 mL, 12.41 mmol) in dichloromethane (1.67 % (w/v)) at ambient temperature. The reaction mixture was stirred for 30 min then quenched with water (1×20 mL), the organic layer was separated, washed twice more with water (2×20 mL), dried over MgSO_4 , filtered and concentrated *in vacuo*. The residue was purified by chromatography (petrol:ethyl acetate, 9:1) to give the title product (1.13 g, 3.98 mmol, 60%) as a yellow oil that required no further purification. ^1H NMR (501 MHz, CDCl_3) δ = 9.99 (s, 1H, CHO), 7.57 (d, J = 1.9 Hz, 1H, C5H), 7.52 (dd, J = 8.1, 1.8 Hz, 1H, C3H), 7.42 (d, J = 8.2 Hz, 1H, C6H), 4.00 (s, 3H, OCH_3). Lit⁷ ^1H NMR (500 MHz, CDCl_3): δ (ppm) = 9.99 (s, 1H, -CHO), 7.57 (d, J = 1.9 Hz, 1H, Ar-H), 7.52 (dd, J_1 = 8.2 Hz, J_2 = 1.9 Hz, 1H, Ar-H), 7.42 (d, J = 8.2 Hz, 1H, Ar-H), 4.00 (s, 3H, - OCH_3). ^{13}C NMR (126 MHz, CDCl_3): δ = 190.27, 152.26, 142.74, 136.81, 124.09, 123.21, 117.42 (CF_3), 111.79, 56.52. Lit⁷ ^{13}C NMR (125 MHz, CDCl_3): δ (ppm) = 190.33, 152.29, 142.78, 136.85, 124.11, 123.24, 118.74 (q, $J_{\text{C-F}}$ = 312 Hz), 111.84, 56.54.

7.4.2 General procedure for synthesis of aryl tosylates



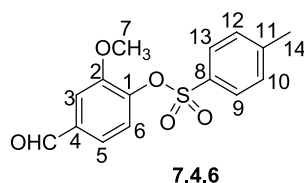
To a solution of phenol (1.00 equiv) in dichloromethane (5% (w/v)) at 0 °C was first added triethylamine (1.00 equiv) followed by *p*-toluenesulfonyl chloride (1.00 equiv). The reaction was warmed to room temperature and stirred for 2 h, then 1M HCl (10 mL) was added and the phases separated. The organic layer was further washed with 1M HCl (2 × 10 mL) followed by saturated aqueous NaHCO₃ (1 × 10 mL) and with brine (1 × 10 mL). The combined organic layers were dried with MgSO₄, filtered and concentrated *in vacuo*.

Guaiacol tosylate^{8,9}



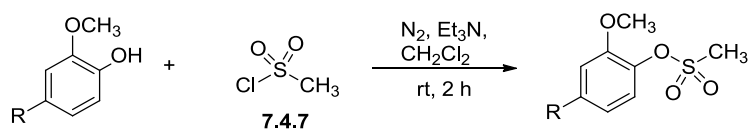
To a solution of guaiacol (1.00 g, 8.06 mmol) in dichloromethane (5% (w/v)) at 0 °C was first added triethylamine (1.10 mL, 7.89 mmol) followed by *p*-toluenesulfonyl chloride (1.53 g, 8.06 mmol). The reaction was allowed to warm to room temperature and stirred for 2 h, then 1M HCl (10 mL) added and the phases separated. The organic layer was further washed with 1M HCl (10 mL × 2) followed by saturated aqueous NaHCO₃ (10 mL) and with brine (10 mL). The combined organic layers were dried with MgSO₄, filtered and concentrated *in vacuo* to give the title product (1.81 g, 6.51 mmol, 81%). ¹H NMR (501 MHz, CDCl₃): δ = 7.79–7.72 (m, 2H, C9H/C13H), 7.33–7.26 (m, 2H, C4H/C5H), 7.23–7.10 (m, 2H, C10H/C12H), 6.94–6.80 (m, 2H, C3H/C6H), 3.56 (s, 3H, OCH₃), 2.44 (s, 3H, C14H₃). Lit⁸ ¹H NMR(300 MHz, CDCl₃): δ = 7.74 (d, *J* = 8.3 Hz, 2 H), 7.28 (d, *J* = 9.2 Hz, 2 H), 7.22–7.17 (m, 1 H), 7.16–7.11 (m, 1 H), 6.88 (dd, *J* = 7.9 and 1.8 Hz, 1 H), 6.85–6.80 (m, 1 H), 3.54 (s, 3 H), 2.43 (s, 3 H). ¹³C NMR (126 MHz, CDCl₃): δ = 151.86, 144.89, 138.49, 133.39, 129.30, 128.63, 127.97, 124.05, 120.62, 112.70, 55.54, 21.66. Lit⁸ ¹³C NMR (75 MHz, CDCl₃): δ = 151.8, 144.9, 138.4, 133.3, 129.3, 128.6, 128.0, 124.0, 120.6, 112.7, 55.5, 21.6. Mpt. (DCM) 83–84 °C; Lit⁹ Mpt. (CHCl₃) 85–86 °C

Vanillin tosylate^{10,11}



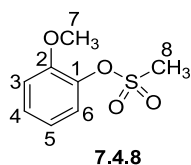
To a solution of vanillin (1.0 g, 6.57 mmole, 1.0 meq.) in dichloromethane (5% (w/v)) at 0 °C was first added triethylamine (1.00 mL, 7.17 mmol) followed by *p*-toluenesulfonyl chloride (1.25 g, 6.57 mmol). The reaction was allowed to warm to room temperature and stirred for 2 h, then 1M HCl (10 mL) added and the phases separated. The organic layer was further washed with 1M HCl (10 mL × 2) followed by saturated aqueous NaHCO₃ (10 mL) and with brine (10 mL). The combined organic layers were dried with MgSO₄, filtered and concentrated *in vacuo* to give the title product (1.42 g, 4.64 mmol, 71%). ¹H NMR (501 MHz, CDCl₃): δ = 9.93 (s, 1H, CHO), 7.76 (d, *J* = 8.3 Hz, 2H, C3H/C5H), 7.43 (dd, *J* = 8.1, 1.8 Hz, 1H, C6H), 7.39–7.28 (m, 4H, C9H/C10H/C12H/C13H), 3.64 (s, 3H, OCH₃), 2.45 (s, 3H, C14H₃). Lit¹⁰ ¹H NMR (300 MHz, CDCl₃): δ = 9.91 (s, 1 H, CHO), 7.75 (d, *J* = 8.3 Hz, 2H, Ar-H), 7.46–7.28 (m, 5H, Ar-H), 3.63 (s, 3H, OCH₃), 2.4 (s, 3H, Ar-CH₃). ¹³C NMR (126 MHz, CDCl₃): δ = 190.77, 152.63, 145.45, 143.06, 135.78, 133.00, 129.50, 128.59, 124.55, 124.32, 111.05, 55.80, 21.71. Lit¹⁰ ¹³C NMR (75 MHz, CDCl₃): δ = 190.7, 152.4, 145.4, 142.8, 135.6, 132.6, 129.4, 128.4, 124.3, 124.1, 110.9, 55.6, 21.5. Mpt. (DCM) 120–121 °C; Lit¹¹ Mpt. (Hexane) 116–117 °C and Lit¹⁰ Mpt. 126–128 °C.

7.4.3 General procedure for synthesis of mesylate



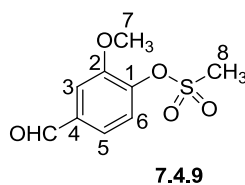
To a solution of phenol (1.00 equiv) in dichloromethane (60 volume equiv.) under nitrogen at room temperature, were added methanesulfonyl chloride (1.30 equiv), and triethylamine (1.50 equiv) as neat liquids. The reaction mixture was stirred for 1 h then diluted with water (60 mL), and the organic phase separated. The aqueous layer was extracted further with dichloromethane (2×15 mL), and the organic layers combined and washed with water and brine (2×30 mL) successively, then dried with MgSO_4 . The solvent was evaporated under reduced pressure.

*Guaiacol mesylate*¹²



To a solution of guaiacol (1.00 g, 8.06 mmol) in dichloromethane (60 mL) under nitrogen at room temperature, were added methanesulfonyl chloride (1.20 g, 10.48 mmol), and triethylamine (1.70 mL, 12.19 mmol) as neat liquids. The reaction mixture was stirred for 1 h then diluted with water (60 mL), and the organic phase separated. The aqueous layer was extracted further with dichloromethane (15 mL \times 2), and the organic layers combined and washed with water and brine (30 mL \times 2) successively, then dried with MgSO₄. The solvent was evaporated *in vacuo* to give the title products (1.59g, 7.87 mmol, 97%). ¹H NMR (300 MHz, CDCl₃): δ = 7.33–7.19 (m, 2H, C3H/C6H), 7.05–6.86 (m, 2H, C4H/C5H), 3.85 (s, 3H, OCH₃), 3.13 (s, 3H, C8H₃). Lit¹² ¹H NMR (300 MHz, CDCl₃): δ = 7.32–7.23 (m, 2H), 7.03–6.92 (m, 2H), 3.88 (s, 3H), 3.17 (s, 3H). ¹³C NMR (75 MHz, CDCl₃): δ = 151.41, 138.34, 128.33, 124.57, 121.12, 112.90, 55.91, 38.24. Lit¹² ¹³C NMR (100 MHz, CDCl₃): δ = 151.25, 138.23, 128.12, 124.39, 120.99, 112.83, 55.91, 38.20.

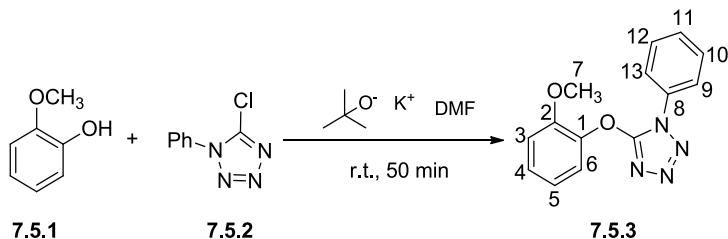
Vanillin mesylate^{13,14}



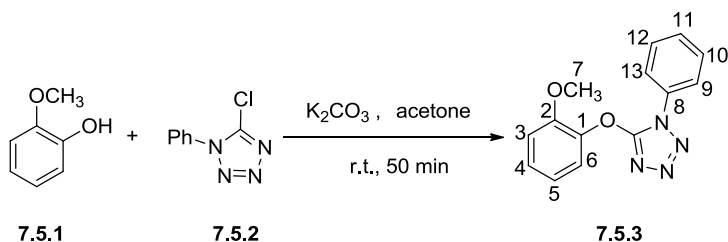
To a solution of vanillin (1.00 g, 6.57 mmol) in dichloromethane (30 mL), under nitrogen at room temperature, were added methanesulfonyl chloride (1.00 g, 8.73 mmol), and triethylamine (1.40 mL, 10.04 mmol) as neat liquids. The reaction mixture was stirred for 1 h then diluted with water (60 mL), and the organic phase separated. The aqueous layer was extracted further with dichloromethane (15 mL \times 2), and the organic layers combined and washed with water and brine (30 mL \times 2) successively, then dried with MgSO₄. The solvent was evaporated *in vacuo* to give the title products (0.94g, 4.09 mmol, 62%). ¹H NMR (501 MHz, CDCl₃): δ = 9.97 (s, 1H, CHO), 7.54 (d, J = 1.7 Hz, 1H, C5H), 7.52–7.47 (m, 2H, C3H/C6H), 3.98 (s, 3H, OCH₃), 3.25 (s, 3H, C8H₃). ¹³C NMR (126 MHz, CDCl₃): δ = 190.67, 152.31, 142.79, 136.01, 124.73, 119.13, 111.32, 56.30, 38.87. LC-MS (ES+ mode): m/z = 230.90 [100%, M⁺]; calculated for C₉H₁₀O₅S requires [M⁺]: m/z = 230.02. IR ν_{\max} / cm⁻¹ (film): 3009, 2914, 1692, 1350, 1147, 1102, 848, 498. Mpt. 88-89 °C; Lit¹³ Mpt. (Methanol/H₂O) 89 °C and Lit¹⁴ Mpt. (ethanol) 93–94 °C

7.5 Synthesis of tetrazoles

5-(2-Methoxy-phenoxy)-1-phenyl-1H-tetrazole^{15,16}



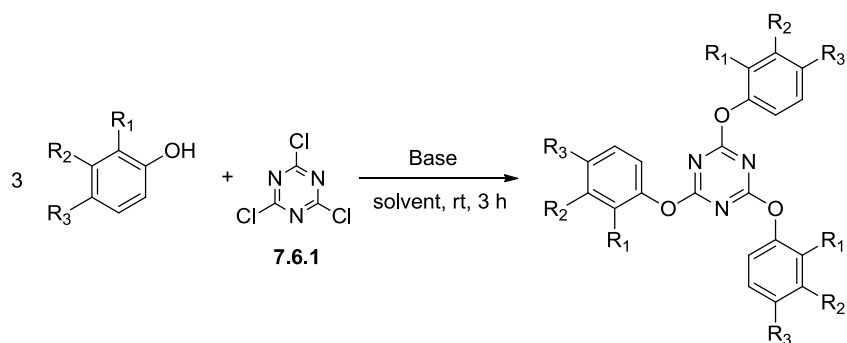
A solution of guaiacol (2.75 g, 22.18 mmol), 5-chloro-1-phenyl-1*H*-tetrazole (4.00 g, 22.15 mmol,) and potassium *tert*-butoxide (2.70 g, 24.06 mmol) in DMF (53 mL) was stirred at room temperature for 1 h. The reaction mixture was quenched with ice–water and the resulting white solid isolated by filtration and recrystallised (from methanol) to give the title compound as a white solid (1.90 g, 7.10 mmol, 32%). ¹H NMR (300 MHz, CDCl₃): δ = 7.93–7.82 (m, 2H, C9H/C13H), 7.65–7.44 (m, 3H, C10H/C11H/C12H), 7.41–7.24 (m, 2H, C4H/C5H), 7.10–6.96 (m, 2H, C3H/C6H), 3.81 (s, 3H, OCH₃). Lit¹⁵ ¹H NMR (300 MHz, acetone-d₆): δ = 7.98–7.48 (m, 9H), 3.76 (s, 3H). ¹³C NMR (75 MHz, CDCl₃): δ = 150.43, 142.50, 133.36, 129.64, 129.22, 127.86, 122.16, 121.58, 121.05, 113.09, 55.96. IR ν_{max}/ cm⁻¹ (film): 3065, 2159, 1591, 1460, 1245, 766, 691. LC-MS (ES+ mode): *m/z* = 269.10 [100%, MH⁺]; calculated for C₁₄H₁₂N₄O₂ requires [MH⁺]: *m/z* = 269.10. Mpt. 109–110 °C; Lit¹⁵ Mpt. 109 °C and Lit¹⁶ Mpt. 111–112 °C



A solution of guaiacol (1.10 g, 8.87 mmol), 5-chloro-1-phenyl-1*H*-tetrazole (1.60 g, 8.86 mmol) and K₂CO₃ (2.45 g, 17.74 mmol) in acetone (25 mL) was stirred at room temperature for 1 h. The reaction mixture was quenched with ice–water and the resulting white solid isolated by filtration and recrystallised from to give the title compound as a white solid (1.78 g, 6.65 mmol, 75%).

Spectroscopic data identical as those reported above.

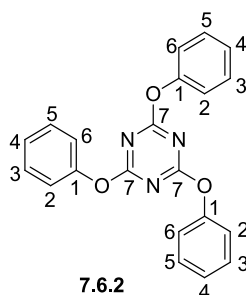
7. 6 Synthesis of 2,4,6-*tris*(aryloxy)-1,3,5-triazine derivatives



General procedure

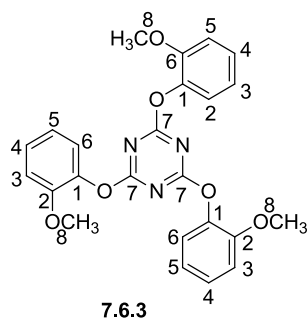
A solution of cyanuric chloride (1.00 equiv) in acetone (300 volume equiv.) was added dropwise to a solution of phenols (3.00 equiv) in water (300 mL) with NaOH (3.00 equiv) and the resulting solution stirred at room temperature for 3 h. The reaction mixture was filtered, the resulting solid was washed with water (2 × 100 volume equiv.) and crystallised from MeOH.

2,4,6-Triphenoxy-1,3,5-triazine¹⁷



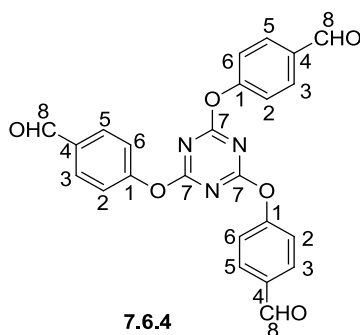
A solution of cyanuric chloride (1.30 g, 7.08 mmol) in acetone (300 mL) was added dropwise to a solution of phenol (2.00 g, 21.25 mmol) in water (300 mL) with NaOH (0.85 g, 21.25 mmol) and the resulting solution stirred at room temperature for 3 h. The reaction mixture was filtered, the resulting solid was washed with water (2 × 100 mL) and crystallised from MeOH to give the title product as a white solid (2.26g, 6.32 mmol, 89%) ¹H NMR (500 MHz, CDCl₃): δ = 7.35 (ddd, *J* = 8.3, 7.4, 0.9 Hz, 9H, C3H/C4H/C5H), 7.16–7.10 (m, 6H, C2H/C6H). Lit ¹H NMR: δ = 7.25–6.60 (m). ¹³C NMR (125 MHz, CDCl₃): δ = 173.68, 151.61, 129.44, 126.03, 121.39. HRMS (ES+ mode): *m/z* = 380.1020 [100%, MNa⁺]; calculated for C₂₁H₁₅N₃O₃ requires [MNa⁺]: *m/z* = 380.1006. Mpt. (MeOH) 230–232 °C; Lit¹⁷ Mpt. (CHCl₃/hexane) 230–231 °C.

2,4,6-Tris(2-methoxyphenoxy)-1,3,5-triazine¹⁸



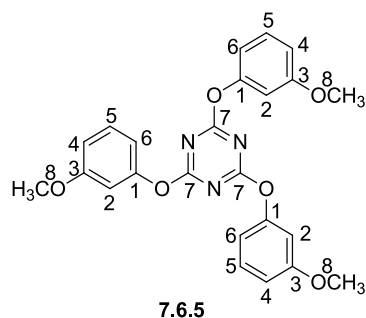
A solution of cyanuric chloride (10.39 g, 56.45 mmol) in acetone (300 mL) was added dropwise to a solution of guaiacol (21.00 g, 169.35 mmol) in water (300 mL) with NaOH (6.77 g, 169.35 mmol, 3.0 equiv) and the resulting solution stirred at room temperature for 3 h. The reaction mixture was filtered, the resulting solid was washed with water (2×100 mL) and crystallised from MeOH to give the title products as white crystals (19.68 g, 44.03 mmol, 78%). ^1H NMR (500 MHz, DMSO- d_6): δ = 7.22 (ddd, J = 8.2, 7.4, 1.6 Hz, 3H, C5), 7.13 (ddd, J = 30.5, 8.1, 1.5 Hz, 6H, C4/C6), 6.93 (td, J = 7.7, 1.4 Hz, 3H, C3), 3.85 (s, 9H, OCH₃). ^{13}C NMR (125 MHz, DMSO- d_6): δ = 173.62, 151.16, 140.86, 126.80, 122.35, 120.60, 112.66, 55.79. HRMS (ES+ mode): m/z = 448.1509 [100%, MH^+]; calculated for $\text{C}_{24}\text{H}_{22}\text{N}_3\text{O}_6$ requires [MH^+]: m/z = 448.1506. IR ν_{max} / cm^{-1} (film): 3017, 2836, 2097, 1695, 1596, 1476, 1253, 1202, 1166, 743. Analysis calculated (%) for $\text{C}_{24}\text{H}_{21}\text{N}_3\text{O}_6$: C, 64.42; H, 4.73; N, 9.39. Found: C, 64.15; H, 4.75; N, 9.25. Mpt. (MeOH) 139–141°C; Lit¹⁸ Mpt. 145 °C

4,4',4''-[1,3,5-Triazine-2,4,6-triyltris(oxy)]tri-benzaldehyde^{19,20}



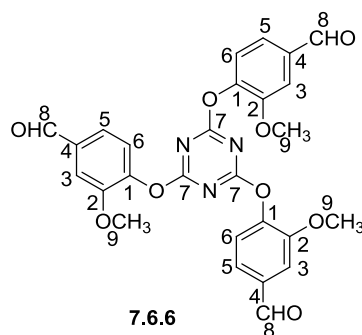
A solution of cyanuric chloride (1.50 g, 8.16 mmol) in acetone (300 mL) was added dropwise to a solution of 4-hydroxybenzaldehyde (2.60 g, 24.50 mmol) in water (300 mL) with NaOH (0.98 g, 24.50 mmol) and the resulting solution stirred at room temperature for 3 h. The reaction mixture was filtered, the resulting solid was washed with water (2×100 mL) and crystallised from MeOH to give the title product as a white solid (3.08 g, 6.97 mmol, 85%). ¹H NMR (500 MHz, CDCl₃): δ = 10.01(s, 3H, CHO), 7.91 (d, J = 2.0, 6H, C3H/C5H), 7.32 (d, J = 8.6, 6H, C2H/C6H). Lit¹⁹ ¹H NMR (400 MHz, CDCl₃): 10.00 (s, 3H, CHO), 7.93 (d, 6H, C3H), 7.31 (d, 6H, C2H). ¹³C NMR (125 MHz, CDCl₃): δ = 190.64, 173.25, 155.71, 134.50, 131.31, 122.21. Lit¹⁹ ¹³C NMR (125 MHz, CDCl₃): 190.9, 173.6, 156.0, 134.8, 131.7, 122.6. HRMS (ES+ mode): m/z = 464.0870 [100%, MNa⁺]; calculated for C₂₄H₁₅N₃O₆ requires [MNa⁺]: m/z = 464.0853. Mpt. (MeOH) 168–170°C; Lit²⁰ Mpt. (EtOAc) 174–176 °C.

2,4,6-Tris(3-methoxyphenoxy)-1,3,5-triazine



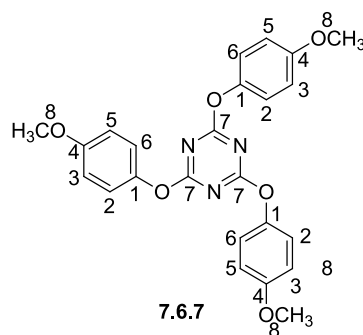
A solution of cyanuric chloride (1.05 g, 5.70 mmol) in acetone (40 mL) was added dropwise to a solution of 3-methoxyphenol (2.12 g, 17.10 mmol) in water (40 mL) with NaOH (0.68 g, 17.10 mmol) and the resulting solution was stirred at room temperature for 3 h. The reaction mixture was filtered, the resulting solid was washed with water (100 mL \times 2) and recrystallised from MeOH to give the product as a white solid (2.34 g, 5.24 mmol, 92%). ^1H NMR (501 MHz, CDCl_3) δ = 7.24 (s, 3H, C5H), 6.75 (dddd, J = 16.1, 8.1, 2.4, 0.8 Hz, 6H, C4H/C6H), 6.69 (t, J = 2.3 Hz, 3H, C2H), 3.76 (s, 9H, OCH_3). ^{13}C NMR (126 MHz, CDCl_3) δ = 173.63, 160.49, 152.45, 129.80, 113.59, 111.88, 107.52, 55.41. LC-MS: m/z = 448.20 [100%, MH^+]; calculated for $\text{C}_{24}\text{H}_{21}\text{N}_3\text{O}_6$ requires [MH^+]: m/z = 448.15. IR ν_{max} / cm^{-1} (film): 3011, 2840, 1576, 1269, 1146, 1040, 776. Mpt. 145–147 $^\circ\text{C}$

4,4',4''-(s-Triazine-2,4,6-triyltrioxy)tri-*m*-anisaldehyde



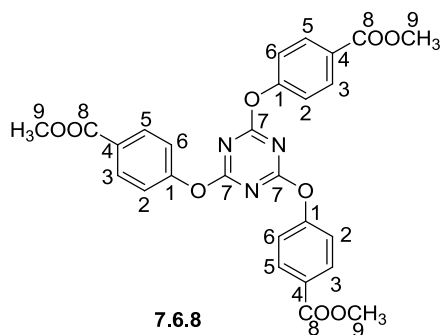
A solution of cyanuric chloride (1.21 g, 6.57 mmol) in acetone (300 mL) was added dropwise to a solution of vanillin (3.00 g, 19.72 mmol) in water (300 mL) with NaOH (0.79g, 19.72 mmol) and the resulting solution stirred at room temperature for 3 h. The reaction mixture was filtered, the resulting solid was washed with water (2×100 mL) and crystallised from MeOH to give the title product as a white solid (2.16 g, 4.07 mmol, 62%). ^1H NMR (500 MHz, CDCl_3): δ = 10.01 (s, 1H, CHO), 7.50 (d, J = 1.8 Hz, 3H, C5H), 7.49 (d, J = 1.8 Hz, 3H, C3H), 7.30 (d, J = 8.4 Hz, 3H, C6H), 3.86 (3H, s, OCH_3). ^{13}C NMR (125 MHz, CDCl_3): δ = 190.79, 173.70, 151.70, 145.04, 135.73, 124.72, 122.71, 111.48, 56.26. HRMS (ES⁺ mode): m/z = 554.1176 [100%, MNa^+]; calculated for $\text{C}_{27}\text{H}_{21}\text{N}_3\text{O}_9$ requires [MNa^+]: m/z = 554.1170. IR ν_{max} / cm^{-1} (film): 3012, 2835, 2563, 2097, 1694, 1593, 1466, 1263, 1202, 1174, 812, 732. Mpt. (MeOH) 238–240 °C.

2,4,6-Tris(4-methoxyphenoxy)-1,3,5-triazine^{21,22}



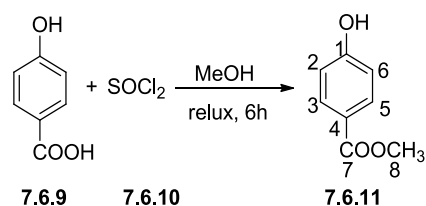
A solution of cyanuric chloride (1.27 g, 6.90 mmol) in acetone (40 mL) was added dropwise to a solution of 4-methoxyphenol (2.57 g, 20.71 mmol) in water (40 mL) with NaOH (0.83 g, 20.71 mmol) and the resulting solution was stirred at room temperature for 3 h. The reaction mixture was filtered, then the resulting solid was washed with water (100 mL \times 2) to give the product as a yellow solid (2.84 g, 6.35 mmol, 92%). ¹H NMR (501 MHz, CDCl₃): δ = 7.05 (d, J = 9.0 Hz, 6H, C2H/C6H), 6.86 (d, J = 9.1 Hz, 6H, C3H/C5H), 3.79 (s, 9H, OCH₃). Lit²¹ ¹H NMR (CDCl₃): 7.08–7.01, 6.92–6.84 (2m, 12H, HAr); 3.79 (s, 9H, OCH₃); ¹³C NMR (126 MHz, CDCl₃): δ = 173.97, 157.37, 145.19, 122.19, 114.46, 55.59. Lit²¹ ¹³C NMR: 174.0, 157.4, 145.2, 122.2, 114.5, 55.6, Mpt. 198–200 °C; Lit²² Mpt. (dioxane) 199–200 °C.

4,4',4''-[1,3,5-Triazine-2,4,6-triyltris(oxy)]tris-benzoic acid trimethyl ester



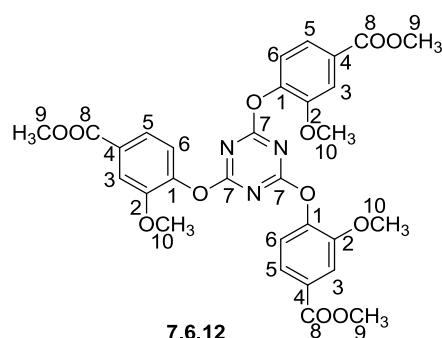
A solution of cyanuric chloride (0.81 g, 4.38 mmol) in THF (20 mL) was slowly added to a solution of methyl 4-hydroxybenzoate (2.00 g, 13.14 mmol) and DIPEA (1.70 g, 13.14 mmol) in THF (50 mL) at room temperature. The resulting solution was heated at reflux for 5 h. The reaction mixture was allowed to cool to room temperature and concentrated *in vacuo* to give the crude products that was purified by column chromatography [petrol/EtOAc (4:1)] and recrystallised from CH₂Cl₂ to give the title product as white solid (1.54 g, 2.90 mmol, 66%). ¹H NMR (501 MHz, CDCl₃): δ = 8.05 (d, *J* = 8.7 Hz, 6H, C3H/C5H), 7.19 (d, *J* = 8.8, 6H, C2H/C6H), 3.93 (3H, s, COOCH₃). ¹³C NMR (125 MHz, CDCl₃): δ = 173.10, 166.80, 159.74, 131.92, 122.87, 115.89, 51.89. HRMS (ES⁺ mode): *m/z* = 554.1176 [100%, MNa⁺]; calculated for C₂₇H₂₁N₃O₉ requires [MNa⁺]: *m/z* = 554.1170. IR ν_{max}/ cm⁻¹ (film): 2986, 1726, 1538, 1357, 1286, 1117, 739. Mpt. 148–151 °C.

4-Hydroxy-benzoic acid methyl ester²³



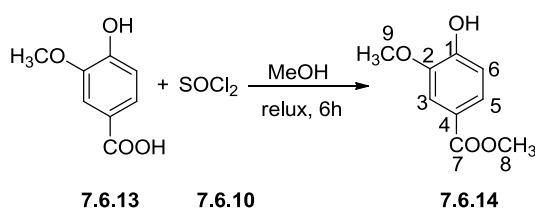
Thionyl chloride (8.61 g, 72.40 mmol) was added to the solution of the 4-hydroxybenzoic acid (5.00 g, 36.20 mmol) in MeOH (60 mL). The resulting solution was heated at reflux for 6 h. The solution was cooled using an ice water bath and neutralised with saturated NaHCO₃ solution (pH 7–8). The reaction mixture was concentrated *in vacuo*, EtOAc (40 mL) and 1M HCl (25 mL) were added to the resulting solid. The organic layer was washed with water (2 × 25 mL) and brine (25 mL). The combined organic layers were dried with Na₂SO₄ and concentrated *in vacuo* to give a brown oil that was triturated with petrol to give the title product as white solid (4.53 g, 29.77 mmol, 82%). ¹H NMR (500 MHz, CDCl₃): δ = 7.96 (d, *J* = 8.8 Hz, 2H, C3H/C5H), 6.85 (d, *J* = 8.8 Hz, 2H, C2/C6), 5.26 (s, 1H, OH), 3.89 (s, 3H, COOCH₃). Lit²³ ¹H NMR (400 MHz, CDCl₃): δ = 7.99 (d, 1H, *J* = 8.0 Hz), 6.90 (d, 1H, *J* = 8.0 Hz), 6.05 (br s, 1H), 3.92 (s, 3H). ¹³C NMR (125 MHz, CDCl₃) δ = 167.22, 159.58, 131.92, 122.96, 115.16, 51.90. Lit²³ ¹³C NMR (200 MHz, CDCl₃) δ = 167.3, 160.1, 132.0, 122.5, 115.3, 52.1.

4,4',4''-[1,3,5-Triazine-2,4,6-triyltris(oxy)]tri-*m*-anisic acid trimethyl ester



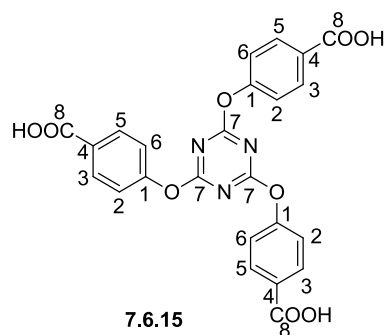
A solution of cyanuric chloride (0.17 g, 0.91 mmol) in THF (20 mL) was slowly added to a solution of 3-methoxy-4-hydroxybenzoic acid methyl ester (0.50 g, 2.74 mmol) and DIPEA (0.35 g, 2.74 mmol) in THF (50 mL) at room temperature. The resulting solution was heated at reflux for 5 h. The reaction mixture was allowed to cool to room temperature and concentrated *in vacuo* to give the crude products that was purified by column chromatography [petrol/EtOAc (4:1)] and recrystallised from CH₂Cl₂ to give the title product as a white solid (0.19 g, 0.30 mmol, 33%). ¹H NMR (500 MHz, CDCl₃): δ = 7.67 (dd, *J* = 8.3, 1.9 Hz, 3H, C5H), 7.62 (d, *J* = 1.9 Hz, 3H, C3H), 7.16 (d, *J* = 8.3 Hz, 3H, C6H), 3.93 (s, 9H, OCH₃), 3.83 (s, 9H, COOCH₃). ¹³C NMR (125 MHz, DMSO-d₆): δ = 166.71, 164.10, 150.84, 142.00, 129.16, 124.62, 117.64, 112.29, 56.19, 52.07. LC-MS: *m/z* = 622.22 [100%, MH⁺]; calculated for C₃₀H₂₇N₃O₁₂ requires [MH⁺]: *m/z* = 622.16. IR ν_{max}/ cm⁻¹ (film): 2975, 1718, 1538, 1357, 1291, 1174, 739. Mpt. 251–253 °C.

4-Hydroxy-3-methoxybenzoic acid methyl ester²⁴



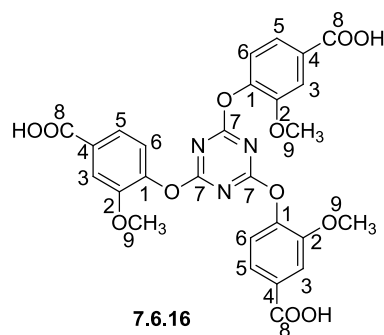
Thionyl chloride (7.08 g, 59.47 mmol) was added to the solution of the 4-hydroxy-3-methoxybenzoic acid (5.00 g, 29.74 mmol) in MeOH (60 mL). The resulting solution was heated at reflux for 6 h. The solution was cooled using an ice water bath and neutralised with saturated NaHCO₃ solution (pH 7–8). The reaction mixture was concentrated *in vacuo*, EtOAc (40 mL) and 1M HCl (25 mL) was added to the resulting solid. The organic layer was washed with water (2 × 25 mL) and brine (25 mL). The combined organic layers were dried with Na₂SO₄ and concentrated *in vacuo* to give a brown oil that was triturated with petrol to give the title product as a white solid (3.73 g, 20.48 mmol, 69%). ¹H NMR (500 MHz, CDCl₃) δ = 7.64 (dd, *J* = 8.3, 1.9 Hz, 1H, C5H), 7.55 (d, *J* = 1.9 Hz, 1H, C3H), 6.94 (d, *J* = 8.3 Hz, 1H, C6H), 5.96 (s, 1H, OH), 3.95 (s, 3H, OCH₃), 3.89 (s, 3H, COOCH₃). Lit²⁴ ¹H NMR (500 MHz, DMSO-d₆): δ = 9.96 (bs, 1H, OH), 7.46–7.48 (dd, 1H, Ar–H), 7.44–7.45 (d, 1H, Ar–H), 6.86–6.88 (d, 1H, Ar–H), 3.82 (s, 3 H, OCH₃), 3.80 (s, 3 H, COOCH₃). ¹³C NMR (125 MHz, CDCl₃): δ = 166.79, 150.61, 146.23, 124.16, 122.29, 114.06, 111.17, 56.16, 51.91. Lit²⁴ ¹³C NMR (125.76 MHz, DMSO-d₆): δ = 166.93, 152.38, 148.22, 124.28, 121.31, 116.06, 113.34, 56.47, 52.58,

2,4,6-Tris-(4-carboxyphenoxy)-1,3,5-triazine²⁵



To a solution of 4-hydroxybenzoic acid (2.00 g, 14.48 mmol, 3.50 equiv.) in water (60 mL) was added NaOH (1.16 g, 28.96 mmol, 7.00 equiv.) and mixed with a solution of cyanuric chloride (0.76 g, 4.14 mmol, 1.00 equiv.) in acetone (50 mL). The resulting solution was stirred at room temperature for 5 h. The reaction mixture was acidified by addition of 2M HCl (7.30 mL) forming a white precipitate. The resulting mixture was stirred for 30 min at 0 °C. After filtration and vacuum drying, the product was obtained as a white solid (1.54 g, 3.15 mmol, 76%). ¹H NMR (501 MHz, DMSO-d₆): δ = 13.00 (br s, 3H, COOH), 7.97 (d, *J* = 8.8 Hz, 6H, C3H/C5H), 7.36 (d, *J* = 8.8 Hz, 6H, C2H/C6H). Lit²⁵ ¹H NMR (DMSO-d₆, 400 MHz): δ = 13.00 (s, 3H, broad), 7.99 (d, *J* = 6.6 Hz, 6H), 7.37 (d, *J* = 7.4 Hz, 6H). ¹³C NMR (126 MHz, DMSO-d₆): δ = 172.70, 166.41, 154.53, 130.90, 128.59, 121.61. HRMS (ES⁺ mode): *m/z* = 490.0883 [100%, MH⁺]; calculated for C₂₄H₁₅N₃O₉ requires [MH⁺]: *m/z* = 490.0881. Mpt. 329–331 °C; Lit²⁵ Mpt. > 300 °C

2,4,6-Tris-(2-methoxy-4-carboxyphenoxy)-1,3,5-triazine

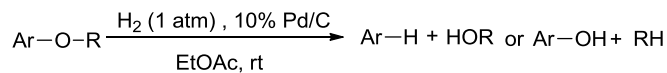


To a solution of vanillic acid (2.00 g, 11.89 mmol, 3.50 equiv..) in water (60 mL), added NaOH (0.95 g, 23.79 mmol, 7.00 equiv.) and mixed with a solution of cyanuric chloride (0.63 g, 3.40 mmol, 1.00 equiv..) in acetone (50 mL). The resulting solution was stirred at room temperature for 5 h. The reaction mixture was acidified by addition of 2M HCl (7.30 mL) forming a white precipitate. The resulting mixture was stirred for 30 min at 0 °C. After filtration and vacuum drying, the product was obtained as a yellow solid (1.40 g, 2.41 mmol, 71% yield). ^1H NMR (501 MHz, DMSO- d_6): δ = 13.04 (brs, 3H, COOH), 7.61–7.50 (m, 6H, C5H/C6H), 7.31 (d, J = 8.3 Hz, 3H, C3H), 3.78 (s, 9H, OCH₃). ^{13}C NMR (126 MHz, DMSO- d_6): δ = 172.74, 166.40, 150.45, 143.24, 129.88, 122.48, 122.11, 113.40, 55.99. HRMS (ES+ mode): m/z = 580.1209 [100%, MH⁺]; calculated for C₂₇H₂₁N₃O₁₂ requires [MH⁺]: m/z = 580.1203. IR ν_{max} /cm⁻¹ (film): 3071, 2957, 1618, 1497, 1367, 1292, 1179, 805. Mpt. 313–315 °C

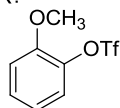
7.7 Hydrogenolysis of lignin monomer compounds

7.7.1 H₂ gas hydrogenolysis in batch

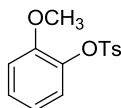
Hydrogenolysis of aryl sulfonates



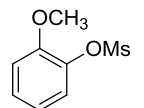
Ar-O-R:



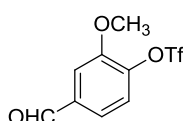
7.7.1



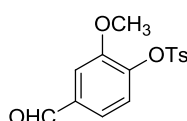
7.7.2



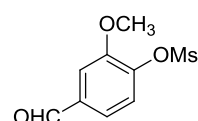
7.7.3



7.7.4



7.7.5



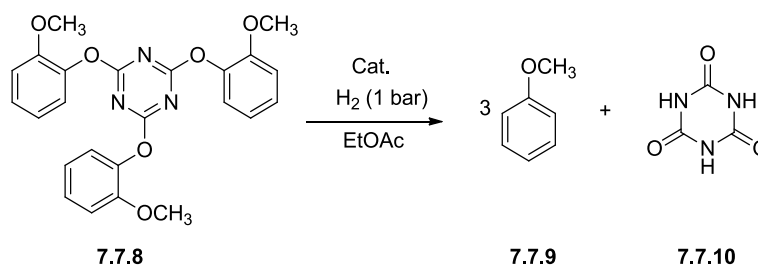
7.7.6

General Procedure

A 250 mL two-necked reaction flask was charged with the aryl sulfonate ester (7.70 mmol) and ethyl acetate (100 mL). 10% palladium on carbon (0.20 g, 10 wt% of the substrate) was then added. Then oxygen was removed by three vacuum/nitrogen cycles at room temperature. The flask was degassed of nitrogen by three vacuum/hydrogen cycles and left under a reservoir of atmospheric pressure hydrogen from a balloon. Separate reactions were stirred for 24–40 h at 20 °C or 40 °C. When the hydrogenation was complete, the catalyst was removed through a plug of celite, washed with ethyl acetate and the filtrate concentrated *in vacuo*. The product was analysed by ¹H NMR spectroscopy and quantitative GC using biphenyl (10 mg/mL) as an internal standard.

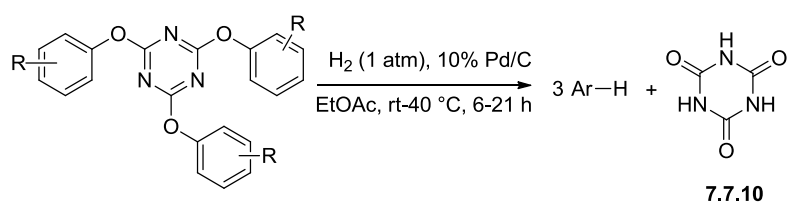
7.7.2 Hydrogenolysis of 2,4,6-*tris*(aryloxy)-1,3,5-triazines

a) Catalyst activity testing

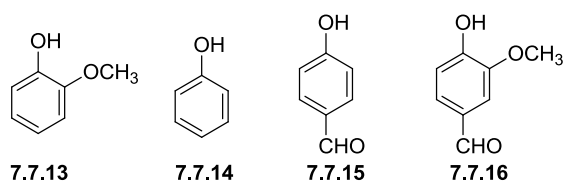
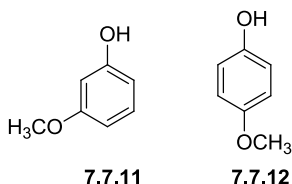


3.00 g of 2,4,6-*tris*(2-methoxyphenoxy)-1,3,5-triazine (6.71 mmol) was dissolved in 70 mL EtOAc and mixed with the catalyst (5 wt% Pd/C, 10 wt% Pd/C, 10 wt% Pt/C, 10 wt% Ru/C and 10 wt% Ni/Al respectively). The flask was degassed of oxygen by three vacuum/nitrogen cycles, followed by three vacuum/hydrogen cycles and left under a reservoir of atmospheric pressure hydrogen from a balloon. The mixture was stirred at room temperature for 24 hours. The reaction mixtures were then filtered and distilled at 70 °C and 156 °C respectively, after removing EtOAc, 1.70 mL (15.66 mmol) of anisole (yield 233% based on theory 300%) was distilled from the reaction using 10 wt% Pd/C. The product anisole was identified and quantified against an authentic standard by GC and GC-MS.

b) Hydrogenolysis of 2,4,6-tris(aryloxy)-1,3,5-triazines



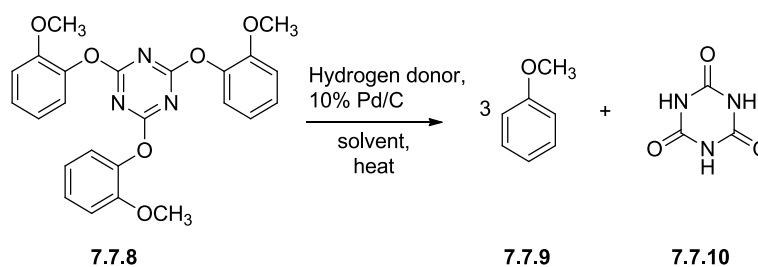
Substrate



General procedure

To a solution of triazines (1.00 equiv.) in ethyl acetate (60 mL) was added 10% Pd/C (10 weight percentage of the substrate) at room temperature. The mixture was degassed of oxygen by three times vacuum/nitrogen cycles. The flask was degassed of nitrogen by three times vacuum/hydrogen cycles and left under a reservoir of hydrogen at atmospheric pressure hydrogen from a balloon. Separate reactions were stirred for 6–21 h at 20 °C or 40 °C. When the hydrogenation was completed, the catalyst was removed by filtering through a plug of celite, the filtrate was washed with water (20 mL) and the organic layer was separated and dried with MgSO₄ and concentrated *in vacuo*. The product was analysed by ¹H NMR spectroscopy and quantitative GC using biphenyl (10 mg/mL) as an internal standard.

7.7.3 Hydrogenolysis using a hydrogen transfer reagent in batch



General procedure

The hydrogen transfer reagent (3.00 equiv.) was added dropwise to a suspension of triazine compound (1.0 equiv) and 10 wt% Pd/C (10% dispersion) in THF (500 mL). The resulting dark suspension was heated at reflux for 12 h. The reaction mixture was filtered and the filtrate analysed by quantitative GC analysis as described, and the GC yield of the product was calculated.

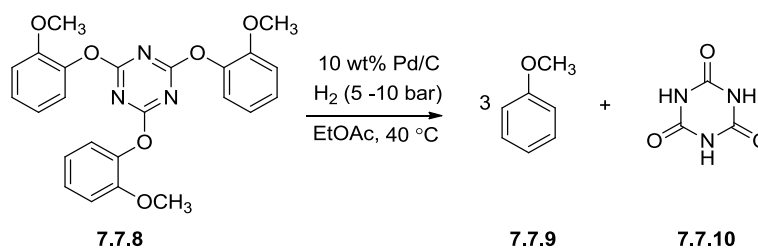
Table 7.2 Transfer hydrogenation for the hydrogenolysis of triazine compound

Hydrogen source	Product	Yield (%)
Hydrazine	Guaiacol	82
Sodium phosphinate	rsm	n/a
2-Propanol	rsm	n/a
Ammonium formate	Guaiacol	43
Glucose	rsm	n/a

* Reaction conditions: triazine (1 equiv.), hydrogen donors (3 equiv.), 10 % Pd/C (10 wt%), solvent: THF, reflux, 12 hour

*‘rsm’ recovered starting material

7.7.4 Hydrogenolysis using Continuous Stirred Tank Reactor (CSTR)



For the hydrogenolysis in CSTR, the concentration of 2,4,6-*tris*(2-methoxyphenoxy)-*s*-triazine in EtOAc was 0.0125 g/mL. The temperature of the reaction was controlled at 40 °C. The hydrogen pressure, flow rate and residence volume were varied to optimise the reaction conditions (Table 7.3). The residence volume could be changed by adjusting the length of the dip tube. After the reaction was complete, the product was obtained by filtering the catalyst *via* celite and analysed by quantitative GC.

Table 7.3 Experimental conditions for CSTR hydrogenolysis

Entry	Pressure (bar)	Flow rate (mL/min)	Residence volume (mL)	Additives
1	10	2	210	n/a
2	10	1	210	n/a
3	10	4	30	n/a
4	10	4	30	Et ₃ N
5*	5	4	30	n/a
6	5	8	30	n/a

* During CSTR hydrogenolysis, the catalyst was recycled after 12 h. The catalyst settled on the bottom of the reactor and was separated, using filter paper if necessary. The recycled catalyst was used for the further hydrogenolysis.

7.6 Reference

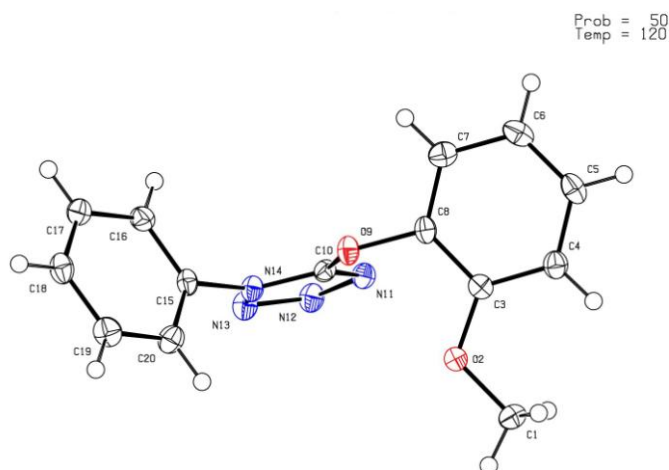
1. Patel, M., *J. Indian Chem. Soc.*, **1928**, *5*, 93.
2. Summerbell, L. J., *J. Chem. Soc. (Resumed)* **1934**, 996–998.
3. Denivelle, L., *Comptes rendus hebdomadaires des séances de l'Académie des sciences*, **1934**, *199*, 211.
4. Ye, H.; Liu, R.; Li, D.; Liu, Y.; Yuan, H.; Guo, W.; Zhou, L.; Cao, X.; Tian, H.; Shen, J.; Wang, P. G., *Org. Lett.*, **2012**, *15*, 18–21.
5. Qin, L.; Ren, X.; Lu, Y.; Li, Y.; Zhou, J., *Angew. Chem. Int. Ed.*, **2012**, *51*, 5915–5919.
6. Seganish, W. M.; DeShong, P., *J. Org. Chem.*, **2004**, *69*, 1137–1143.
7. Speicher, A.; Backes, T.; Hesidens, K.; Kolz, J., *Beilstein J. Org. Chem*, **2009**, *5*, 71.
8. Schade, M. A.; Metzger, A.; Hug, S.; Knochel, P., *Chem. Commun.*, **2008**, *26*, 3046–3048.
9. Burton, H.; Hoggarth, E., *J. Chem. Soc. (Resumed)* **1945**, 14–18.
10. Reddy, C. R.; Rao, N. N.; Srikanth, B., *Eur. J. Org. Chem.*, **2010**, *2010*, 345–351.
11. Collado, D.; Perez-Inestrosa, E.; Suau, R.; Navarrete, J. T. L., *Tetrahedron*, **2006**, *62*, 2927–2935.
12. Fujikawa, N.; Ohta, T.; Yamaguchi, T.; Fukuda, T.; Ishibashi, F.; Iwao, M., *Tetrahedron*, **2006**, *62*, 594–604.
13. Helferich, B.; Papalambrou, P., *Justus Liebigs Annalen der Chemie*, **1942**, *551*, 235–241.
14. Battersby, A. R.; Sheldrake, P. W.; Staunton, J.; Williams, D. C., *J. Chem. Soc., Perkin Trans. 1*, **1976**, 1056–1062.
15. Gol'tsberg, M. A.; Koldobskii, G. I., *Chemistry of Heterocyclic Compounds*, **1996**, *32*, 1300–1304.
16. Musliner, W. J.; Gates, J. W., *J. Am. Chem. Soc.*, **1966**, *88*, 4271–4273.
17. Jones, P. R.; Shelnut, J. G., *J. Org. Chem.*, **1979**, *44*, 696–699.
18. Grigat, E.; Pütter, R., *Chemische Berichte*, **1964**, *97*, 3012.
19. Machakanur, S. S.; Patil, B. R.; Badiger, D. S.; Bakale, R. P.; Gudasi, K. B.; Annie Bligh, S., *J. Mol. Structure*, **2012**, *1011*, 121–127.
20. Duan, H.; Wang, L.; Qin, D.; Li, X.; Wang, S.; Zhang, Y., *Synth. Commun.*, **2011**, *41*, 380–384.
21. Menicagli, R.; Samaritani, S.; Signore, G.; Vaglini, F.; Dalla Via, L., *J. Med. Chem.*, **2004**, *47*, 4649–4652.
22. Wear, R. L. Phenoxy-*s*-triazine chain coupler for polyesterification and novel polyesters. Patent US 3966680 A, **1976**.
23. Yang, D.; An, B.; Wei, W.; Jiang, M.; You, J.; Wang, H., *Tetrahedron*, **2014**, *70*, 3630–3634.

24. Legrand, S.; Nordlander, G.; Nordenhem, H.; Borg-Karlson, A. K.; Unelius, C. R., *Zeitschrift für Naturforschung B*, **2004**, 829–835.
25. Aakeroy, C. B.; Desper, J.; Urbina, J. F., *CrystEngComm*, **2005**, 7, 193–201.

Appendix

A1 X-Ray Crystal Structure data and refinement for 5-(2-methoxy-phenoxy)-1-phenyl-1H-tetrazole

Molecular Formula: C₁₄H₁₂N₄O₂



Measurements were carried out at 120K on an Agilent SuperNova diffractometer equipped with an Atlas CCD detector and connected to an Oxford Cryostream low temperature device using mirror monochromated Cu K α radiation ($\lambda = 1.54184 \text{ \AA}$) from a Microfocus Nova X-ray source. The structure was solved by direct methods using SHELXS¹ and refined by a full matrix least squares technique based on F^2 using SHELXL97.¹

The compound crystallised as colourless needles. The compound crystallised in a monoclinic cell and was solved in the $P2_1/n$ space group, with one molecule in the asymmetric unit.

All non-hydrogen atoms were located in the Fourier Map and refined anisotropically. All hydrogen atoms were placed in calculated positions and refined isotropically using a “riding model”.

Pictures are presented with non-hydrogen atoms displayed as displacement ellipsoids, which are set at the 50% probability level.

Table 1 Crystal data and structure refinement.

Identification code	YZ_Tet_Cu
Empirical formula	C ₁₄ H ₁₂ N ₄ O ₂
Formula weight	268.28
Temperature/K	120.00(10)
Crystal system	monoclinic
Space group	P2 ₁ /n
a/Å	10.6453(2)
b/Å	9.6562(2)
c/Å	12.4988(3)
α /°	90.00
β /°	96.510(2)
γ /°	90.00
Volume/Å ³	1276.50(5)
Z	4
$\rho_{\text{calc}}/\text{cm}^3$	1.396
μ/mm^{-1}	0.804
F(000)	560.0
Crystal size/mm ³	0.18 × 0.07 × 0.05
Radiation	CuK α (λ = 1.54184)
2 θ range for data collection/°	10.36 to 134.16
Index ranges	-12 ≤ h ≤ 12, -11 ≤ k ≤ 11, -14 ≤ l ≤ 7
Reflections collected	5338

Independent reflections	2230 [$R_{\text{int}} = 0.0385$, $R_{\text{sigma}} = 0.0410$]
Data/restraints/parameters	2230/0/182
Goodness-of-fit on F^2	1.069
Final R indexes [$I \geq 2\sigma(I)$]	$R_1 = 0.0391$, $wR_2 = 0.0960$
Final R indexes [all data]	$R_1 = 0.0490$, $wR_2 = 0.1035$
Largest diff. peak/hole / $e \text{ \AA}^{-3}$	0.22/-0.27

Table 2 Fractional Atomic Coordinates ($\times 10^4$) and Equivalent Isotropic Displacement Parameters ($\text{\AA}^2 \times 10^3$). U_{eq} is defined as 1/3 of of the trace of the orthogonalised U_{ij} tensor.

Atom	x	y	z	U_{eq}
C1	9868.5(16)	-2659.2(18)	-1182.7(14)	26.1(4)
O2	9123.4(10)	-1677.2(11)	-671.8(9)	22.5(3)
C3	8862.1(13)	-469.1(16)	-1207.7(12)	18.5(3)
C4	9246.7(14)	-123.1(17)	-2201.1(13)	21.8(3)
C5	8923.0(14)	1156.7(18)	-2662.0(13)	23.0(3)
C6	8225.2(14)	2107.8(17)	-2148.6(14)	24.4(4)
C7	7827.6(14)	1773.7(16)	-1155.4(13)	22.3(3)
C8	8146.3(13)	502.8(16)	-707.0(12)	18.2(3)
O9	7796.2(9)	210.1(11)	330.5(8)	19.9(3)
C10	6827.1(13)	-649.6(15)	362.4(12)	16.6(3)
N11	6151.7(12)	-1297.7(14)	-433.9(10)	19.4(3)
N12	5268.8(12)	-2024.8(14)	51.6(11)	22.1(3)
N13	5393.7(12)	-1830.2(14)	1081.4(11)	22.0(3)
N14	6394.4(11)	-955.1(13)	1302.3(10)	18.1(3)

C15	6715.4(13)	-368.7(16)	2358.0(12)	17.6(3)
C16	5949.4(15)	669.2(16)	2684.7(13)	21.2(3)
C17	6232.9(16)	1233.5(17)	3705.7(13)	24.0(3)
C18	7266.8(15)	750.2(17)	4379.6(13)	23.2(4)
C19	8024.8(14)	-292.8(18)	4036.4(14)	24.9(4)
C20	7753.3(14)	-864.3(17)	3018.3(13)	23.1(4)

Table 3 Anisotropic Displacement Parameters ($\text{\AA}^2 \times 10^3$). The Anisotropic displacement exponent takes the form:

$$-2\pi^2[h^2a^2U_{11}+2hka*b*U_{12}+\dots]$$

Atom	U_{11}	U_{22}	U_{33}	U_{23}	U_{13}	U_{12}
C1	29.1(8)	24.2(8)	25.4(9)	-0.6(7)	4.6(6)	8.1(6)
O2	28.0(6)	20.9(6)	19.4(6)	2.8(4)	6.7(4)	4.8(4)
C3	16.0(7)	19.9(7)	19.2(8)	1.1(6)	0.6(6)	-1.7(5)
C4	19.4(7)	25.7(8)	20.4(9)	0.0(6)	3.5(6)	-1.5(6)
C5	17.7(7)	32.2(9)	18.7(8)	6.3(7)	0.0(6)	-4.6(6)
C6	18.6(7)	25.1(8)	28.7(9)	9.3(7)	-0.7(6)	-1.8(6)
C7	16.8(7)	21.6(8)	28.2(9)	-0.3(6)	1.8(6)	-0.2(6)
C8	16.8(7)	22.7(8)	15.0(8)	-0.8(6)	2.0(6)	-3.8(5)
O9	20.2(5)	23.5(6)	16.8(6)	-2.1(4)	4.7(4)	-5.5(4)
C10	15.7(6)	17.6(7)	16.9(8)	-0.6(6)	2.9(5)	2.3(5)
N11	19.9(6)	20.5(6)	17.7(7)	-2.1(5)	1.8(5)	-0.8(5)
N12	21.3(6)	24.2(7)	21.0(8)	-3.7(5)	3.4(5)	-3.3(5)
N13	21.5(6)	23.4(7)	21.2(8)	-3.9(5)	3.6(5)	-5.1(5)
N14	18.0(6)	19.3(6)	17.1(7)	-2.7(5)	3.2(5)	-3.1(5)
C15	19.8(7)	19.0(7)	14.5(8)	-1.3(6)	4.0(5)	-5.1(5)
C16	24.9(7)	20.4(8)	17.9(8)	0.6(6)	0.5(6)	1.4(6)
C17	30.7(8)	22.4(8)	18.8(8)	-1.8(6)	3.1(6)	1.9(6)
C18	26.1(8)	26.7(8)	16.4(8)	-3.4(6)	0.9(6)	-6.5(6)

C19	19.4(7)	31.3(9)	22.9(9)	0.6(7)	-2.8(6)	-1.1(6)
C20	18.6(7)	26.3(8)	24.8(9)	-2.4(6)	3.9(6)	0.8(6)

Table 4 Bond Lengths

Atom	Atom	Length/Å	Atom	Atom	Length/Å
C1	O2	1.4321(19)	C10	N14	1.342(2)
O2	C3	1.3581(19)	N11	N12	1.3689(18)
C3	C4	1.392(2)	N12	N13	1.2927(19)
C3	C8	1.400(2)	N13	N14	1.3632(18)
C4	C5	1.390(2)	N14	C15	1.441(2)
C5	C6	1.384(2)	C15	C16	1.383(2)
C6	C7	1.394(2)	C15	C20	1.387(2)
C7	C8	1.376(2)	C16	C17	1.389(2)
C8	O9	1.4177(18)	C17	C18	1.389(2)
O9	C10	1.3283(19)	C18	C19	1.389(2)
C10	N11	1.318(2)	C19	C20	1.387(2)

Table 5 Bond Angles

Atom	Atom	Atom	Angle/°	Atom	Atom	Atom	Angle/°
C3	O2	C1	116.21(12)	C10	N11	N12	104.59(12)
O2	C3	C4	125.58(14)	N13	N12	N11	111.63(12)
O2	C3	C8	116.53(13)	N12	N13	N14	106.35(12)
C4	C3	C8	117.90(14)	C10	N14	N13	107.26(12)
C5	C4	C3	119.94(15)	C10	N14	C15	130.22(13)
C6	C5	C4	121.24(15)	N13	N14	C15	121.85(11)
C5	C6	C7	119.50(15)	C16	C15	N14	117.95(13)

C8	C7	C6	118.92(14)	C16	C15	C20	122.08(15)
C3	C8	O9	119.20(14)	C20	C15	N14	119.96(14)
C7	C8	C3	122.50(14)	C15	C16	C17	118.80(15)
C7	C8	O9	118.18(13)	C18	C17	C16	120.01(15)
C10	O9	C8	115.95(12)	C19	C18	C17	120.32(15)
O9	C10	N14	120.55(14)	C20	C19	C18	120.27(15)
N11	C10	O9	129.28(14)	C19	C20	C15	118.53(15)
N11	C10	N14	110.16(13)				

Table 6 Torsion Angles

A	B	C	D	Angle/°	A	B	C	D	Angle/°
C1	O2	C3	C4	0.6(2)	C10	N11	N12	N13	0.19(16)
C1	O2	C3	C8	-179.28(13)	C10	N14	C15	C16	95.86(18)
O2	C3	C4	C5	-179.54(14)	C10	N14	C15	C20	-85.2(2)
O2	C3	C8	C7	179.22(14)	N11	C10	N14	N13	-0.42(16)
O2	C3	C8	O9	3.10(19)	N11	C10	N14	C15	-171.06(14)
C3	C4	C5	C6	0.3(2)	N11	N12	N13	N14	-0.45(16)
C3	C8	O9	C10	-78.60(17)	N12	N13	N14	C10	0.52(16)
C4	C3	C8	C7	-0.6(2)	N12	N13	N14	C15	172.11(13)
C4	C3	C8	O9	-176.76(13)	N13	N14	C15	C16	-73.61(18)
C4	C5	C6	C7	-0.6(2)	N13	N14	C15	C20	105.33(17)
C5	C6	C7	C8	0.3(2)	N14	C10	N11	N12	0.15(16)
C6	C7	C8	C3	0.3(2)	N14	C15	C16	C17	179.08(13)

C6	C7	C8	O9	176.50(13)	N14	C15	C20	C19	-178.98(13)
C7	C8	O9	C10	105.11(15)	C15	C16	C17	C18	-0.3(2)
C8	C3	C4	C5	0.3(2)	C16	C15	C20	C19	-0.1(2)
C8	O9	C10	N11	1.5(2)	C16	C17	C18	C19	0.3(2)
C8	O9	C10	N14	-177.69(13)	C17	C18	C19	C20	-0.2(2)
O9	C10	N11	N12	-179.07(14)	C18	C19	C20	C15	0.1(2)
O9	C10	N14	N13	178.88(13)	C20	C15	C16	C17	0.2(2)
O9	C10	N14	C15	8.2(2)					

Table 7 Hydrogen Atom Coordinates ($\text{\AA}\times 10^4$) and Isotropic Displacement Parameters ($\text{\AA}^2\times 10^3$).

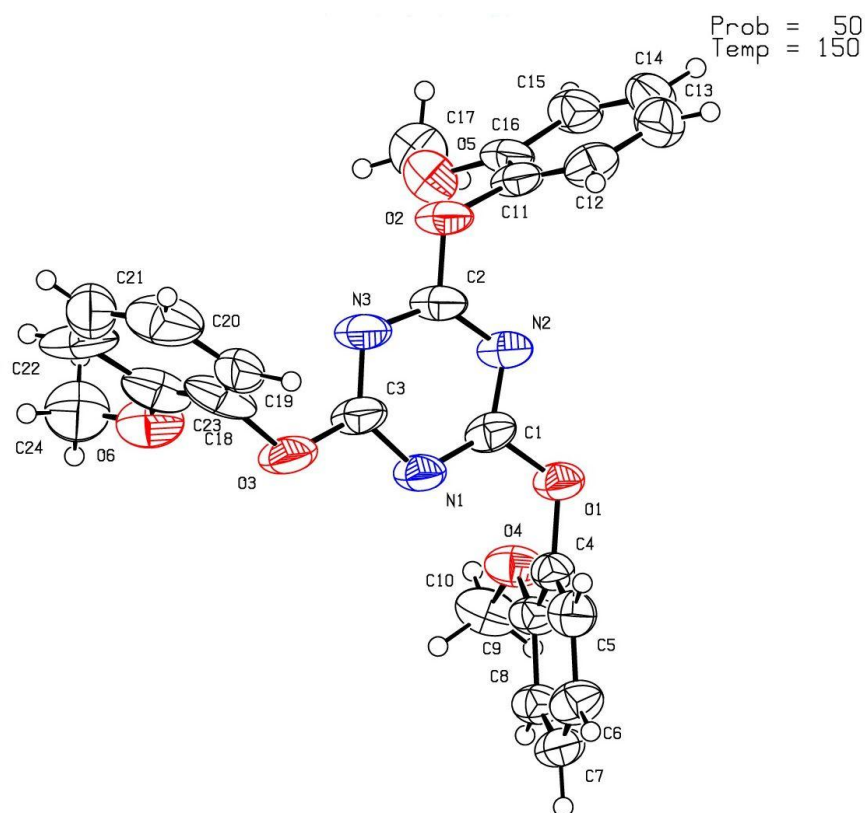
Atom	x	y	z	U(eq)
H1A	9424	-2932	-1861	39
H1B	10019	-3458	-730	39
H1C	10661	-2245	-1300	39
H4	9720	-747	-2556	26
H5	9180	1378	-3328	28
H6	8023	2963	-2464	29
H7	7355	2400	-802	27
H16	5257	984	2229	25
H17	5730	1935	3938	29
H18	7452	1127	5064	28
H19	8717	-610	4491	30
H20	8256	-1564	2784	28

References

1. Sheldrick, G. M., *Acta Crystallogr. Sect. A: Found. Crystallogr.* **2007**, *64*, 112-122.

A2 X-Ray Crystal Structure data and refinement for 2,4,6-tris(2-methoxyphenoxy)-1,3,5-triazine

Molecular formula: C₂₄H₂₁N₃O₆



Measurements were carried out at 150 K on a Bruker-Nonius Apex X8 diffractometer equipped with an Apex II CCD detector and using graphite monochromated Mo-K α radiation from a FR591 rotating anode generator. The structure was solved by direct methods using SHELXLS-97 and refined using SHELXL-97.¹ Compound crystallises in the monoclinic space group $P2_1/c$ with one molecule and one MeOH in the asymmetric unit. All non-hydrogen atoms were refined anisotropically. Hydrogen atoms were placed in calculated positions and refined using a riding model. All Uiso(H) values were constrained to be 1.2 times (1.5 for methyl) Ueq of the parent atom. Crystals were very thin plates and subsequently the data collected were weak, leading to high residuals on refinement.

Pictures are presented with non-hydrogen atoms displayed as displacement ellipsoids, which are set at the 50% probability level.

Table 1 Crystal data and structure refinement.

Identification code	zhaotmpt
Empirical formula	C ₂₄ H ₂₁ N ₃ O ₆
Formula weight	479.48
Temperature/K	150.00
Crystal system	monoclinic
Space group	P2 ₁ /n (No. 14)
a/Å	11.008(4)
b/Å	16.489(4)
c/Å	14.423(4)
α /°	90.00
β /°	101.804(15)
γ /°	90.00
Volume/Å ³	2562.6(13)
Z	4
ρ_{calc} /cm ³	1.243
μ /mm ⁻¹	0.092
F(000)	1008
Crystal size/mm ³	0.01 x 0.12 x 0.14
Radiation	MoKa 0.71073
Theta Min-Max [Deg]	2.5, 23.6
Dataset	-12: 12 ; -18: 13 ; -16: 15
Tot., Uniq. Data, R(int)	13583, 3712, 0.123

Observed data [I > 2.0 sigma(I)]	1831
Nref, Npar	3712, 321
R, wR2, S	0.1165, 0.3846, 1.16
w	= where P=(Fo ² +2Fc ²)/3
1/[s ² (Fo ²)+(0.2000P) ²]	
Max. and Av. Shift/Error	0.00, 0.00
Min. and Max. Resd. Dens.	-0.39, 0.82
[e/Ang ³]	

Table 2 Final Coordinates and Equivalent Isotropic Displacement Parameters of the non-Hydrogen.

Atom	x	y	z	U(eq)
O1	0.2988(5)	0.1458(3)	0.8409(3)	0.0564(19)
O2	0.1779(5)	0.4075(2)	0.8937(3)	0.0617(19)
O3	-0.0452(6)	0.1896(3)	0.9729(5)	0.108(3)
O4	0.1737(5)	0.0664(3)	0.6849(3)	0.0650(19)
O5	0.1003(5)	0.4477(3)	0.7114(3)	0.068(2)
O6	-0.2714(7)	0.2296(3)	0.8835(4)	0.085(3)
N1	0.1206(6)	0.1635(3)	0.9050(4)	0.061(2)
N2	0.2411(6)	0.2761(3)	0.8613(4)	0.055(2)
N3	0.0617(7)	0.3032(3)	0.9311(5)	0.070(3)
C1	0.2152(7)	0.1977(4)	0.8707(4)	0.051(3)
C2	0.1613(8)	0.3257(4)	0.8942(5)	0.061(3)
C3	0.0485(9)	0.2226(4)	0.9347(6)	0.072(3)
C4	0.2830(6)	0.0592(4)	0.8464(5)	0.046(3)

C5	0.3347(7)	0.0173(4)	0.9293(5)	0.058(3)
C6	0.3326(7)	-0.0685(4)	0.9310(5)	0.061(3)
C7	0.2761(7)	-0.1109(4)	0.8491(6)	0.062(3)
C8	0.2195(7)	-0.0681(4)	0.7644(5)	0.056(3)
C9	0.2229(7)	0.0175(4)	0.7632(5)	0.053(3)
C10	0.1009(8)	0.0242(5)	0.6005(5)	0.069(3)
C11	0.2701(8)	0.4395(4)	0.8443(6)	0.059(3)
C12	0.3949(9)	0.4489(4)	0.8924(6)	0.063(3)
C13	0.4811(8)	0.4851(5)	0.8432(7)	0.075(4)
C14	0.4392(9)	0.5107(5)	0.7487(7)	0.074(4)
C15	0.3129(9)	0.5010(4)	0.7014(6)	0.067(3)
C16	0.2263(8)	0.4624(4)	0.7501(5)	0.055(3)
C17	0.0523(8)	0.4723(5)	0.6130(5)	0.082(4)
C18	-0.1195(12)	0.2500(5)	1.0247(7)	0.089(5)
C19	-0.0596(8)	0.2744(5)	1.1117(7)	0.071(3)
C20	-0.1473(13)	0.3279(6)	1.1577(8)	0.113(6)
C21	-0.2704(10)	0.3418(6)	1.1042(8)	0.086(4)
C22	-0.3204(12)	0.3133(4)	1.0176(7)	0.095(5)
C23	-0.2294(11)	0.2608(5)	0.9710(7)	0.083(4)
C24	-0.3937(12)	0.2454(6)	0.8302(9)	0.114(5)

U(eq) = 1/3 of the trace of the orthogonalized U Tensor

Table 3 Anisotropic Displacement Parameters ($\text{\AA}^2 \times 10^3$).

Atom	U_{11}	U_{22}	U_{33}	U_{23}	U_{13}	U_{12}
O1	0.079(4)	0.037(3)	0.060(3)	-0.005(2)	0.030(3)	0.000(2)
O2	0.104(4)	0.029(3)	0.062(3)	0.002(2)	0.040(3)	-0.001(2)
O3	0.140(6)	0.036(3)	0.184(7)	0.000(4)	0.119(6)	0.009(3)
O4	0.099(4)	0.046(3)	0.052(3)	0.007(2)	0.020(3)	-0.007(3)
O5	0.076(4)	0.076(4)	0.051(3)	0.001(3)	0.014(3)	-0.013(3)
O6	0.125(6)	0.066(4)	0.065(4)	-0.001(3)	0.022(4)	-0.001(4)
N1	0.090(5)	0.035(3)	0.071(4)	-0.005(3)	0.045(4)	-0.002(3)
N2	0.090(5)	0.035(3)	0.045(3)	0.000(3)	0.025(3)	0.000(3)
N3	0.105(6)	0.032(4)	0.087(5)	0.000(3)	0.053(5)	-0.001(3)
C1	0.077(6)	0.042(4)	0.038(4)	-0.006(3)	0.022(4)	0.008(4)
C2	0.097(7)	0.032(4)	0.059(5)	0.000(3)	0.031(5)	-0.004(4)
C3	0.110(7)	0.036(5)	0.091(6)	0.009(4)	0.067(6)	0.009(4)
C4	0.054(5)	0.038(4)	0.049(4)	-0.005(3)	0.018(4)	-0.002(3)
C5	0.067(5)	0.057(5)	0.053(5)	-0.001(4)	0.020(4)	-0.002(4)
C6	0.080(6)	0.052(5)	0.053(5)	0.012(4)	0.016(4)	0.010(4)
C7	0.082(6)	0.039(4)	0.075(5)	0.006(4)	0.042(5)	0.008(4)
C8	0.079(6)	0.042(4)	0.055(5)	-0.001(4)	0.031(4)	-0.003(4)
C9	0.075(5)	0.039(4)	0.053(5)	0.005(4)	0.030(4)	-0.004(3)
C10	0.103(7)	0.065(5)	0.036(4)	0.011(4)	0.008(4)	-0.019(5)
C11	0.089(7)	0.029(4)	0.068(5)	0.007(4)	0.041(5)	0.009(4)
C12	0.080(7)	0.051(5)	0.058(5)	-0.011(4)	0.011(5)	0.008(4)

C13	0.075(6)	0.067(6)	0.090(7)	-0.013(5)	0.033(6)	-0.009(4)
C14	0.079(7)	0.058(5)	0.096(7)	-0.004(5)	0.043(6)	-0.014(4)
C15	0.091(7)	0.051(5)	0.068(5)	0.005(4)	0.036(5)	-0.004(4)
C16	0.085(6)	0.031(4)	0.056(5)	0.002(3)	0.028(5)	-0.006(4)
C17	0.094(7)	0.089(6)	0.065(6)	-0.010(5)	0.023(5)	-0.007(5)
C18	0.127(10)	0.057(6)	0.076(7)	0.025(5)	0.008(7)	-0.042(6)
C19	0.066(6)	0.054(5)	0.093(7)	0.021(5)	0.018(6)	-0.004(4)
C20	0.189(13)	0.072(7)	0.098(8)	-0.029(6)	0.078(9)	-0.033(7)
C21	0.070(7)	0.081(7)	0.110(9)	0.037(6)	0.026(6)	0.009(5)
C22	0.202(11)	0.031(4)	0.075(7)	-0.001(4)	0.084(8)	0.003(5)
C23	0.118(9)	0.058(6)	0.067(6)	0.013(5)	0.002(7)	-0.031(6)
C24	0.114(10)	0.098(8)	0.131(10)	0.012(7)	0.030(8)	0.002(7)

The Temperature Factor has the Form of $\text{Exp}(-T)$ Where $T = 8 * (\text{Pi}^{**2}) * U * (\text{Sin}(\text{Theta}) / \text{Lambda})^{**2}$, for Isotropic Atoms $T = 2 * (\text{Pi}^{**2}) * \text{Sum}_{ij} (h(i) * h(j) * U(i,j) * \text{Astar}(i) * \text{Astar}(j))$, for Anisotropic Atoms. $\text{Astar}(i)$ are Reciprocal Axial Lengths and $h(i)$ are the Reflection Indices.

Table 4 Bond Lengths

Atom	Atom	Length/Å	Atom	Atom	Length/Å
O1	C1	1.388(9)	C12	C13	1.427(13)
O1	C4	1.443(8)	C13	C14	1.411(14)
O2	C2	1.361(7)	C14	C15	1.427(14)
O2	C11	1.453(10)	C15	C16	1.443(12)
O3	C3	1.377(11)	C18	C23	1.308(17)
O3	C18	1.571(12)	C18	C19	1.354(14)
O4	C9	1.403(8)	C19	C20	1.553(15)

O4	C10	1.486(9)	C20	C21	1.434(18)
O5	C16	1.406(10)	C21	C22	1.343(15)
O5	C17	1.467(8)	C22	C23	1.575(16)
O6	C23	1.354(11)	C5	H5	0.95
O6	C24	1.431(15)	C6	H6	0.95
N1	C1	1.363(10)	C10	H10B	0.98
N1	C3	1.379(10)	C10	H10A	0.98
N2	C2	1.355(10)	C10	H10C	0.98
N2	C1	1.337(8)	C12	H12	0.95
N3	C2	1.364(11)	C13	H13	0.95
N3	C3	1.339(8)	C14	H14	0.95
C4	C5	1.397(10)	C15	H15	0.95
C4	C9	1.423(10)	C17	H17C	0.98
C5	C6	1.415(9)	C17	H17A	0.98
C6	C7	1.404(11)	C17	H17B	0.98
C7	C8	1.438(11)	C19	H19	0.95
C8	C9	1.412(9)	C20	H20	0.95
C11	C16	1.398(11)	C21	H21	0.95
C11	C12	1.415(13)	C22	H22	0.95
C24	H24C	0.98			
C24	H24A	0.98			
C24	H24B	0.98			

Table 5 Bond Angles

Atom	Atom	Atom	Angle/°	Atom	Atom	Atom	Angle/°
C1	O1	C4	119.9(5)	C4	C9	C8	118.8(6)
C2	O2	C11	118.1(6)	O2	C11	C16	116.0(7)
C3	O3	C18	116.4(6)	C12	C11	C16	123.7(8)
C9	O4	C10	116.4(5)	O2	C11	C12	120.3(7)
C16	O5	C17	117.9(6)	C11	C12	C13	118.7(8)
C23	O6	C24	122.4(8)	C12	C13	C14	119.1(8)
C1	N1	C3	110.6(6)	C14	C15	C16	119.5(8)
C1	N2	C2	112.4(6)	O5	C16	C11	117.1(7)
C2	N3	C3	112.8(7)	O5	C16	C15	125.4(6)
O1	C1	N2	113.4(6)	C11	C16	C15	117.5(8)
N1	C1	N2	129.2(7)	O3	C18	C23	108.2(8)
O1	C1	N1	117.5(6)	C19	C18	C23	136.4(11)
O2	C2	N3	113.0(6)	O3	C18	C19	115.3(9)
N2	C2	N3	127.1(6)	C18	C19	C20	109.7(9)
O2	C2	N2	119.9(7)	C19	C20	C21	117.5(9)
O3	C3	N1	111.8(6)	C20	C21	C22	127.4(11)
O3	C3	N3	120.3(8)	C21	C22	C23	114.5(10)
N1	C3	N3	128.0(8)	O6	C23	C22	118.8(9)
O1	C4	C5	120.3(6)	C18	C23	C22	114.5(9)
O1	C4	C9	118.2(6)	O6	C23	C18	126.8(10)
C5	C4	C9	121.4(6)	C4	C5	H5	120
C4	C5	C6	120.3(6)	C6	C5	H5	120

C5	C6	C7	119.3(6)	C5	C6	H6	120
C6	C7	C8	120.7(6)	C7	C6	H6	120
C7	C8	C9	119.5(6)	C8	C7	H7	120
O4	C9	C4	115.9(6)	C6	C7	H7	120
O4	C9	C8	125.3(6)	C7	C8	H8	120
C9	C8	H8	120	C20	C19	H19	125
O4	C10	H10B	110	C18	C19	H19	125
O4	C10	H10C	110	C19	C20	H20	121
O4	C10	H10A	109	C21	C20	H20	121
H10A	C10	H10C	109	C22	C21	H21	116
H10B	C10	H10C	109	C20	C21	H21	116
H10A	C10	H10B	109	C21	C22	H22	123
C13	C12	H12	121	C23	C22	H22	123
C11	C12	H12	121	O6	C24	H24B	110
C12	C13	H13	120	O6	C24	H24C	109
C14	C13	H13	120	O6	C24	H24A	110
C13	C14	H14	119	H24A	C24	H24C	109
C15	C14	H14	119	H24B	C24	H24C	109
C16	C15	H15	120	H24A	C24	H24B	109
C14	C15	H15	120				
O5	C17	H17A	109				
O5	C17	H17B	109				
H17A	C17	H17B	109				
H17A	C17	H17C	109				

O5	C17	H17C	110
H17B	C17	H17C	109

Table 6 Torsion Angles

A	B	C	D	Angle/°	A	B	C	D	Angle/°
C4	O1	C1	N1	0.4(8)	O1	C4	C9	O4	-5.8(10)
C4	O1	C1	N2	-179.8(5)	O1	C4	C9	C8	172.8(6)
C1	O1	C4	C5	-87.6(8)	C5	C4	C9	O4	179.4(7)
C1	O1	C4	C9	97.6(7)	C5	C4	C9	C8	-2.0(11)
C11	O2	C2	N2	9.3(10)	C4	C5	C6	C7	-1.1(11)
C11	O2	C2	N3	-171.6(6)	C5	C6	C7	C8	-0.7(12)
C2	O2	C11	C12	-89.0(8)	C6	C7	C8	C9	1.2(12)
C2	O2	C11	C16	93.4(7)	C7	C8	C9	O4	178.6(7)
C18	O3	C3	N1	170.0(7)	C7	C8	C9	C4	0.2(11)
C18	O3	C3	N3	-9.1(12)	O2	C11	C12	C13	-176.2(6)
C3	O3	C18	C19	-75.8(10)	C16	C11	C12	C13	1.2(11)
C3	O3	C18	C23	106.9(9)	O2	C11	C16	O5	-3.7(9)
C10	O4	C9	C4	-174.7(6)	O2	C11	C16	C15	174.7(6)
C10	O4	C9	C8	6.9(11)	C12	C11	C16	O5	178.7(6)
C17	O5	C16	C11	179.2(6)	C12	C11	C16	C15	-2.9(11)
C17	O5	C16	C15	1.0(10)	C11	C12	C13	C14	0.4(11)
C24	O6	C23	C18	-179.8(10)	C12	C13	C14	C15	-0.2(12)
C24	O6	C23	C22	2.7(12)	C13	C14	C15	C16	-1.6(12)
C3	N1	C1	O1	177.9(6)	C14	C15	C16	O5	-178.8(7)

C3	N1	C1	N2	-1.9(10)	C14	C15	C16	C11	3.0(10)
C1	N1	C3	O3	-177.8(6)	O3	C18	C19	C20	-175.4(7)
C1	N1	C3	N3	1.3(12)	C23	C18	C19	C20	0.9(16)
C2	N2	C1	O1	-177.6(5)	O3	C18	C23	O6	-3.4(13)
C2	N2	C1	N1	2.2(10)	O3	C18	C23	C22	174.2(7)
C1	N2	C2	O2	177.1(6)	C19	C18	C23	O6	-179.9(10)
C1	N2	C2	N3	-1.8(11)	C19	C18	C23	C22	-2.2(17)
C3	N3	C2	O2	-177.7(7)	C18	C19	C20	C21	0.3(13)
C3	N3	C2	N2	1.4(11)	C19	C20	C21	C22	0.4(16)
C2	N3	C3	O3	177.9(7)	C20	C21	C22	C23	-1.7(15)
C2	N3	C3	N1	-1.1(12)	C21	C22	C23	O6	-179.8(8)
O1	C4	C5	C6	-172.2(7)	C21	C22	C23	C18	2.4(12)
C9	C4	C5	C6	2.5(11)					

References

1. Sheldrick, G. M., *Acta Crystallogr. Sect. A: Found. Crystallogr.* **2007**, *64*, 112-122.